

https://dspace.org/

Systematic synthesis framework for the generation of CO2 and H2 sinks: the P-Graph approach

Jugmohan, Jaimee

2020

https://hdl.handle.net/10539/31329

Jugmohan, Jaimee. (2019). Systematic synthesis framework for generation of CO2 and H2 Sinks :the P-Graph approach. University of the Witwatersrand, https://hdl.handle.net/10539/31329

Downloaded from a DSpace repository. https://dspace.org/

SYSTEMATIC SYNTHESIS FRAMEWORK FOR THE GENERATION OF CO_2 AND H_2 SINKS:

The P-Graph Approach



Jaimee Jugmohan

797664

797664@students.wits.ac.za or jaimeejugmohan@gmail.com

Professor Thokozani Majozi (University of the Witwatersrand)

Sustainable Process Engineering Research

Chemical Engineering

University of the Witwatersrand

This dissertation is submitted for the degree of MSc Chemical Engineering

March 2020

Dedication

This dissertation is dedicated to my family. A special thanks to my parents, Stephen and Nadira Jugmohan, for their support and motivation. You have moulded me into the person that I am today. Thank you for not only being a parent to me but also being a teacher and mentor. I can always count on you both in the most difficult of times. I love you and I will always be grateful for the life that you have given to me.

A huge thanks to my sister, Nikita Jugmohan, for always using comforting words when my motivtion levels were low. Your determination and effort gives me strength. Words cannot begin to describe how much I appreciate everything that you have done for me, and how thankful I am to have a sister like you.

Thank you to Professor Thokozani Majozi, Dr. Brian North and Dr. Peter Mukoma for their help and guidance throughout the course of this research. The insight that you have provided into some of the stumbling blocks of my research was invaluable.

Lastly, I would like to express my thanks to the National Research Foundation (NRF) for funding this research.

UNIVERSITY OF THE WITWATERSRAND, JOHANNESBURG

SCHOOL OF CHEMICAL AND METALLURGICAL ENGINEERING
Faculty of Engineering & the Built Environment

Degree	MSc (Chemical Engineering)
Task	Master's Dissertation
Title	Systematic Synthesis Framework for the Generation of CO_2 and H_2 Sinks: The P-Graph Approach
Year	2020
Supervisor	Prof. Thokozani Majozi
Co-Supervisor #1	Dr. Brian North
Co-Supervisor #2	Dr. Peter Mukoma

Plagiarism Declaration

- I am aware that plagiarism (the use of someone else's work without their permission and/or without acknowledging the original source) is wrong.
- I confirm that the work submitted in this dissertation is my own unaided work.
- I have followed the required conventions in referencing the thoughts and ideas of others.
- I understand that the University of the Witwatersrand may take disciplinary action against me if there is a belief that this is not my own unaided work or that I have failed to acknowledge the source of the ideas or words in my writing.

Student Number	Name	Signature
797664	Jaimee Jugmohan	J Jugmohan

Table of Contents

Synopsis 1

1. Introduction 2

1.1. Background information 2

1.2. Motivation 5

1.3. Aims and Objectives 8

1.4. Problem statement 9

1.5. References 10

2. Literature review 12

2.1. Background information & the gap in the field 12

2.2. Greenhouse gases and CO_2 emissions 15

2.3. Greenhouse gas emissions in South Africa 18

2.4. The production of methanol 19

2.5. The production of dimethyl ether 27

2.6. The production of formaldehyde 28

2.7. The production of methane 30

2.8. The production of formic acid 35

2.9. The production of formate 38

2.10. The production of hydrocarbons (alkanes and alkenes) 39

2.11. The P-Graph 43

2.12. References 44

3. Framework Development 51

4. Model development through P-Graph 54

4.1. Methodology for P-Graph development 54

4.2. Reaction pathway database 56

4.3. Initial P-Graph model 61

4.4. P-Graph conditions 62

4.4.1. Condition 1 62

4.4.2. Condition 2 64

4.4.3. Condition 3 64

4.5. Revised P-Graph model 65

4.6. References 66

5. P-Graph analysis 70
5.1. The development of Aspen Plus ® Simulations 70
5.2. The costing of unit operations 71
5.2.1. Costing procedure 72
5.2.2. Costing capacity limits 74
5.2.3. Breakdown of unit operations 75
5.3. Model constraints 76
5.4. Analysis criteria 79
5.4.1. Criterion 1: Economic viability 79
5.4.2. Criterion 2: Environmental impact 80
5.4.3. Criterion 3: Analysis of the payback period 81
5.4.4. Criterion 4: Catalyst cost and performance index 82
5.5. References 83
6. Application of systematic framework 84
6.1. Data utilized in analysis 84
6.1.1. Cost of reactants and utilities 84
6.1.2. Cost of catalysts 85
6.1.3. Sales potential of products 86
6.1.4. Additional data utilized 87
6.2. Application of reduction criteria 1 to 3 87
6.3. Application of reduction criterion 4 88
6.3.1. Costing of the catalysts 88
6.3.2. Analysis of the methanol production pathways 89
6.3.3. Analysis of the DME production pathways 90
6.4. Final ranking of reduced search space 92
6.5. References 92
7. Limitations of framework 95
7.1. Data subject to change 95
7.2. Effect on most viable pathway 96
7.3. References 97
8. Optimization of most viable reaction pathway 98
8.1. Reactor operating conditions 98
8.1.1. Reaction kinetics and reaction constants 98

8.1.2. Initial pre-reactor optimization basis 100
8.1.3. Aspen Plus ® reaction kinetic parameters 101
8.1.4. Optimization model specifications in Aspen Plus ® 102
8.1.5. Objective function 104
8.1.6. Optimization model – Observations and results 104
8.2. Compressor/Heat exchanger configuration 107
8.2.1. Pre-reactor configuration superstructure 107
8.2.2. Superstructure analysis and scenario description 108
8.2.3. Optimization model specifications in Aspen Plus ® 111
8.2.4. Objective function 112
8.2.5. Observations and results 113
8.3. Number of pre-reactor unit operations 114
8.3.1. Optimization model specifications in Aspen Plus ® 114
8.3.2. Objective function 115
8.3.3. Optimization model – Observations and results 116
8.4. CO_2/H_2 feed ratio 117
8.4.1. Optimization model specification in Aspen Plus ® 117
8.4.2. Objective function 118
8.4.3. Optimization model – Observations and results 119
8.5. Post-reactor flash drum conditions 120
8.5.1. Optimization model specifications in Aspen Plus ® 120
8.5.2. Objective function 121
8.5.3. Optimization model – Observations and results 121
8.6. The recycle structure 123
8.6.1. Optimization model specifications in Aspen Plus ® 123
8.6.2. Objective function 124
8.6.3. Optimization model – Observations and results 124
8.7. The distillation column 126
8.8. Energy saving analysis and heat integration 128
8.8.1. Final process flow diagram before heat integration 128
8.8.2. Possible solutions and design changes 129
8.8.3. Final process flow sheet with heat integration and utilities 132
8.9. Summary of optimization results 133

8.10. References 133
9. Conclusion 135
10. Appendices 137
10.1. Appendix A – Case studies evaluated 137
10.2. Appendix B – Case study data (based on formulae) 147
10.3. Appendix C - Costing procedure (constants and graphs) 163
10.3.1. Purchased equipment cost constants 163
10.3.2. Pressure factors for non-pressure driven unit operations 164
10.3.3. Bare module and material factors for heat exchangers, process vessels and pumps 165
10.4. Appendix D – MATLAB ® codes for costing equipment 170
10.4.1. Code for the costing of compressors 170
10.4.2. Code for the costing of heat exchangers 172
10.4.3. Code for the costing of pumps 178
10.4.4. Code for the costing of turbines 181
10.4.5. Code for the costing of process vessels 183
10.4.6. Code for the costing of towers 185
10.4.7. Code for the costing of trays 187

List of Figures

Figure 1: Global CO_2 emissions by various world regions (Ritchie & Roser, 2017) 3
Figure 2: Global CO_2 emissions from fossil fuels (2010 – 2018) (Le Quere et al., 2018) 4
Figure 3: Diagrammatic representation of a food chain 4
Figure 4: Onion diagram of process design (Smith & Linnhoff, 1988) 6
Figure 5: Complete overview of systematic framework developed 53
Figure 6: Preliminary P-Graph based on the reaction pathway database before implementing conditions 61
Figure 7: Final revised P-Graph after the implementation of the conditions 65
Figure 8: Generic flowsheet structure of Aspen Plus ® Simulations 70
Figure 9: Diagrammatic representation of the breakdown of unit operations 76
Figure 10: Tornado diagram showing the effect of various factors on the payback period of the most viable pathway (Case study 8) 96
Figure 11: Preliminary flowsheet utilized in the optimization of the reactor operating conditions 101
Figure 12: Line graph showing the effect of temperature and pressure on the hourly production of MeOH 105
Figure 13: Line Graph showing the effect of temperature and pressure on the objective function 106
Figure 14: 3D Surface plot showing the effect of temperature and pressure on the objective function of the pre-reactor system 107
Figure 15: Pre-reactor compressor/heat exchanger superstructure 108
Figure 16: Line graph showing the change in the objective function as the number of heat exchangers increase 117
Figure 17: Line graph showing the effect that the hydrogen flow rate has on the hourly profit 119
Figure 18: 3D Surface plot showing the effect of temperature and pressure on the objective function of the post-reactor system 123
Figure 19: Bar graph of the total sizes of the heat exchanger areas for the various possible recycle structure options 125
Figure 20: Final process flow diagram before heat integration 128

Figure 21: Final process flowsheet after heat integration (colour coded with utility streams) 132
Figure 22: Material factors for the equipment in Table 40 167
Figure 23: Material factors for the equipment in Table 42 169

List of Tables

Table 1: Reaction pathway database based on data extracted from various literature sources 56
Table 2: Preliminary P-Graph results before the addition of conditions 62
Table 3: List of mutual exclusions applied to the preliminary P-Graph 63
Table 4: P-Graph results after all conditions were implemented 66
Table 5: Unit operation capacity limits associated with the costing procedure and equations 74
Table 6: Cost of raw materials or reactants required for the case studies and the utility required 84
Table 7: Cost of each individual component required for the catalysts needed in each case study 85
Table 8: Catalyst costs with their respective mass compositions 86
Table 9: Sales potential of products that are produced via the various case studies 86
Table 10: Other factors that are required for the case studies to be analysed 87
Table 11: Catalysts and compositions required for the production of MeOH from the reduced case study workspace 88
Table 12: Catalysts and compositions required for the production of DME from the reduced case study workspace 89
Table 13: Important data for final MeOH production workspace 89
Table 14: Important data for final DME production workspace 91
Table 15: Final ranking of the reduced workspace in order of viability 92
Table 16: Factors that are subject to change during this analysis 95
Table 17: Characteristics of the TMC-3/1 catalyst utilized in reaction kinetics derivation 99
Table 18: Kinetic parameter constants 99
Table 19: CZA catalyst operating conditions constraints 100
Table 20: Kinetic parameters required for Aspen Plus ® reactor modelling 102
Table 21: Optimization variables with their step sizes 102
Table 22: Optimization constraints for reactor operating conditions 103
Table 23: Pressure and temperature ranges for which the catalyst is not in operation within the predetermined constraints 105
Table 24: List of all possible compressor/heat exchanger configurations based on the superstructure 109

Table 25: Data for the various scenario evaluated in the optimization of the unit operation configuration 113
Table 26: Results obtained from the optimization model on Aspen Plus ® 116
Table 27: Temperature showing the pressure and temperatures for which the flash drum is inoperable 122
Table 28: Specifications of the distillation column required in the separation of the MeOH /water mixture 126
Table 29: Physical specification of the distillation column required 127
Table 30: Current heat exchanger data for the process depicted in Section 8.8.1 129
Table 31: Potential savings of the process based on Aspen Energy Analyzer ® 130
Table 32: Detailed analysis of the hot and cold utilities required for the process 130
Table 33: Possible solutions in order to reduce the energy consumption of the current plant 131
Table 34: Changes to the heat exchanger network by employing Solution 1 131
Table 35: Final design summary based on all optimization models 133
Table 36: Case studies to be evaluated based on the P-Graph developed 137
Table 37: Detailed case study data extracted from Aspen Plus ® 147
Table 38: Equipment cost data to be utilized with Equation (33) 163
Table 39: Pressure factors for process equipment utilized in Equation (34) 164
Table 40: Identification numbers for material factors for heat exchangers, process vessels and pumps 165
Table 41: Constants for bare module factors utilized in Equation (36) 167
Table 42: Identification numbers for material factors for the rest of the unit operations 168

Nomenclature

Symbol	Value Represented	Symbol	Value Represented
C_p^o	Purchased Cost at Ambient Conditions ($)	W_{Total}	Total Work Done by Units (kW)
$K_1 \rightarrow K_3$	Purchased Cost Constants	W_j	Work Done by Individual Units (kW)
A	Unit Operation Capacity (kW, m^2 or m^3)	E_{Total}	Total Energy Required (kW)
F_P	Pressure Factor	m_{NG}	Mass of Natural Gas Needed (tons)
$C_1 \rightarrow C_3$	Pressure Factor Constants	HV_{NG}	Heat Value of Natural Gas (GJ/kg)
P	Pressure (barg)	$m_{CO_2\ Produced}$	Mass of CO_2 Produced (tons/year)
D	Diameter of Vessel (m)	M_{CH_4}	Molar Mass of Methane (kg/kmol)
C_{BM}	Bare Module Cost ($)	M_{CO_2}	Molar Mass of CO_2 (kg/kmol)
$B_1 \rightarrow B_2$	Bare Module Cost Constants	$C_{Total\ NG}$	Annual Cost of Natural Gas ($)
F_M	Material Factor	C_{NG}	Cost of Natural Gas ($/MMBtu)
F_{BM}	Bare Module Material Factor	$m_{CO_2\ Purchased}$	Mass of CO_2 Purchased (tons/year)
F_q	Quantity Factor	$m_{CO_2\ Fed}$	Mass of CO_2 in Feed (tons/year)
N	Number of Trays	C_{RM}	Annual Cost of Raw Materials ($)
n	Number of Unit Operations in Case Study	m_k	Mass Flow of Raw Material (tons)

HE_{Total}	Total Cost of Heat Exchangers ($)	C_k	Cost of Raw Material ($/kg)
$C_{i_{HE}}$	Cost of Individual Heat Exchanger ($)	a	Number of Reactant Feed Streams
P_{Total}	Total Cost of Pressure Changing Units ($)	$SP_{Products}$	Annual Sales of Products ($)
C_{i_P}	Cost of Individual Pressure Changing Units ($)	m_l	Mass Flow of Products (tons)
S_{Total}	Total Cost of Separation Units ($)	SP_l	Selling Price of Product ($/kg)
C_{i_S}	Cost of Individual Separation Units ($)	b	Number of Product Streams
C_{Total}	Total Cost of Unit Operations ($)	$Profit$	Annual Profit ($)
Q_{Total}	Total Heat Released from Plant (kW)	PBP	Payback Period (years)
Q_i	Heat Released by Individual Units (kW)	CRF	Capital Recovery Factor
r	Annual Discount Rate (%)	ACC	Annualized Capital Cost ($/annum)
n	Lifespan of the Plant (years)		

List of Appendices

Appendix A – Case studies evaluated.....137
Appendix B – Case study data 147
Appendix C - Costing procedure (constants and graphs) 163
Purchased equipment cost constants.....163
Pressure factors for non-pressure driven unit operations 164
Bare module and material factors for heat exchangers, process vessels and pumps.....165
Appendix D – MATLAB ® codes for costing equipment.....170
Code for the costing of compressors 170
Code for the costing of heat exchangers.....172
Code for the costing of pumps.....178
Code for the costing of turbines 181
Code for the costing of process vessels 183
Code for the costing of towers.....185
Code for the costing of trays.....187

Conference Presentations

The work detailed in this Master's dissertation has been presented at the following conferences:

1. 2019 AIChE Spring Meeting and 15th Global Congress on Process Safety held in New Orleans, United States of America
2. 7th International Conference on Biorefineries (ICB 2019) held in Johannesburg, South Africa

Synopsis

Economies have become increasingly reliant on the use of fossil fuels as the primary energy source in order to meet energy demands of a growing population. The combustion of fossil fuels results in greenhouse gas (GHG) emissions, particularly carbon dioxide (CO_2). This has resulted in CO_2 emissions increasing at a rate that is detrimental to climate. To curb the detrimental effects of these emissions, whilst providing for the energy requirements of the population, a carbon negative energy source should ideally be introduced into the energy mix.

In this dissertation, a P-Graph superstructure approach is utilized to encompass a wide array of CO_2 reaction pathways that produce methanol (MeOH) and dimethyl ether (DME), both of which have proven to be prominent in the energy industry. A total of 85 reaction pathways were simulated using Aspen Plus ® software. These case studies were then analyzed from an environmental and economical perspective, in order to determine the most viable pathways to produce the aforementioned products. The framework developed was able to systematically reduce the search space from 85 possible scenarios, to 6 viable case studies, which is a 93% reduction in the original search space. The use of a $CuO/ZnO/Al_2O_3$ catalyst at 240^oC and 80 bar pressure, was found to be the most viable option to produce MeOH. The most viable scenario for the production of DME, on the other hand, is to produce MeOH over the aforementioned catalyst, and then further dehydrate the MeOH over an Al/Si catalyst at 400^oC and 25 bar pressure. The production of MeOH is deemed to be more feasible than the production of DME.

With the most viable reaction pathway being known as the production of MeOH via a $CuO/ZnO/Al_2O_3$ catalyst, the focus is shifted outside of the framework, to the optimization of this reaction pathway. Post-optimization, it is found that the use of a $CuO/ZnO/Al_2O_3$ (TMC-3/1 industrial ZA Tarnow) catalyst at 201^oC and 29 bar pressure, is the most viable reaction conditions involved in the direct hydrogenation of CO_2 to MeOH. This pathway is able to yield a 97.69% conversion of CO_2, thereby exhibiting the highest environmental and economic benefits after optimization.

This dissertation details the systematic framework used in the synthesis and analysis of the P-Graph when arriving at the reduced search space, as well as the optimization procedure that is followed for the most viable reaction pathway.

1. Introduction

Energy supports all forms of life, and is becoming increasingly fundamental in ensuring survival. Due to major increases in global population, and the social orders associated therewith, excessive strain is being put on the current energy sector. The integration of energy into our daily lives has been deemed critical to sustainable development, destitution mitigation, economic advancement and ecological sustainability (Department of Environmental Affairs, 2015).

1.1. Background information

The most common way to meet current global energy requirements, is through the use of fossil fuels as the primary energy source. An example of such an economy is the South African economy, with coal accounting for 77% of the primary energy supply, and more than 90% of electricity generation (Department of Environmental Affairs, 2015).

Two main concerns arise when using fossil fuels to meet daily energy requirements. The first concern lies in the fact that fossil fuels are considered to be a non-renewable resource. A non-renewable resource is defined as a finite resource that is unable to renew itself at a sufficient rate for it be extracted within meaningful human time frames, thereby not promoting sustainable development (Covert et al., 2016).

Furthermore, an inverse proportionality relationship exists between the cost of fossil fuel extraction and the amount of fossil fuels available. As the amount of fossil fuels begins to decrease, the resource becomes increasingly difficult to extract. This will, in turn, lead to more specialized equipment being required, as well as an increase in the labour required to extract these resources. Therefore, as fossil fuel reserves begin to diminish, the cost of extraction increases. This will likely lead to the point at which fossil fuels become too costly to harvest, resulting in humanity being forced to turn to alternative resources (Covert et al., 2016).

The second major concern with non-renewable resources are the toxic emissions that result due to the combustion of fossil fuels. The byproducts of the combustion process, commonly sulfur dioxide, smoke and CO_2, have proven to be damaging to human health, and are linked to the

impairment of cognitive and behavioral development, respiratory illnesses and other chronic diseases (Perera, 2017). CO_2 is a GHG, and due to the excessive use of fossil fuels in the South African economy, South Africa has been ranked among the top 15 CO_2 emitters globally (Department of Environmental Affairs, 2015). The significant increases in global CO_2 emissions can be depicted by means of Figure 1, which details the annual global CO_2 emissions, as well as the amount that each country or region contributes to this annual amount (Ritchie & Roser, 2017).

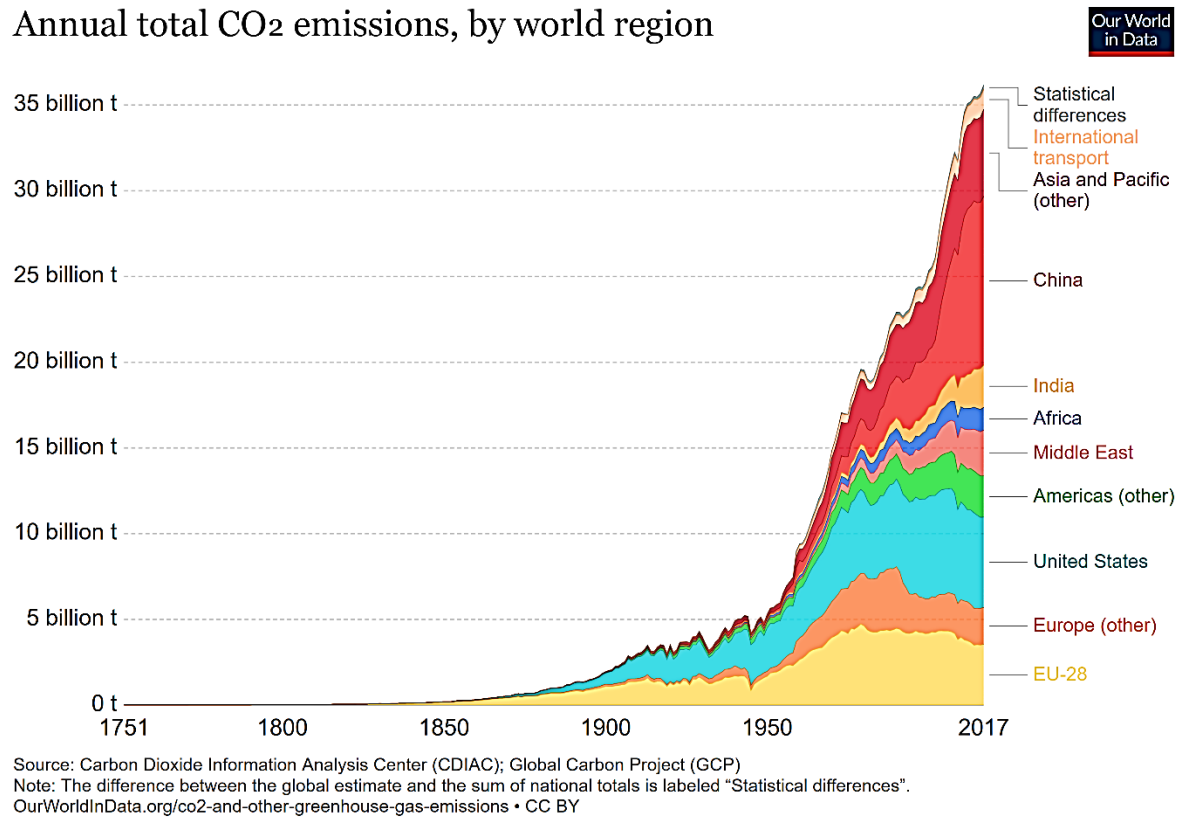

Figure 1: Global CO_2 emissions by various world regions (Ritchie & Roser, 2017)

Europe, China and the United States of America were the largest contributors of CO_2 emissions, between the years of 1800 and 2017. This was due to the level of development in these regions. Developing countries and continents (such as Africa) also contributed to the global CO_2 emissions to a lesser extent.

Figure 2 shows the CO_2 emissions derived from fossil fuel usage over the last 8 years (2010 – 2018), indicating that CO_2 emissions in 2018 was at an astounding 31.70 gigatons. This is a 2.50% increase from 2017 (Le Quere et al., 2018). Furthermore, Figure 2 shows that over the

last 8 years, there has been a 4.00 gigaton increase in CO_2 emissions caused by fossil fuel usage.

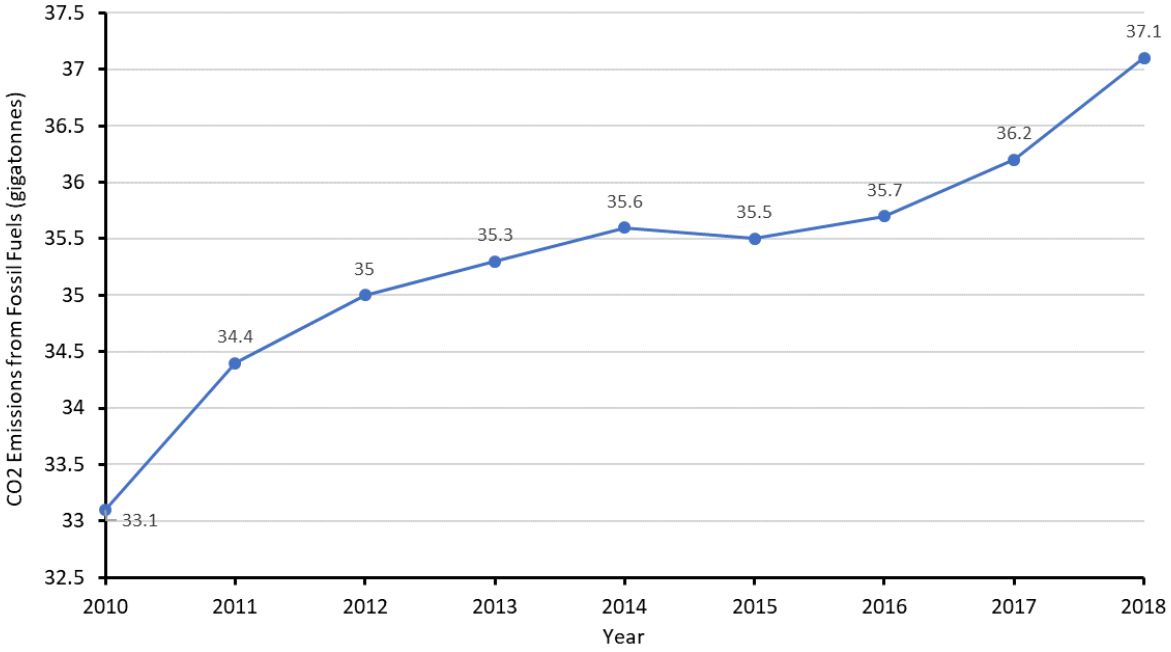

Figure 2: Global CO_2 emissions from fossil fuels (2010 – 2018) (Le Quere et al., 2018)

These fossil fuel emissions place considerable pressure on the environment, resulting in ozone depletion and subsequent climate changes. Such changes are extremely catastrophic to biological systems, as well as the environment in which they exist (Department of Environmental Affairs, 2015). An adequate representation of the chain reaction caused by fossil fuel emissions is depicted in Figure 3.

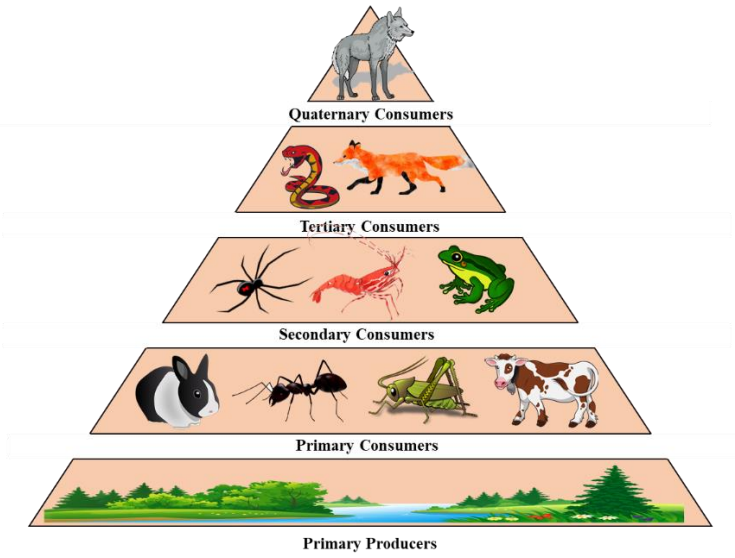

Figure 3: Diagrammatic representation of a food chain

Figure 3 considers the ecosystems, and the interaction of these ecosystems, as a building structure, with the primary producers, such as plants and trees, being the foundation of the building. Much of these primary producers survive within specific climates, and thus alterations to this climate, brought about by the GHG emissions, could result in many primary producers dying off. This affects the foundation of the ecological system, in turn affecting all other living organisms.

Currently, non-renewable energy sources are being utilized at an alarming rate. In order to reduce the rate at which these resources are being diminished, whilst still providing for the energy needs of a growing population, a carbon negative energy technology needs to be created. The term carbon negative is defined as a process that takes in more CO_2 than it emits, thereby having an overall reduction on current atmospheric CO_2 levels.

One method by which to utilize CO_2 as a reactant, is through hydrogenation. This allows for CO_2 to be converted to a value-added product, such as MEOH and DME, whilst simultaneously providing a convenient manner by which to store hydrogen. These value-added products can be utilized in the generation of electricity.

Recently, focus has been placed on the generation of electricity from renewable energy sources and hydrogen-based storage of excess electricity, via the "Power to X" (PtX) principle. PtX alludes to transformation advances that take into consideration the decoupling of energy from the electricity sector, so that it may be utilized in different sectors, i.e. the transport and chemical industries (Schnettler & Schmiedel, 2018). An example of a PtX system is the hydrogenation of CO_2 to methanol, which is one of the pathways explored further in this dissertation.

1.2. Motivation

The motivation behind this research was threefold, i.e. the extensive resources that are expended during the initial stages of designing a process, the depleting fossil fuel reserves, and the consequences of GHG emissions, specifically CO_2.

Firstly, the basis for any design and optimization model can be represented by means of an onion diagram, which details the hierarchical approach taken during the design of any chemical

process. The onion diagram can be represented diagrammatically as shown in Figure 4 (Smith & Linnhoff, 1988).

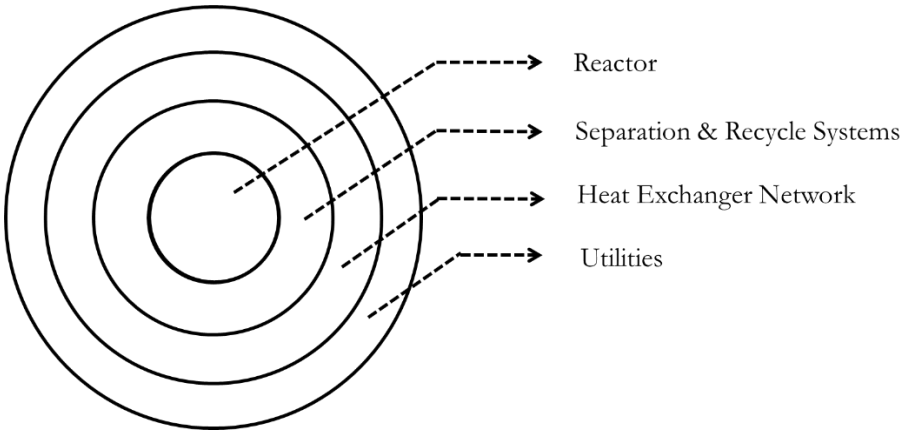

Figure 4: Onion diagram of process design (Smith & Linnhoff, 1988)

Figure 4 follows the 'onion logic', which involves building an irreducible structure. This diagram shows that at the center of any process, exists the reactor design, followed by the design of the separation and recycle systems. In each stage of this design process, decisions are made based on the information available in that stage, as well as the information obtained in previous stages of the design (Smith & Linnhoff, 1988). This shows that the reactor is the foundation of a chemical process, with all other decisions and designs being made around this unit operation.

Many of the current studies focus on improving existing processes, rather than developing processes from scratch. However, it is possible that a better reaction pathway could be implemented in a process, resulting in greater efficiencies or possibly lower costs. The concern lies in finding this reaction pathway without expending too many resources during the early design stages.

To solve this problem a systematic framework needs to be developed, as is detailed in this dissertation. This framework utilizes a database containing all of the reaction pathways that currently focus on the production of a desired product, and systematically reduce this search space to the most feasible pathways. The reaction pathways in the reduced search space are ranked in order of their viability, taking into account both environmental and economic benefits. The strength of such a framework lies in the fact that it is based on a comprehensive database, thereby not limiting its application to only certain reactive systems. This makes the framework more practical and generic in its application. Furthermore, the reduction in the reaction pathway search space allows for resources to be more efficiently utilized, with the

most efficient and viable pathway being known at an early stage, prior to extensive design and optimization procedures.

Secondly, as detailed in Section 1.1, there are currently major concerns surrounding the utilization of fossil fuels globally. Currently the global fossil fuel reserves are as follows (BP plc, 2019):

- Coal – 1.05 billion metric tons
- Natural gas (NG) – 196.90 trillion cubic meters
- Crude Oil – 1.73 billion barrels

Although this appears to be a large reserve, the global energy demand increased by 2.30% in 2018, which is twice the average rate of increase over the last decade. Increased use of fossil fuels covered 70% of the global increase in energy demand with NG covering almost 45% of total demand growth (International Energy Agency, 2019). Therefore, at the current rate of fossil fuel consumption, the fossil fuel reserves are predicted to become exhausted as follows (BP plc, 2019):

- Coal – year 2169
- NG – year 2068
- Crude Oil – year 2066

This increase in fossil fuel usage does not promote sustainable development. This could be catastrophic in meeting the energy requirements of future generations. In order to reduce the usage of fossil fuels, alternative energy sources need to be explored. This could either be in the form of renewable energy sources, such as solar and hydro power, or through the conversion of current detrimental GHG emissions to valuable products.

Lastly, GHGs are defined as gases that absorb and emit radiant energy within the thermal infrared range, with one such gas being CO_2. CO_2 is produced during the combustion of fossil fuels. These gases trap heat in the atmosphere resulting in both ozone depletion and climate changes (Darkwah et al., 2018). Such climate changes are catastrophic to biological systems and the environment in which they exist. Primary producers, and the species that rely on them, are highly sensitive to environmental changes, and only survive within specific climates. Changes in the climate results in these species dying off. Studies show that over 40% of insects are currently being threatened with extinction (Sanchez-Bayo & Wyckhuys, 2019).

This climate change has been increasingly evident in recent months. The National Oceanic and Atmospheric Administration announced that the January-July 2019 period had a combined global land and ocean surface temperature increase of 0.95^{o}C. This is the second highest January-July period since global records began in 1880 (NOAA National Centers for Environmental Information, 2019). This heat wave has also caused major concerns in Greenland, melting its ice sheets at a significant rate. Approximately 197 billion tons of ice melted into the Atlantic Ocean in July 2019, with a maximum of 12 billion tons of ice being melted in a single day. The rate of the ice melting in July is 36% more than scientists expect within a year (Lewis, 2019).

If fossil fuel usage continues at the current rate, it is predicted that global temperatures could increase by 5°C by 2100. According to the Intergovernmental Panel on Climate Change (IPCC), this could cause sea levels to rise by more than 2 meters by the end of this century. This rise in sea level could result in land losses of 1.79 million square kilometers, and potentially the displacement of 187 million people (Bamber et al., 2019).

In order to reduce the usage of fossil fuels and their emissions thereof, a carbon negative fuel source should ideally be introduced into the energy mix. This fuel source aims to utilize atmospheric CO_2, in an attempt to reduce CO_2 levels and the subsequent anthropogenic climate changes. The systematic framework that is developed in this dissertation, is applied to a CO_2/H_2 system, with the hope of demonstrating its application and benefit.

1.3. Aims and Objectives

The aim of this research is to develop a systematic method for the determination of the most viable reaction pathway, which utilized both CO_2 and H_2, to produce a synthetic fuel. The most viable reaction pathway is then optimized, covering the following scope:

- Reactor operating conditions, accounting for both conversion and economic implications
- Feed ratio of CO_2 and H_2
- Pre-reactor unit operation configuration and number of unit operations
- Recycle structure
- Post-reactor conditions for unreacted gas separation

- Heat integration and other possible energy savings

The following list details the objectives of this research, in order to achieve the aforementioned aim:

- To develop a reaction pathway superstructure containing pathways with H_2 and CO_2.
- To become familiar with the software that is utilized in the construction of P-graphs and the relevant solvers that are involved.
- To determine the number of achievable reaction pathway combinations.
- To design processes for each pathway and determine their respective mass balances, energy balances, and unit operation sizes (with the exception of the reactor units).
- To conduct a feasibility/economic analysis on each process in order to determine the most feasible pathways.
- To further optimize the most viable reaction pathway determined from the systematic framework.

1.4. Problem statement

Given a reaction pathway database (RPD) containing the following information:

- Reaction pathway mechanism, i.e. sub reactions involved in the reaction system
- Reaction operating conditions, i.e. temperature and pressure
- Catalyst required and its associated composition
- Products produced in the system
- Conversion of CO_2
- Selectivity required in cases where multiple products are produced
- Inlet feed ration of CO_2 to H_2

Develop:

- A systematic framework that is able to reduce the search space to a manageable region containing the most feasible reaction pathway.
- Identify and optimize the most viable pathway in the search space

The validity and usefulness of this systematic framework is demonstrated by applying it to a CO_2/H_2 system in order to determine which reaction pathway is able to produce a carbon negative fuel source, whilst still being both environmentally and economically beneficial.

1.5. References

Bamber, J. L., Oppenheimer, M., Kopp, R. E., Aspinall, W. P., & Cooke, R. M. (2019). Ice sheet contributions to future sea-level rise from structured expert judgment. Proceedings of the National Academy of Sciences of the United States of America, 116(23), 11195-11200. doi:10.1073/pnas.1817205116

BP plc. (2019). BP Statistical Review of World Energy 68th Edition. London: Pureprint Group Limited.

Covert, T., Greenstone, M., & Knittel, C. R. (2016). Will We Ever Stop Using Fossil Fuels? Becker Friedman Institute for Research in Economics Working Paper No. 2720633. doi:10.2139/ssrn.2720633

Darkwah, W. K., Odum, B., Addae, M., & Koomson, D. (2018). Greenhouse Effect: Greenhouse Gases and Their Impact on Global Warming. Journal of Scientific Research and Reports, 17(6), 1-9. doi:10.9734/JSRR/2017/39630

Department of Environmental Affairs. (2015). Chapter 12 - Energy. In *Environment Outlook* (pp. 238 - 276). Johannesburg.

International Energy Agency. (2019). Global Energy & CO_2 Status Report: The latest trends in energy and emissions in 2018. France: IEA Publications.

Le Quere, C., Andrew, R. M., Friedlingstein, P., Sitch, S., Hauck, J., Pongratz, J., . . . Zheng, B. (2018). Global Carbon Budget 2018. Earth System Science Data, 10(4), 2141–2194. doi:10.5194/essd-10-2141-2018

Lewis, S. (2019, August 2). 11 billion tons of ice melted in Greenland — in just one day. (CBS NEWS) Retrieved August 28, 2019, from https://www.cbsnews.com/news/11-billion-tons-of-ice-melted-greenland-just-one-day/

NOAA National Centers for Environmental Information. (2019). State of the Climate: Global Climate Report for July 2019. North Carolina.

Perera, F. (2017). Pollution from Fossil-Fuel Combustion is the Leading Environmental Threat to Global Pediatric Health and Equity: Solutions Exist. International Journal of Environmental Research and Public Health, 15(16).

Ritchie, H., & Roser, M. (2017). CO_2 and Greenhouse Gas Emissions. United Kingdom: University of Oxford.

Sanchez-Bayo, F., & Wyckhuys, K. A. (2019). Worldwide decline of the entomofauna: A review of its drivers. Biological Conservation, 232, 8-27. doi:10.1016/j.biocon.2019.01.020

Schnettler, A., & Schmiedel, G. (2018, July 5). Catalysts of the Transition to a new Energy Mix.

Smith, R., & Linnhoff, B. (1988). The design of separators in the context of overall processes. Chemical Engineering Research and Design, 195-228.

2. Literature review

This chapter provides a background of this research field, identifying the gap in the field that this dissertation aims to address, as well as details the previous work that has been conducted around the reaction pathways that utilize CO_2 and H_2. These pathways, and their associated experimental data, was utilized in the development of a reaction pathway database, as is shown in Section 4.2 of this dissertation.

2.1. Background information & the gap in the field

Due to the fact that reaction pathway synthesis is often considered to be the main area within process synthesis, it is crucial to develop a systematic method whereby desirable reactions can easily be identified. This desirability can be subject to a number of factors, with the most important two being the economic and environmental benefit of the reaction pathway. However, taking into consideration all engineering factors, can prove to be a difficult task. Therefore, simplifying assumptions can be made to create a more manageable task.

In 1982, the possibility of exploring new reaction pathways to produce a chemical product was investigated using a systematic analytical framework. This framework considered the Gibbs free energy and temperature of a reaction, when determining its feasibility. The search space included both single-step and multiple-step reaction pathways. This showed an optimization problem with two degrees of freedom. The advantages in utilizing the Gibbs free energy phenomenon in such a case, is that alternative reaction pathways can be identified and considered (Rotstein et al., 1982). The shortcoming of this research was that the Gibbs free energy and temperature space considered, resulted in an infinite number of reaction pathways.

The procedure was later furthered by evaluating the thermodynamic feasibility of the reaction pathways, creating an initial screening process to reduce the infinite search space. This created a bounded feasible region within the space of the Gibbs free energy and temperature variable, generating a more accurate reaction pathway search algorithm (Fornari et al., 1989). An additional screening mechanism was to consider the economics, processing and safety of the reaction pathways (Fornari & Stephanopoulos, 1994).

Later that year, an optimization problem was developed, whereby its solution was able to yield the reaction pathway that is thermodynamically, economically and environmentally feasible (Li et al., 2000).

In 2000, a hierarchical optimization procedure for reaction pathway synthesis was developed. This optimization procedure looked at economic potential, thermodynamic feasibility and kinetic desirability. In cases where an overall reaction is deemed profitable, yet thermodynamically unachievable, a reaction decomposition method was applied. This involved adding intermediates into the reaction pathway, allowing the product to be produced via several thermodynamically feasible division reactions (Li et al., 2000).

This hierarchical optimization procedure was demonstrated using a case study involving the production of vinyl chloride. A total of 17 overall reactions were derived for the production of vinyl chloride, with each being analyzed from a stoichiometric and gross profit perspective (Li et al., 2000). The shortcoming of this research was that the reaction pathways considered did not account for the conversion of each reaction, the cost of the equipment required in developing a chemical plant to achieve the reaction, and the environmental impact of the reaction in question.

The P-Graph algorithm (Section 2.11) is able to provide a superstructure network, detailing all possible combinations. Although initially developed for solving process network synthesis (PNS) problems, the recent applications of the P-Graph algorithm include separation network synthesis, reaction pathway identification, scheduling and supply-chain optimization (Varbanov et al., 2017).

The P-Graph model was first applied to reaction pathway identification and synthesis in 1997 (Fan & Friedler, 1997). In 2001, a new axiomatic system specifically targeting reaction pathway synthesis in catalytic conditions was developed (Fan et al., 2001). This was verified later that year (Seo et al., 2001). In 2008, the P-Graph algorithm was used in determining the reaction pathway mechanism behind the catalytic partial oxidation of methanol (Tan et al., 2018). It was formally proved that the new reaction pathway synthesis algorithms, based on the P-Graph concept, was able to generate a complete set of reaction pathways, identical to those found using linear algebraic approaches (Barany et al., 2012).

Recent developments in this area looked at reducing the number of feasible pathways, by adding search criteria (Liu et al., 2015), or taking into account experimental data to confirm the reaction pathways (Diaz-Alvarado et al., 2018).

Reaction pathway synthesis can be defined as determining how many reaction pathway combinations are possible through the use of elementary reactions. The resulting search space is then used in selecting the preferred reaction mechanism. In order for a reaction pathway combinatorial to be classified as feasible, whilst simultaneously reducing the search space, it is required to meet one of the following six axioms (Lakner et al., 2018):

i. Every starting reactant and final product are represented in the reaction pathway.
ii. Each elementary reaction represented in the reaction pathway is defined.
iii. Every chemical species represented has at least one path leading to the final product of the overall reaction.
iv. Every chemical species represented must be a reactant for, or a product from, at least one elementary reaction represented in the reaction pathway.
v. A reactant of any elementary reaction represented in the reaction pathway is a starting reactant, if it is not a product of any elementary reaction represented in the reaction pathway.
vi. The reaction pathway includes at most either the forward or the reverse step of each elementary reaction.

Furthermore, a reaction pathway must also be considered ‘startable’ for it to be part of the possible combination search space. A startable reaction is defined as a reaction that is able to achieve steady state when only the reactants, of that reaction, are available. This prevents intermediate reactions from being classified as their own reaction pathway combination (Lakner et al., 2018).

As can be seen by the six axioms above, the term ‘feasibility’ in reaction pathway synthesis, is simply an indication of whether a reaction pathway is considered possible, without taking into account conversions, production rates and current economics. This is one of the main aspects that is aimed to be addressed in this dissertation, thereby increasing the application of this methodology to industrial processes.

In 2018, an investigation was conducted into the design of a carbon, hydrogen and oxygen symbiosis network, in order to enable the systematic integration of multiple plants and to determine chemical conversion, separation, and allocation schemes through a multiscale atomic targeting approach. This model took into account seasonal variabilities and multiple modes of operation throughout the year. The model aimed to maximize profits of the system

in question, and also address CO_2 emissions, by reducing emissions and converting CO_2 to value added products (Al-Fadhli et al., 2018).

The research conducted looked at determining economic and environmental feasibility, however, the case studies were based on chemical plants that have already been constructed and are in operation. The information required in this study included mass balances, design vectors and the fixed capital investment (Al-Fadhli et al., 2018).

Apart from considering economic and environmental concerns, social sustainability must also be considered during the economic assessment of a chemical plant. Social sustainability involves considering market uncertainty as well as the price/cost volatility. This is important in analyzing the feasibility of any chemical plant as the sales potential of the product will be highly dependent on the market for the product, i.e. the supply and demand chain (Sepiacci & Manca, 2015).

Presented in this dissertation is the systematic framework to reduce the reaction pathway search space to a smaller region containing the optimum reaction pathway. This systematic framework aims to address the aforementioned shortcomings in a single novel framework, by using an RPD, containing the conversion and operating conditions of various reaction pathways. This framework looks at the mass balances, energy balances, possible energy savings by heat integration and physical sizing and costing of each unit operation within the case studies, prior to their construction.

Furthermore, an environmental and economic analysis will be conducted on each possibility. The usefulness of this framework is demonstrated through its application with a CO_2/H_2 reactive system. This allows for the creation of a carbon negative fuel source that is both environmentally and economically beneficial.

2.2. Greenhouse gases and CO_2 emissions

To meet the energy requirements of a rapidly growing population, many countries have become increasingly reliant on fossil fuel usage (Bellotti et al., 2017). Fossil fuels account for almost 90% of the world's energy requirements. Developing countries contribute 80% towards the global population, but only 49% of the world's energy consumption, as is to be expected based on technological developments (Hashimoto et al., 2016).

Unfortunately, one of the byproducts during the combustion of fossil fuels is CO_2, which is a GHG. GHGs have rapidly become one of the most pressing environmental concerns, with much of these effects being traced back to the aforementioned CO_2 emissions (Bellotti et al., 2017).

CO_2 emissions have major effects on the environment, resulting in global warming. Unfortunately, these emissions also contribute to urban smog, acid rain, and many health problems, including cancer (Vanhove, 2015). The global energy demand is expected to double between the year 2017 and 2050, thereby increasing the emphasis that is being placed on renewable energy sources as an alternative and cleaner energy provider (Bellotti et al., 2017). The concern with renewable energy lies in its intermittent and fluctuating nature, making it extremely unstable for communities to rely solely on renewable energy sources (Hashimoto et al., 2016).

Furthermore, with CO_2 often being considered as a by-product or waste stream during the combustion of fossil fuels, one needs to consider its utilization as a possible 'Waste to Energy' process. During a waste to energy process, a trade-off exists between the energy that is generated from the system, and the energy expelled during the collection, transport and treatment of a waste stream (Ng et al., 2013). Process equipment and energy required to capture CO_2 are one of the major CO_2 concerns. Some of the performance indicators utilized in this trade-off, include cost, Waste Energy Potential Utilisation (WEPU) and the carbon footprint (Ng et al., 2013).

In 2017, the absorption capacity of coal for CO_2, after adding SO_2 to the feed mixture, was investigated. This investigation found that increasing the pressure of CO_2 absorption to a sub-critical state, was able to enhance the CO_2 adsorption capacity of coal (Khanyisile et al., 2017). Thereby, demonstrating one possibility in which coal can be captured for future utilization.

Daramola reported that much of the CO_2 storage systems in South Africa, was attributed to deep unmineable coal seams which have a capacity of approximately 150 gigatons of CO_2 (Daramola, 2015). Unfortunately, little effort was being focused on CO_2 capture and transport in South Africa, which is essential for developing systems that utilize CO_2. The main concern with implementing carbon capture in the South African infrastructure was due to financial restrictions and the lack of technical expertise (Yoro & Sekoai, 2016). In hopes of rectifying this, Daramola had focused on CO_2 capture, with one such work looking into the synthesis and evaluation of carbon nanotubes composite adsorbent for CO_2 capture (Osler et al., 2017).

In order to lower the energy requirements of carbon capture systems, heat and mass integration could be utilized. A recent review on the process integration techniques that could be used to minimize both energy and materials, found that the use of inhibitors and additives are the most common strategy used in lowering the energy requirements of the carbon capture process. However, this only worked with gas-liquid systems. Heat and mass integration, on the other hand, eliminated this limitation, and allowed for the application of both liquid and solid absorbents. This was found to increase the efficiency of the capture process (Yoro et al., 2019).

There are three proposed methods by which to reduce the levels of anthropogenic CO_2. The first is to reduce the amount of CO_2 that is produced by targeting the emission sources, i.e. creating processes that release less CO_2 waste. The next is to store or sequester the CO_2 underground, however, this has its limitation, due to geological space constraints (Matzen & Demirel, 2016). Lastly, CO_2 could be utilized in chemical processes. The four main uses of CO_2 are as follows (Vanhove, 2015):

- CO_2 can be used as an inert. This is common in the food industry, in products such as carbonated beverages.
- CO_2 can be utilized as a working fluid. Recent research has shown that supercritical CO_2 can be used in heat exchanger unit operations.
- CO_2 can be used as a solvent, to increase the recovery of hydrocarbons.
- CO_2 can be reacted to form valuable products, such as MeOH and DME.

The conversion of CO_2 to useful and valuable products has become increasingly important in many industries, especially with the restrictions and penalties that are required to be paid for each ton of CO_2 emitted (Van der Ham et al., 2012). The main concern with the utilization of CO_2 is that it is a thermodynamically stable molecule, and therefore, is extremely costly to utilize as a reactive chemical compound (Gaikwad et al., 2016). To overcome this, a catalyst is utilized. The use of a catalyst will lower the operating conditions or shorten the required reaction time (Matzen & Demirel, 2016).

A commonly increasing solution to the rising energy demand globally is the power to gas and power to liquid strategy (Burkhardt et al., 2015). This involves the storage of excess electricity from the grid in a gas or liquid form, allowing for subsequent use of the stored energy at a later time (Bellotti et al., 2017). An example of such a reactive system that is used in excess electricity storage, is seen between CO_2 and H_2, with H_2 either being available through electrolysis or the use of a hydrogen donor (Zhao et al., 2018).

2.3. Greenhouse gas emissions in South Africa

South Africa is an example of one of the economies that are heavily reliant on fossil fuels, and are suffering from excess GHG emissions. The World Resources Institute Climate Analysis Indicator Tool (WRI CAIT) reports that the energy sector is dominating South Africa's GHG profile, accounting for approximately 84% of South Africa's total emissions in 2012. Of this, 60% of energy emissions were due to electricity and heat, 15% to manufacturing and construction, 12% to transportation, and the remaining 12% to other, smaller energy subsectors. Agriculture, one of the most prominent industries in South Africa, is the second highest emitting sector (USAID, 2015).

South Africa meets most of its energy needs through the use of coal as a fossil fuel. However, the use of coal has two major concerns. The first concern is that this process emits large amounts of CO_2, which is extremely harmful to the environment. The second major concern is that coal is a non-renewable resource, and therefore, its constant use does not promote sustainable development. The U.S. Energy Information Administration reported that most coal power plants in South Africa are outdated, poorly maintained, and working at their maximum capacity (USAID, 2015).

In hopes of rectifying this, South Africa is diversifying its electricity generation mix and is expanding its renewable electricity generation capacity through the Renewable Energy Independent Power Producer Procurement Program (REIPPPP). This expansion has resulted in the emissions from agriculture, forestry, and other land-use dropping by 15.7%. However, this decrease was also attributed partly to the livestock numbers diminishing between the years of 2000 and 2010 (USAID, 2015).

South Africa is aware that it is a significant contributor to global climate change, with significant GHG emissions from its energy-intensive, fossil-fuel powered economy, noting this fact in its National Climate Change Response Strategy. With the carbon intensity of South Africa's economy being almost 4 times the world average, there is much potential to reduce South Africa's GHG emissions relative to gross domestic product (GDP). South Africa has also been developing policy tools, including a carbon tax (Carbon Tax Act 15 of 2019), desired emission reduction outcomes (DEROs) for particular sectors, company-level carbon budgets, and regulatory standards and controls for specific GHG pollutants and emitters (USAID, 2015).

One of the prominent research areas in South Africa, is the conversion of CO_2 to valuable products. The sections to follow detail the literature surrounding CO_2 hydrogenation to valuable products.

2.4. The production of methanol

MeOH is a colourless, volatile and flammable organic compound. Although it is considered to be a toxic chemical, MeOH has become essentially integrated into much of our everyday lives, with it being used extensively in the production of everyday products such as certain shampoos and plastics. Other products for which MeOH is utilized as a feedstock include acetic acid and formaldehyde, which in turn are used in the production of adhesives, foams, solvents and windshield washer fluid (Leonzio, 2018).

Furthermore, MeOH is an alternative, cleaner source of energy. In 2006, 23% of the global methanol produced was used in energy-related applications. By 2015, this had increased to 36%, reaffirming the focus being placed on introducing methanol into the energy mix (IHS Chemical, 2015). MeOH can be used on its own as a vehicle fuel or blended directly into gasoline to produce a high-octane, efficient fuel with lower emissions than conventional gasoline (Leonzio, 2018).

Direct-methanol fuel cells are unique in their low temperature, atmospheric pressure operation, allowing them to be miniaturized to an unprecedented degree (Olah, 2005). Combined with the relatively easy and safe storage and handling of MeOH, this may open the possibility of fuel cell-powered consumer electronics, such as laptop computers and mobile phones (Olah, 2005).

Prior to 1998, the most popular method for MeOH synthesis was through the use of a ZnO-supported Cu catalyst, which was promoted by Al_2O_3. An investigation conducted in 1998 aimed to enhance the performance of the copper/zinc/alumina catalyst by adding palladium. The CZA catalyst had a nominal composition of 55:30:15, in the atomic ratio of Cu:Zn:Al, and was prepared through co-precipitation (Cabrera et al., 1998).

The reaction was performed at an overall pressure of 40 bar, and with reaction temperatures ranging from 433 K to 473 K. The incorporation of Pd to the base Cu/ZnO(Al_2O_3) catalyst enhanced the CO_2 conversion and selectivity to MeOH at all temperatures and time points

along the reaction process. Palladium, however, is a rare, expensive transition metal, making its use in such processes extremely costly (Cabrera et al., 1998).

MeOH can be synthesized via the reverse water gas shift (RWGS) reaction, by means of Equation (1) and Equation (2) (Van der Ham et al., 2012).

$$CO_2 + H_2 \leftrightarrow CO + H_2O \quad (1)$$

$$CO + 2H_2 \leftrightarrow CH_3OH \quad (2)$$

In the investigation conducted by Van der Ham et al. (2012), the CO_2 feed stream was first purified through the use of a monoethanolamine (MEA) scrubbing system, with the H_2 feed being purified by a membrane system. The hydrogenation of CO_2 can be completed in one of two mechanisms, either by direct synthesis where both reactions occur simultaneously within the same reactor unit, or by indirect synthesis where two reactors are utilized; one for each reaction. This investigation utilized a single reactor unit operation.

The reactor utilized in the system was a fluidized bed membrane reactor, equipped with a $Cu/ZnO/Al_2O_3$ catalyst. Zeolite membranes were present to remove the MeOH, resulting in a shift in the equilibrium of the reaction and promoting the production of MeOH to a larger extent. One of the main concerns, however, was the deactivation of the catalyst, caused by both the water produced in the reaction, as well as the exothermic nature of the reaction. Based on this, a wall-cooled fluidized bed reactor was selected with the advantage being that the catalyst can easily be removed and regenerated (Van der Ham et al., 2012).

In the final design, 15.4 kt/y of CO_2 was needed in order to produce 10 kt/y MeOH. Although this was a significant reduction in the CO_2 levels, the process was not deemed to be economically feasible in 2012 and was unable to turn over a profit. This plant could be revisited in the future, when there are more technological advancements in this area of research, or when the price of MeOH has increased enough to deem the process economically feasible.

However, in order to determine how to optimize this reaction further, reaction kinetics were required. The production of MeOH via the RWGS reaction is termed the CAMERE process. Joo (n.d) looked into this reaction kinetics, deeming that the main limiting factor of the conversion of CO_2 to MeOH, were in the conditions experienced in the RWGS reaction (Joo, n.d).

All of the kinetic equations published on the RWGS reaction were obtained over copper containing catalysts at low temperatures (Joo, n.d). Joo investigated the kinetics related with a commercial Fe_2O_3/Cr_2O_3 (Fe:Cr = 9:1 in molar ratio) catalyst, specifically looking at the RWGS reaction. This experiment was conducted in a tubular catalytic reactor, with the reaction pressure being maintained at 1 atm, and the temperature ranging between 670 K and 823 K. The catalyst over feed ratio (W/F) ranged between 0.05 and 3.7 g-cat.hr/mole of CO_2 in the feed. Using these conditions, Joo (n.d) was able to derive the following reaction kinetics:

$$r = \frac{\frac{P_{CO2}P_{H2}}{P_{CO}} + \frac{P_{H2O}}{K}}{\frac{1}{K_1 k} + \frac{P_{CO2}}{kP_{CO}}} \quad (3)$$

In Equation (3) the rate of reaction (r) was calculated using the partial pressure of the reaction components (P_{CO2}, P_{H2}, P_{CO}, P_{H2O}), the reaction rate constant (k) and the equilibrium constant (K). Joo (n.d) also noted that by constantly removing the water from the RWGS reaction, the equilibrium was readjusted. As a result, the amount of recycled gas in the CAMERE process was decreased by four times. The major concern with this research was the lack of detail provided. For example, even though a reaction rate equation had been given, there was no indication as to the kinetic parameters used or the manner in which this equation was derived.

Hong (2013) noted that during the production of MeOH through CO_2 hydrogenation, heterogeneous catalysis was generally applied, as homogeneous catalysis uses Ru, a rare transition metal, thereby increasing the cost of the process (Hong, 2013).

The CHEMIK company (2014) also looked into the production of MeOH via the RWGS reaction. This research found that the cost of a process that utilizes only CO_2 as a feed reactant was deemed to be much more expensive than a feed stream that contains a CO_2/CO mixture. Many of the catalysts used are specific to the hydrogenation of CO and deactivate under large amounts of CO_2. As a result, numerous case studies are being dedicated to improving the efficiency of a catalyst for CO_2 hydrogenation (CHEMIK, 2014).

One of the catalysts receiving a lot of focus, is the Cu/ZnO (70:30) catalyst with the addition of promoters, to increase the surface area, thermal stability, and selectivity within the reactive system. Research conducted by Maria et al. (2014) at CHEMIK, looked into the enhancement of this catalyst using various promoters. During this investigation, a tubular flow, high pressure, fixed bed reactor was utilized, with catalyst particles ranging from 0.8 to 1.0 mm in diameter. The reaction temperature for this investigation ranged between 433 K and 513 K, with pressure

being maintained throughout the investigation. The feed ratio of H_2 to CO_2 was 3:1, with 12 mol% of inert nitrogen (CHEMIK, 2014).

This investigation yielded the following results (CHEMIK, 2014):

- The addition of Cr and Pd to a Cu/Zn/Zr catalyst improved the catalyst surface area, however, the copper active area was at its highest when using Cr and Ga as the promoters.
- The best selectivity was found to occur with the palladium promoter, however, should a high temperature range be used, gallium was the preferred promoter.
- The highest MeOH yields at low temperatures were obtained with La, Cr or Ce promoters.

Jadhav et al. (2014) conducted a review of all recent studies in MeOH synthesis. One such study looked into the production of MeOH from natural gas (NG) through the syngas route, which involves steam reforming of CH_4 to produce a syngas mixture. The syngas was then converted to MeOH at operating temperatures ranging from 250°C to 300°C, and at pressures ranging between 5 and 10 MPa. The following reactions were expected to occur within this system:

$$CH_4 + H_2O \leftrightarrow CO + 3H_2 \quad (4)$$

$$CH_4 + 2H_2O \leftrightarrow CO_2 + 4H_2 \quad (5)$$

$$CO_2 + 3H_2 \leftrightarrow CH_3OH + H_2O \quad (6)$$

$$CO + H_2O \leftrightarrow CO_2 + H_2 \quad (7)$$

$$CO + 2H_2 \leftrightarrow CH_3OH \quad (8)$$

Unfortunately, the conversion of CO to MeOH was generally limited at around 20% for commercial application, and therefore, this would need to be looked into in order to optimize the process (Jadhav et al., 2014).

The methanol economy proposed by Olah et al. (2014) aimed to utilize the CO_2 captured from various processes, in order to create MeOH in a carbon neutral cycle. This implies that the carbon produced or unreacted within the system would be recycled back as a feed into the system, thereby allowing for the process to have no net CO_2 emissions. This was a vital concern, as the MeOH production plant could only be deemed as being environmentally benign

if it was able to utilize more CO_2 than that which was produced during the manufacturing process (Jadhav et al., 2014).

The thermodynamics for MeOH production from H_2 and CO_2 are not as favourable as those for production of MeOH from H_2 and CO. For example, the equilibrium yield of MeOH from CO_2 at 200◦C is slightly less than 40%, whereas the yield from CO is greater than 80%. $CuO/ZnO/Al_2O_3$ catalysts, which facilitate MeOH production from syngas, exhibit poor activity for CO_2 hydrogenation at low temperatures, i.e. less than 250◦C. An increase in temperature, however, facilitates the activation of CO_2. Unfortunately, such high temperatures promote the RWGS reaction and results in the production of CO and water (Jadhav et al., 2014).

According to Mahajan and Goland (2003), approximately 30 MPa pressure was required to achieve high CO_2 conversions, i.e. greater than 80%, at 125ºC. Cu, Zn, Cr, and Pd catalysts are commonly used to minimize by-product formation, i.e. hydrocarbons, and maximize MeOH yield and selectivity. There are many research groups looking into the possibility of merging the reactor and separation unit into a single unit operation. This will allow for the product to be constantly removed from the system, thereby constantly readjusting the equilibrium within the reactor, thus promoting the formation of MeOH as the main product (Jadhav et al., 2014).

The thesis put forward by Arthur Vanhove (2015) looked at further optimizing an existing MeOH production plant using Aspen Plus ® software. The following conclusions were noted in this optimization investigation (Vanhove, 2015):

- In order to decrease the amount of electricity that was utilized by the plant, the number of compressors within the system could be increased. As opposed to having a single compressor going from 1 bar to 300 bar, multiple compressor units could be utilized with smaller pressure step ups.
- The cooling requirements of the heat exchangers could also be optimized by running the water used in one heat exchanger through another, in an integrated loop, thereby reducing the water requirements of the process. This is especially important in the current times of water crisis.
- Recycle streams could also be used to improve the process and reduce wastage.

Gaikwad et al. (2016) investigated the synthesis of MeOH via the direct hydrogenation of CO_2 as well as the indirect RWGS mechanism. This reactive system occurred by means of Equation (9), (10) and (11) (Gaikwad et al., 2016).

$$CO_2 + 3H_2 \leftrightarrow CH_3OH + H_2O \quad (9)$$

$$CO_2 + H_2 \leftrightarrow CO + H_2O \quad (10)$$

$$CO + 2H_2 \leftrightarrow CH_3OH \quad (11)$$

The direct hydrogenation of CO_2 to MeOH is exothermic; however, the water gas shift reaction is an endothermic reaction. Therefore, in order to favour MeOH production in this reactive system, low temperatures and high pressures are required. However, in order to reduce the pressures required, a highly active, and economic, Cu-ZnO based catalyst was utilized (Gaikwad et al., 2016).

The investigation, conducted by Gaikwad, et al. (2016) in Barcelona, looked into various factors that could affect the hydrogenation of CO_2 to MeOH over a $Cu/ZnO/Al_2O_3$ catalyst. The experiment was performed in a fixed bed reactor and utilized an 8 mol% argon composition in the feed stream. The following results were noted from this experiment (Gaikwad et al., 2016):

- An increase in pressure increased the conversion of CO_2 and the selectivity to MeOH.
- An increase in temperature resulted in a rapid decrease in the MeOH selectivity.
- An increase in the flowrate resulted in a decrease in both the conversion and the selectivity. This was due to the fact that the contact time between the surface area of the catalyst and the reactants decreased. Increasing the flow rate also decreased the residence time.
- Smaller catalyst particles were found to increase the conversion and the selectivity, due to the increased surface area.

These results were later verified by Hus et al. (2017), who conducted experiments to also show that an increase in temperature compromises on MeOH selectivity, due to the RWGS reaction (Hus et al., 2017).

A further investigation conducted by Fan and Wu (2016), looked at the use of reduced graphene oxide (rGO) as the novel support for copper-based catalysts. This experiment was completed using a fixed bed reactor, and CZZA catalyst – comprised of 20 wt% $CuO\text{-}ZnO\text{-}ZrO_2\text{-}Al_2O_3$ (CZZA) and 80 wt% GO. The CZZA catalyst has a ratio of 4/3/1.5/1.5. The reactor unit utilized was a single column stainless steel reactor, with a back-pressure regulator, in order to control the reaction pressure and condense the water and MeOH being produced (Fan & Wu, 2016).

The following conclusions were drawn by Fan and Wu (Fan & Wu, 2016):

- The addition of the rGO to the CZZA catalyst drastically increased the surface area of the catalyst.
- The H_2 and CO_2 adsorption properties of catalysts depend on the surface area and Cu dispersion, which affects the CO_2 conversion.
- The MeOH production was reduced upon an increase in temperature, as was expected in the case of an exothermic reaction.
- The CO_2 conversion and MeOH selectivity increased with an increase in pressure.
- An increase in the space velocity caused a decrease in the conversion and selectivity, mainly due to the lower contact and residence times.

The main shortcoming of this research was the catalyst composition. The catalysts utilized in the investigation had a composition of 20 wt% CZZA and 80 wt% rGO. Unfortunately, there was no indication in this research article as to how this composition was arrived at, and also the effect that the varying of rGO would have on the catalyst cost and the activity of the catalyst.

The research conducted by Bellotti et al. (2017) showed that it was possible to isolate the direction hydrogenation of CO_2 to MeOH via the following reaction:

$$CO_2 + 3H_2 \leftrightarrow CH_3OH + H_2O \quad (12)$$

The hydrogenation of CO_2 to MeOH occurs over a $CuO/ZnO/Al_2O_3$ (CZA) catalyst, at a temperature of between 250 – 300°C and a pressure ranging from 50 to 100 bar. At these operating conditions, Bellotti et al. (2017) reported a 96% conversion of CO_2 to MeOH.

Bellotti et al. (2017) looked at the feasibility of a German methanol production plant, employing the reaction shown in Equation (12). The most important parameters looked at during the feasibility study was the effect on Net Present Value (NPV) and the Discounted Pay Back Period (DPBP). DPBP is the time required, after start-up, to recover the fixed capital costs required for a project with all cash flows discount back to time zero. The CO_2 utilized in this plant was obtained from a power plant, and therefore, did contain trace amounts of other impurities, the nature of which was not explicitly stated in the study (Bellotti et al., 2017).

This feasibility study found that as the production rate of the plant begins to increase, the capital cost of the plant per ton of MeOH decreases significantly (Bellotti et al., 2017). Therefore, large plants proved to be the most feasible, even though they required the largest capital investment. This resulted in a lower DPBP. Furthermore, Bellotti et al. (2017) found that the

sale of oxygen, a by-product produced during the electrolysis process, is mandatory for the plant to be profitable, as the most expensive part of the plant was deemed to be the Proton Exchange Membrane (PEM) electrolyzer unit.

Unfortunately, this study did not account for the unit operations that were involved in the purification of the CO_2 that was needed in order to operate the plant. Furthermore, the cost of electricity, inflation rate, and income tax were deemed to be constant over the entire 15-year lifespan of the plant. This is highly unlikely and should be revised in future studies of this nature. It is possible that these changes could drastically affect the NPV and DPBP of the plant, and may even result in a lower feasibility than was determined within this study.

In 2017, the first pilot plant for MeOH production was constructed in Japan and had a production rate of 50 kg/hr of MeOH. This plant employed a SiO_2-modified CuO/ZnO catalyst, with the unreacted feed, i.e. CO_2 and H_2, being recycled back into the process. A MeOH selectivity of 99.9% was achieved in this plant, after monitoring the plant for around 8000 hours of operation, during which the operating conditions were set at 250^oC and 5 MPa (Tursunov et al., 2017).

Kar et al. (2018) derived a four-factor criterion that needs to be considered, when deciding on the optimal catalyst to be used in a MeOH synthesis pathway. These four criteria are as follows:

- The catalyst should preferentially not contain any noble base metals.
- The catalyst should be able to operate at low temperatures and pressures.
- The catalyst should have a high turnover number (TON) and turnover frequency (TOF).
- The catalyst should have a long lifetime, in order to reduce the costs.

Currently, bulk of the known catalysts for MeOH synthesis utilize ruthenium; however, this is an extremely rare transition metal and should be avoided as a catalyst moment due to its expensive nature. Utilizing a catalyst with ruthenium increases the cost of the catalyst, in turn reducing profits. However, when a $Ru(CO)_{12}$ catalyst was used, it was found that at temperatures below 160^oC, carbon monoxide (CO) was formed. This aids in the MeOH production plant operating at higher temperatures to achieve higher CO_2 conversions (Kar et al., 2018).

2.5. The production of dimethyl ether

DME is a clean, colourless gas that is easy to liquefy and transport. It has remarkable potential for increased use as an automotive fuel, for electric power generation, and in domestic applications such as heating and cooking (Fleisch et al., 2012).

DME can be derived from many sources, including renewable materials, i.e. biomass, waste and agricultural products, and fossil fuels, i.e. NG and coal. DME has been used for decades in the personal care industry, as a benign aerosol propellant, and is now increasingly being exploited for use as a clean-burning alternative to liquefied petroleum gas (LPG), diesel and gasoline (Fleisch et al., 2012).

Like LPG, DME is gaseous at normal temperatures and pressures but changes to a liquid when subjected to modest pressure or cooling. This easy liquefaction makes DME easy to transport and store. This and other properties, including a high oxygen content, lack of sulfur or other noxious compounds, and ultra clean combustion make DME a versatile, promising solution in the mixture of clean, renewable and low carbon fuels under consideration worldwide (Fleisch et al., 2012).

MeOH production plants typically use NG as their feedstock, with the production of DME being the dehydration of MeOH. The investigation conducted by Matzen and Demirel (2016) in the United States of America utilized Aspen Plus ® software to conduct a life-cycle assessment for novel MeOH and DME production. The life cycle assessment looks at the activities in the course of a product's life.

The production of DME generally occurs over alumina-based catalysts, in a fixed bed reactor, at a temperature and pressure of 250-400°C and 25 bar respectively. The selectivity of this reaction is usually extremely high with small amounts of formaldehyde being formed (Matzen & Demirel, 2016).

$$2CH_3OH \rightarrow CH_3OCH_3 + H_2O \quad (13)$$

The assessment conducted by Matzen and Demirel (2016) used the CO_2 that was produced from a biomass fermentation process, and the H_2 supplied by a wind-powered water electrolysis process. The MeOH that is formed in the initial stages of this process will either be converted into DME or used directly as a fuel.

The 4.1 kWh/Nm^3 electrolyzer unit utilized, was able to produce 485 Nm^3/hr of H_2 gas. The main ratios that were looked at in this analysis were the fossil fuel energy ratio (FER) and the carbon fixation fraction (CFF) (Matzen & Demirel, 2016). The FER is the ratio of the energy that is able to be obtained from the MeOH and DME produced, to the energy utilized in the production of MeOH and DME. Ideally, this ratio should be greater than 1 for a process to be deemed viable. The CFF is the fraction of carbon that is converted into organic products, i.e. MeOH and DME, and is an indication of the conversion of CO_2 achieved in the process.

MeOH showed higher metrics in FER and CFF, due to the heating requirements of the DME columns in the production stage of this process, leading the MeOH production to be deemed more efficient and economical than the production of DME (Matzen & Demirel, 2016).

The concern with the DME plant is that formaldehyde is a known carcinogen and is the by-product of the DME production facility. Even after waste treatment, the effects of the formaldehyde are quite substantial and therefore is a major risk factor when designing such a process (Matzen & Demirel, 2016).

Both fuels, MeOH and DME, have lower energy densities than typical petroleum fuels, which would require minor changes or adjustments to current combustion engines. The minor modifications required would be built from the existing infrastructure and could possibly be a cheaper and more feasible option than building from scratch, allowing these petrochemicals to be easily introduced into our current energy systems in the future (Matzen & Demirel, 2016).

2.6. The production of formaldehyde

Formaldehyde is a commonly used feedstock in over 50 different industries, with over 30 million tonnes being produced globally in 2011 alone. Research conducted by Chan et al. (2017), identified two possible routes that can be utilized in the production of formaldehyde, with the main difference lying in the intermediates that exist. For the sake of this literature review, these two routes will be referred to as Route A and Route B and will be explained and detailed in the paragraphs to follow.

Route A involves the hydrogenation of CO_2 into formic acid (HCOOH), before being further hydrogenated to produce formaldehyde and water. This occurs by means of the following reactions (Chan et al., 2017):

$$CO_2 + H_2 \leftrightarrow HCOOH \qquad \Delta G = -3.17\ kJ/mol \qquad (14)$$

$$HCOOH + H_2 \leftrightarrow HCHO + H_2O \qquad \Delta G = 8.09\ kJ/mol \qquad (15)$$

Route B, on the other hand, employs the RWGS reaction, leading to the same overall reaction experienced in Route A, but having the following intermediate reaction steps (Chan et al., 2017):

$$CO_2 + H_2 \leftrightarrow CO + H_2O \qquad \Delta G = 12.54\ kJ/mol \qquad (16)$$

$$CO + H_2 \leftrightarrow HCHO \qquad \Delta G = -7.62\ kJ/mol \qquad (17)$$

Gibbs Free Energy is an indication as to the spontaneity of the reaction, with a negative value representing a spontaneous reaction and a positive value representing a non-spontaneous reaction. Focusing solely on the Gibbs Free Energy values of each sub-reaction, Route A has its first step being spontaneous, whereas Route B has its second step being spontaneous (Chan et al., 2017).

The catalyst utilized in this experiment was an alumina catalyst, that was either supported by Cu or Ni and promoted using Pt or Ru. Furthermore, the experiment conducted by Chan et al. (2017), occurred in a batch reactor for 22 hours at a temperature and pressure of 298 Kelvin and 70 bar respectively. This research focused on the feasibility of Route A, and was able to conclude the following:

- A Pt-Cu catalyst was found to be approximately three times more effective than a Pt-Ni catalyst.
- The effectiveness of the catalysts over the 22-hour period was given as Pt-Cu>Pt-Ni=Ru-Ni>Ru-Cu.
- An increase in the H_2 to CO_2 ratio increased the yield of formaldehyde.

The main concern with this research was noted during the analysis of the experimental data. Although a significant amount of formaldehyde was formed, there was almost no formic acid detected. This resulted in Chan et al. (2017) concluding that there is a 100% selectivity in this experiment. However, there was some confusion regarding the actual route that was

investigated in this experiment, and whether or not it was actually Route B that was being investigated instead of Route A.

However, in subsequent experimental runs, where formic acid was produced as the intermediate, it was noted that the formic acid being produced was less than the amount of formaldehyde that was being produced. This implies unwanted products also being formed, thereby nullifying the statement made by Chan et al. (2017) that there is a 100% selectivity in this experiment.

2.7. The production of methane

Methane (CH_4) can be produced through the direct hydrogenation of CO_2, via a biochemical process, and with the use of a catalyst. The bacteria that is utilized in such a process is hydrogenotrophic methanogenic archaea. These are generally utilized in conventional biogas digesters or fermenters at sewage treatment plants (Burkhardt & Busch, 2013).

The biological process by which to produce CH_4 from CO_2 and H_2 is an anaerobic process, i.e. occurs without oxygen, and occurs at an optimal pH of 6.8-7.2. A sufficient amount of nutrients must also be present for the bacteria to operate. Furthermore, these microorganisms are extremely sensitive to temperature, with their optimum operating temperature lying in the mesophilic range (37°C) or thermophilic range (55°C). The methanation reaction occurs by means of the following equation (Burkhardt & Busch, 2013):

$$4H_2 + CO_2 \rightarrow CH_4 + 2H_2O \quad (18)$$

Research conducted by Burkhardt and Busch (2013) utilized a trickle bed bioreactor as opposed to a fixed bed reactor, due to an increase in the residence time. A higher residence time often leads to better conversions. The results that were able to be drawn from this experiment were as follows:

- Almost full conversion to CH_4 was able to be achieved, with the concentration of the H_2 reactant decreasing by 94-99% within the first 2.25 hours of the residence time.
- In a fixed bed reactor, the retention time was too low, and therefore a residence time of 4 hours was needed to achieve the same conversion as the trickle bed reactor.

- This is a more economically feasible approach than the Sabatier reaction, as it does not require an expensive catalyst.
- As opposed to feeding gases into the system, liquid or solid waste can be fed into the system.

Unfortunately, the research conducted by Burkhardt and Busch (2013) did not look at how the presence of impurities would affect the conversion to methane.

Burkhardt et al. (2015) furthered their research, by investigating the possibility of adding a hollow membrane to the trickle bed reactor system. The aim of adding this membrane was to cause a more efficient distribution of gases in the reactor unit, subsequentially increasing the conversion of the system. This investigation was conducted under anaerobic conditions and utilized an 88 litre, trickle bed reactor. The system was operated under mesophilic temperatures (37^oC) and ambient pressures. The reactor system was subjected to a pH of between 7.2 and 7.4, with the H_2 to CO_2 ratio being maintained as the stoichiometric ratio of 4:1 (Burkhardt et al., 2015).

By allowing the bioreactor to have a residence time of 4 hours, an almost complete conversion of H_2 was achieved, with the CH_4 purity stream being around 98%. This was a continuous process, with no recycle stream. It was found that traces of contaminants did not affect the system; however, it was necessary that these contaminants be removed before the CH_4 is put into storage. To reach that variety of methanogens, anaerobic sludge of a local sewage plant was used as the inoculum. Therefore, archaeal species like Methanococcus spp., Methanobacterius spp., Methanomicrobium and also Methanosaeta spp. could be confirmed (Burkhardt et al., 2015).

Later that year, Alitalo et al. (2015) also looked into the biological production of methane, via methanogenic archaea micro-organisms. This process is known as biological methanogenesis. In order to build on the work conducted by Burkhardt et al. (2015), this investigation aimed to investigate the effect of agitation on the system, as well as the implementation of a recycle stream (Alitalo et al., 2015).

Due to the low solubility of gases, especially H_2, an efficient supply of gases to the micro-organisms was a decisive factor in this process. Mechanical agitation, or stirring, is the most common means by which to enhance the transfer of gases and other substances in the bioreactor. However, agitation consumes high amounts of energy, thereby increasing operating costs (Alitalo et al., 2015).

Experiments conducted by Alitalo et al. (2015) in Finland, utilized two bioreactors in series – each having a capacity of 2 litres. The H_2 utilized in the system was produced using a PEM electrolyzer, with the total reactor system having a residence time set at 144 hours.

The following observations were noted throughout the course of this investigation:

- The CH_4 production rate from the reactor was approximately 4.64 litres of CH_4 per litre of reactor volume, per day.
- A decrease in the H_2 entering the reactor system resulted in a decrease in the conversion to below 20%.
- The addition of a recycle stream, with small amounts of sodium sulfide and ammonium carbonate, increased the productivity to 6.3 litres of CH_4 per litre of reactor volume per day.
- Despite the larger size of the reactor, blockage of the granular support by excess cell mass was observed with time. Thus, the information obtained can hardly be used for modelling and scale-up of biological CH_4 production.

The addition of sodium sulfide in the recycle stream, to increase productivity, could prove to be disadvantageous as well, as it results in the production of hydrogen sulfide, by means of the following reaction (Alitalo et al., 2015):

$$Na_2S + 2H_2O + CO_2 \rightarrow Na_2CO_3 + H_2S \tag{19}$$

This process does show that CH_4 can be produced from biological processes, with minimal agitation, however, there were two major concerns with this process. The first concern was the production of hydrogen sulfide, which is extremely poisonous. The second concern was with the scale-up of the plant, which does not seem to be possible at this stage (Alitalo et al., 2015).

Moving away from the biological production of methane, Miguel et al. (2015) investigated the direct hydrogenation of CO_2 to MeOH and methane from post-combustion exhaust streams. This reactive system occurs by means of the following two chemical equations:

$$CO_2 + 4H_2 \leftrightarrow CH_4 + 2H_2O \tag{20}$$

$$CO_2 + 3H_2 \leftrightarrow CH_3OH + H_2O \tag{21}$$

Looking at these stoichiometric equations, it can be seen that the MeOH production pathway utilizes less H_2. Furthermore, MeOH has a higher energy density. However, the production of

CH_4 could be beneficial as it will allow for the product to be transported and utilized in the current NG infrastructure (Miguel et al., 2015).

The investigation conducted by Miguel et al. (2015), in Portugal, aimed to determine the effect of pressure, temperature, H_2 to CO_2 feed ratio, and the presence of impurities, on the conversion, yield, and selectivity of the system. This analysis was completed using the Aspen Plus ® simulation software and employs the Soave-Redlich-Kwong (SRK) equation of state.

During this investigation, only the two reactions detailed above were considered, with all other side reactions being completely disregarded. The following conclusions were drawn from this simulation (Miguel et al., 2015):

- An increase in pressure results in an increase in the conversion of CO_2.
- In order to produce MeOH, the feed stream is required to be compressed quite considerably, whereas, in the production of CH_4, this conversion can take place at atmospheric pressures.
- Focusing solely on the CH_4 reaction, the conversion decreased with an increase in temperature.
- The conversion of CO_2 to CH_4 increased when increasing the H_2 to CO_2 feed ratio.
- The presence of water in the feed stream decreased the equilibrium conversion.
- The presence of oxygen in the feed stream also significantly decreased the conversion, due to the presence of side reactions occurring in the system.

The main concern with the methanation process was that water needed to be constantly removed from the system, in order for the equilibrium to readjust and favour the production of CH_4 (Miguel et al., 2015).

Hashimoto et al. (2016), looked at the production of H_2 gas via seawater electrolysis, before then catalytically reacting this H_2 with CO_2 in the production of methane. This research was able to highlight the following conclusions:

- With the use of a Ni-Fe-C alloy cathode and a MnO_2 anode, only 8% of the electricity consumed produced chlorine at the anode, with the rest of the electricity being used in the production of H_2, at the cathode, and oxygen, at the anode.
- Using a Ni-0Zr catalyst, a rapid conversion with complete selectivity was noted for the hydrogenation of CO_2 to CH_4. This selectivity occurred at temperatures of 100^oC and above.

Unfortunately, this research does not look into the effect that pressure will have on the system, nor does it specify a pressure at which the investigation was conducted, thereby leaving a lot of room for uncertainty. Furthermore, the investigation looked at 'pure' seawater, i.e. not containing any impurities. This investigation did not consider other possible impurities that may exist in seawater and how these will be filtered out before entering the electrolysis unit.

Zamani and Abdullah (2018) noted that the main concern in the methanation process is the high operational cost and the high H_2 gas consumption. In order to address the high levels of H_2 gas required, Zamani and Abdullah (2018) aimed to investigate the possibility of producing hydrogen by means of aluminium and an alkaline solution.

This reaction occurred in the presence of sodium hydroxide (NaOH) and aluminium was extracted from recycled materials such as soft drink cans. As an additional benefit to this approach, the by-product ($Al(OH)_3$) could be used in various wastewater treatment processes, as well as in the pharmaceutical industry. One gram of aluminium is able to generate 1.2 litres of H_2 gas at ambient temperatures. This occurred by means of the following reaction system (Zamani & Abdullah, 2018):

$$Al(s) + 3H_2O(l) \xrightarrow[NaOH]{} Al(OH)_3(l) + 1.5\, H_2(g) \quad (22)$$

$$CO_2(g) + 4H_2(g) \rightarrow CH_4(g) + 2H_2O\ (l) \quad (23)$$

The reaction was optimized by means of the H_2 to CO_2 ratio (X_1), catalyst weight loading (X_2), and the reaction temperature (X_3). The following equation was developed based on the experimental data obtained, and is able to determine the predicted CO_2 conversion, using these three parameters (Zamani & Abdullah, 2018):

$$Y = 91.32 + 7.53X_1 + 7.25X_2 + 32.80X_3 - 11.20X_1X_2 + 4.25X_1X_3 - 0.25X_2X_3 \quad (24)$$

Comparing the experimental data individually, led to the following conclusions being drawn from this research (Zamani & Abdullah, 2018):

- The temperature was the most influential parameter in the CO_2 conversion, followed by the H_2 to CO_2 ratio and lastly the catalyst weight.
- As temperature increased, so did CO_2 conversion.
- An increase in the catalyst weight and feed ratio also increased CO_2 conversion, with the optimal ratio being 4.2.

- The differences between the predicted and observed values was 2.99%, which was deemed insignificant, as the observed values were within the 5% level of significance.

2.8. The production of formic acid

One of the most limiting factors to a hydrogen-based economy is the problems that are associated with the storage of H_2. Formic acid has proven to be a promising molecule for H_2 storage, with it containing 4.4 wt% H_2 and a flash point of 69°C. This is much higher than that of gasoline. Furthermore, the hydrogenation of CO_2 to formic acid is fast, but controllable, with the concern in this reaction lying in finding an efficient manner to catalyze the reaction (Laurenczy & Dyson, 2014).

The research conducted by Laurenczy and Dyson (2014), found that the production of formic acid was usually catalyzed using a homogeneous catalyst in an aqueous solution. This reaction was found to be highly sensitive to the pH levels of the solutions, with a direct proportionality relationship existing between the pH, conversion and reaction rate. The dissolution of the gases to form an aqueous solution decreases the Gibbs Free Energy of the reaction significantly, with the addition of a base being able to decrease the Gibbs Free Energy even further. This can be seen in the following chemical equations (Laurenczy & Dyson, 2014):

$$CO_2(g) + H_2(g) \rightarrow HCOOH\ (g) \quad \Delta G = 32.9\ kJ/mol \tag{25}$$

$$CO_2(aq) + H_2(aq) \rightarrow HCOOH\ (aq) \quad \Delta G = -4\ kJ/mol \tag{26}$$

$$CO_2(aq) + H_2(aq) + NH_3(aq) \rightarrow HCOO^-_{(aq)} + NH_4^+(aq) \quad \Delta G = -35.4\ kJ/mol \tag{27}$$

If a ruthenium catalyst is utilized in the above reaction, the need for a base is decreased. Unfortunately, this is a rare transition metal and will cause a significant increase in the cost of the process. The homogeneous catalytic decomposition of formic acid in aqueous solutions provides an efficient in situ method for H_2 production, that operates over a wide range of pressures, under mild conditions, and at a controllable rate (Laurenczy & Dyson, 2014).

Research conducted by Zargari et al. (2017) in the United States of America, also looked at the hydrogenation of CO_2 to formic acid, however, this research incorporated the use of an NHC-Amidate Pd (II) complex, in addition to the bases used in 2014.

The following conclusions were drawn from this investigation (Zargari et al., 2017):

- At equal reactant pressure, i.e. 10 atm, of CO_2 and H_2 gas were stirred at 160^oC for 3 hours, 32.2 µmol of formic acid was produced as the major product, while MeOH and formaldehyde were produced in trace amounts, less than 0.5 µmol. It is important to note, however, that this initial experiment was conducted in the presence of 5 µmol of an alkaline aqueous solution.
- The catalyst turnover number (TON) of the complex was 6.4. This shows the number of moles of the substrate that a mole of catalyst can convert before becoming inactivate.
- An increase in the reaction temperature resulted in an increase in the TON of the catalyst/reaction system.
- In the absence of any base solution, there was no product being formed. Therefore, KOH needed to be present for the reaction system to begin – thereby confirming the research conducted by Laurenczy and Dyson (2014).
- An increase in pressure also resulted in an increase in conversion.

The major concern of the research conducted in 2017, was found upon analysis of the products being formed within the system. These products contained traces of potassium carbonate, which leads to the possibility that the carbon source that was reacting with the complex was in fact carbonate, and not CO_2, as it was previously thought to be (Zargari et al., 2017). Further research would need to be conducted to determine the validity of this statement.

Roger et al. (2018) looked at the production of formic acid, via the production of formate as an intermediate. However, as opposed to using the catalyzed reactive approach, this research opted to use the ability of living organisms, in order to perform this reaction biologically.

The formate hydrogenlyase (FHL) enzyme from Escherichia coli normally oxidizes formic acid to CO_2 and H_2. However, this research was able to unlock the reverse reaction. During this process, CO_2 and H_2 are placed under a pressure of up to 10 bar, allowing for the conversion of CO_2 to formic acid to be close to 100 % (Roger et al., 2018).

Henry's law states that the amount of gas that is able to dissolve in a solvent is directly proportional to the applied pressure. Therefore, the system put forward was designed bearing in mind the need to regulate the temperature and pH, due to the very condition specific nature of biological production mechanisms. The following conclusions were drawn (Roger et al., 2018):

- An increase in residence time increases the amount of formate that is produced, and also increases the change in pressure in the reactor unit operation. However, due to the increased formation of formic acid, the pH also decreases with time.
- Maintaining the pressure of the gas mixture in the headspace of 10 bar, combined with the fine control of the reaction pH, lead to over 20 times more formate being produced than was produced at ambient pressures.
- The number of cells that are required for optimum formate production decreases significantly under pressure.

The major concern with this research was the reported CO_2 conversion. This research claims that at 10 bar pressure, the CO_2 conversion was approximately 103%. This cannot be physically possible, as the reaction cannot react more CO_2 than was taken into the system.

Another system of importance that should be noted, was detailed in Germany in 2012. Although many years before the above-mentioned research, a German research group noted that the major concern with the production of formic acid was that the equilibrium of the reaction heavily favours the reactants. Therefore, the formic acid would need to be constantly removed from the system, in order to increase its productivity by readjusting the equilibrium of the reaction (Wesselbaum et al., 2012).

The journal Angewandte Chemie aimed to address this concern through the utilization of CO_2 as a reactant, and in its supercritical state, allowing for solvent separation. A team led by Walter Leitner developed a continuous process by which they were able to integrate the reaction and separation steps into a single unit operation. Supercritical CO_2 flows through the reactor at 74 bar and 31°C, and selectively removes the formic acid from the mixture, allowing the product to be constantly flushed from the reactor unit operation (Wesselbaum et al., 2012).

The concern with this dual unit operation system was that it was only able to operate stably for approximately 200 hours. It is necessary to delve deeper into optimizing the lifespan of this unit operation, as this method could be extremely useful in overcoming thermodynamic restrictions that are in place during the hydrogenation of CO_2 to formic acid (Wesselbaum et al., 2012).

2.9. The production of formate

There are many processes, especially in the Germany and Iceland region that employ the RWGS reaction, in order to curb the detrimental effects of CO_2 on the environment. By using this reaction pathway system, CO_2 can be converted to CO, which can then be further hydrogenated in order to make fuels such as MeOH, DME and CH_4. The RWGS reaction is generally employed as the first step in many CO_2-based reactions, as CO is more reactive than CO_2 (Watari et al., 2017).

Homogeneous catalysts are generally based on transition metals and are used to perform selective reactions under mild conditions. Nozaki et al. (2009) began their research to develop a homogenous catalyst that could produce formate using CO_2 and H_2 as the feed. Through this research, they were able to develop an iridium complex that created formate (CHOO-) with a TON of 3,500,000. This catalyst operated at pressures of approximately 60 atm, and temperatures up to 120^oC. The H_2 to CO_2 ratio utilized during this investigation was a 1 to 1 ratio (Watari et al., 2017).

Watari et al. (2017) then picked up this research, looking at the hydrogenation of CO_2 over a Cu/1,8-Diazabicyclo[5.4.0]undec-7-ene (DBU)/bidentate ligand catalyst system. These experiments found that the addition of any nitrogen bidentate ligand was able to improve both the conversion and the TON of the catalyst, due to its electronic properties. However, further research needs to be conducted into the use of copper catalysts in this reaction, as copper is a relatively cheap metal.

Zhao et al. (2018) explored the possibility of not feeding hydrogen gas into the system, but rather using a hydrogen donor in the reactive system. The use of the hydrogen donor was explored as a cheaper alternative as hydrogen donors are much cheaper than electrolysis units. Furthermore, hydrogen donors are reactive materials that are involved in the reaction, whereas electrolysis involves separate unit operations. Therefore, the cost of electrolysis is also increased by factors such as equipment purchases and maintenance.

Based on the research that was conducted by Zhao et al. (2018), potassium borohydride was found to be a better hydrogen donor than sodium borohydride. This conclusion was reached upon analysis of their costs and stability, as potassium borohydride is cheaper and has a higher stability in water. Furthermore, this research looked at the hydrogenation of CO_2 at low

temperatures and atmospheric pressures, using potassium borohydride as the hydrogen donor. The results of this investigation were as follows (Zhao et al., 2018):

- Any impurities in the CO_2 reactant stream, i.e. NOx and oxygen, had no significant impact on product formation. This shows no competition or inhibition taking place by these impurities.
- An increase in the concentration of potassium borohydride resulted in an increase in the conversion.
- High temperatures were used to increase molecular diffusion, however, above 50^oC the conversion decreased, due to the lower CO_2 stability.

This research, however, has two major shortcomings or concerns that need to be addressed. The first of these concerns is the regeneration of potassium borohydride. This is an energy-intensive process, thereby increasing the cost of the process. Secondly, it is important to note that this investigation was conducted on a small scale, with a homemade reactor unit operation, and therefore, the validity of these results in an industrial application cannot be guaranteed.

2.10. The production of hydrocarbons (alkanes and alkenes)

In much of the research geared towards the hydrogenation of CO_2, CH_4 is produced as the primary product. Although a good fuel, this limits the fuel potential of CO_2 hydrogenation. The possible production of higher hydrocarbons from this process has proven to be more beneficial, as they are able to store more energy – acting as a more fuel-efficient energy storage source (Zhanghuai & Yuan, 2000).

Zhanghuai and Yuan (2000) aimed to look at the catalytic activity and the product distribution over TiO_2, ZrO_2, and Al_2O supported iron oxide catalysts. The catalysts were prepared with 5 wt% Fe and set up in a stainless steel, fixed bed microreactor. The H_2 to CO_2 feed flow rate was kept in a molar ratio of 2:1 respectively, with the operating temperatures being tested at both 573 K and 623 K. The pressure of the system was constant, at 1.5 MPa, with the residence time ranging from between two to four hours.

The following conclusions were drawn from this research (Zhanghuai & Yuan, 2000):

- Catalysts with low metal loading usually gave low activities, with poor selectivities to C2+ hydrocarbons.
- When the iron loading was increased to 5 wt%, the catalyst was able to reach its maximum conversion at 17% of CO_2, with a selectivity of 38% to C2+ hydrocarbons.
- A certain amount of CO was detected in the product stream, over all Fe/ZrO_2 and Fe/TiO_2 catalysts. However, the higher the catalyst activity, the better the selectivity to C2+ hydrocarbons, thus lessening the amount of CO produced. This supports the view that CO is an intermediate in the hydrogenation of CO_2.
- Both the ZrO_2 and TiO_2 catalyst promoters showed good catalytic activities and selectivities to C2+ hydrocarbons.
- The best result that was achieved in this experiment was a conversion of 20% with a selectivity 69% to C2+ hydrocarbons, over a 15 wt% Fe/ZrO_2.
- The optimum temperature of a 5 wt% Fe/ZrO_2 was 723 K, which was lower than the optimum temperature of a 5 wt% Fe/TiO_2 catalyst, which is 773 K. This was also economically beneficial, as Zr is cheaper than Ti.

The investigation conducted by Jun et al. (n.d) in Korea, followed a similar approach as that employed by Zhanghuai and Yuan (2000), however, the scope of the investigation was broadened to incorporate the effect of Fe on the catalyst, as well as the effect of potassium (K). This research found that if the potassium content of the iron catalyst was increased, the selectivity to C2+ hydrocarbons also increased significantly (Jun et al., n.d).

The investigation utilized a fixed bed reactor, at a temperature of 573 K and a pressure of 1 atm. The results of the temperature programmed decarburization showed that weak interaction between iron and the support existed with Fe/Al_2O_3 and strong interaction existed with Fe/TiO_2. This led to the conclusion that the use of titanium in the catalyst will lead to a much higher conversion and selectivity towards C2+ hydrocarbons, when potassium was added to the catalyst structure (Jun et al., n.d). However, as with research conducted by Zhanghuai and Yuan (2000), titanium is much more costly than iron, and therefore this economic factor would also need to be considered.

More often than not, the hydrogenation of CO_2 to hydrocarbons and oxygenates occurs in two steps, with the first step being the RWGS reaction, followed by the hydrogenation of CO. This can be referred to as the Fischer Tropsch (FT) process (Zhenya et al., 2013).

Zhenya et al. (2013) aimed to first replicate the results of Zhanghuai and Yuan (2000), as well as Jun et al. (n.d), before moving on to investigate the possible addition of alkali metals into the iron catalysts in order to increase the conversion of CO_2 and the selectivity to olefins. The initial part of the investigation was able to confirm that iron catalysts were not very effective in the FT process, as they are geared towards increasing the selectivity of CH_4 and also deactivate at rapid rates (Zhenya et al., 2013).

Furthermore, the addition of supporters and promoters, such as a K-modified Fe/Al_2O_3 catalyst, i.e. involving the addition of potassium, at 673K, was able to yield CO_2 conversions of approximately 69%, with the C2 – C4 olefin (alkene) selectivity being 40%. In this scenario, the selectivity to CH_4 is suppressed to a mere 20% (Zhenya et al., 2013).

In order to investigate the effect of alkali metal on the conversion and selectivity in this reactive system, Zhenya et al. (2013) utilized a stainless-steel fixed bed reactor, operating at a pressure of 2 MPa and a temperature of 613 K. The feed contained H_2, CO_2, and argon, with a ratio of 69/23/8 respectively. The reaction time was approximately 10 hours (Zhenya et al., 2013). This was the same conditions utilized when confirming the relationships obtained by Zhanghuai and Yuan (2000), as well as Jun et al. (n.d).

The following conclusions were drawn from this investigation (Zhenya et al., 2013):

- Where there was no modification to the Fe catalyst, there was a low activity, with the conversion of CO_2 being 5.6 % at 613 K. Furthermore, there was no olefin formation.
- The addition of alkali metals significantly enhanced the activity for CO_2 hydrogenation.
- The alkali metals were able to suppress the selectivities for CH_4, and paraffin and was able to enhance the olefin selectivity significantly.
- The C2-C4 olefins selectivity increased in the following order: Fe < Li mod < Na mod < Cs mod < K mod < Rb mod. This shows that a catalyst with an alkali metal ion that has a stronger basicity exhibited a more significant promoting effect for the hydrogenation of CO_2 to light olefins.
- Increasing the K value above 10 wt% led to a decrease in CO_2 conversion and yield of olefins.
- The doping of boron with the K modified catalyst was able to further enhance the activity.

The shortcoming of this research was that it was completed at a constant reaction temperature and pressure. Therefore, the activity or operating range of each catalyst was not known. It is possible that at higher temperatures or pressures, that the physical structure of the catalyst may break down or that the catalyst may begin to operate at even higher activities.

Gnanamani et al. (2015) aimed to investigate the effect of cobalt-based catalysts on the FT synthesis process. Under FT synthesis conditions, cobalt has a very low water gas shift activity and acts primarily as a methanation catalyst when CO_2 is used as a feedstock, instead of CO. It is highly desirable to lower the hydrogenation activity of cobalt, such that CO_2 can be converted into higher hydrocarbons - either by first forming CO or partially hydrogenated CO intermediates (Gnanamani et al., 2015).

Owen et al. (2013) was able to show that cobalt has the ability to hydrogenate CO_2 at atmospheric pressure. Through the addition of alkali promoters, like Na and K, the selectivity of C5+ hydrocarbons were greatly enhanced. Gnanamani et al. (2015) utilized a calcined cobalt catalyst that was pre-treated at different conditions, in order to obtain various forms of cobalt. This pre-treatment was dependent on whether the catalyst was set to achieve H_2 activation, syngas activation, or CO activation (Gnanamani et al., 2015).

The experiment was conducted in a stainless-steel fixed bed reactor, with 2.5 grams of calcined cobalt catalyst that was diluted with 10 grams of glass beads. The feed entering the reactor unit operation comprised of 75% H_2 and 25% CO_2, with the reactor temperature and pressure being maintained at 220°C and 1.89 MPa respectively. The following results/conclusions were drawn from this experiment (Gnanamani et al., 2015):

- There was a decrease in the BET surface area from 351 to 247 m^2/g with a loading of 20 wt% Co onto the silica support. Adding 1 wt% sodium altered the BET surface area of the catalyst, which dropped further to 201 m^2/g.
- The catalyst reduced at 350°C, thereby displaying higher initial CO_2 conversions, which then proceeded to decrease from 23.5% to 18.0% within 20 hours of time-on-stream.
- When the sodium promoted cobalt catalyst was pre-treated with H_2, the selectivity of CH_4 was extremely high, lying within the range of 70% to 80% of the total CO_2 converted.
- By utilizing CO in the pre-treatment phase, the selectivity of CH_4 was found to decrease significantly, to a range of between 8% and 16%, with the selectivity of alcohol rising significantly to between 62% and 73%.

Ando (2016) aimed to determine the effect of metal additives, i.e. Li, Na, K, Cs, Ca and La, on the Fe-Cu catalyst activity in the FT process. The Fe-Cu catalyst typically used in the FT process consists of 95 mol% Fe with 5 mol% of Cu. During this investigation, the metal nitrates added during the modification process were added in 0.7 wt% (Ando, 2016).

For this investigation, a stainless-steel fixed bed reactor was utilized, with the reactant, or feed stream, containing 25% CO_2 in H_2. At a constant pressure of 5 MPa, the following were noted (Ando, 2016):

- An increase in the temperature increases the CO_2 conversion – with the optimal temperature being 623 K.
- With the exception of Li, the addition of alkali metals significantly increased the conversion of CO_2. In terms of alkene selectivity, cesium was deemed to be the most effective additive among the alkali metals.
- The addition of SiO_2 or MgO to the catalyst resulted in only CO being produced.
- Increasing the space velocity decreases the conversion of CO_2, due to the lower residence time and contact time, however, small improvements to alkene selection were noted. These small improvements, however, were around 0.1% selectivity and did not account for the 20% decrease in conversion, thereby nullifying the benefit of increasing the space velocity.

Unfortunately, this research also fell short in the same area as that conducted by Zhenya et al. in 2013, as it did not delve into the relationship that exists between pressure and conversion, or more importantly, the relationship between pressure and catalyst activity.

2.11. The P-Graph

The P-Graph was initially created to address Process Network Synthesis (PNS) problems. It is a bipartite graph that contains two vertices, i.e. process units, represented by horizontal bars, and material streams, represented by dots, with the type of dot being used to represent whether the material is a raw material, intermediate or product. Arcs are then used to join these two together, showing the relationship between the process units and the respective material streams. The P-Graph methodology is based on the following five axioms (Friedler et al., 1998):

- Every final product must be represented in the graph.
- A material vertex has no input if, and only if, it represents a raw material.
- Every horizontal bar must represent an operating unit that has been defined in the synthesis problem.
- Every operating bar has at least one path that is leading to a material vertex that is representing a final product.
- If a material vertex belongs to the graph, it must be an input to or an output from at least one operating unit vertex in the graph.

A P-Graph can be constructed using the P-Graph Studio ® software. This software is able to analyze P-Graph models, by means of employing three different algorithms. These algorithms are as follows (Aviso et al., 2016):

- Accelerated Branch and Bound (ABB) Algorithm – This algorithm is used to optimize an objective function and lower limit constraints.
- Maximal Structure Generation (MSG) Algorithm – This algorithm undergoes mathematical calculations to determine the maximal structure based on the five axioms. Essentially this tries to prove that all conditions have been met for the algorithms to follow.
- Solution Structure Generation (SSG) Algorithm – This algorithm is to find the most feasible combination from the maximal substructure. This feasible combination will be a subset of the structure.

The P-Graph model is a superstructure that encompasses all of the possible ways in which streams and unit operations can interact with one another, with the optimum plant configuration being a subset of this superstructure (Aviso et al., 2016).

2.12. References

Al-Fadhli, F. M., Mukherjee, R., Wang, W., & El-Halwagi, M. M. (2018). Design of Multiperiod C–H–O Symbiosis Networks. ACS Sustainable Chemistry and Engineering, 6(7), 9130-9136. doi:10.1021/acssuschemeng.8b01462

Alitalo, A., Niskanen, M., & Aura, E. (2015). Biocatalytic methanation of hydrogen and carbon dioxide in a fixed bed bioreactor. Bioresource Technology, Issue 196, 600-605. doi:10.1016/j.biortech.2015.08.021

Ando, H., 2016. Selective Alkene Production by the Hydrogenation of Carbon Dioxide over Fe-Cu Catalyst. ScienceDirect - Energy Procedia, Issue 89, pp. 421-427. doi:10.1016/j.egypro.2016.05.056

Aviso, K., Lee, J.-Y. & Tan, R. R., 2016. A P-Graph Model for Multi-period Optimization of Isolated Energy Systems. Chemical Engineering Transactions, Volume 52, pp. 865-870. doi:10.3303/CET1652145

Barany, M., Bertok, B., Imreh, C., Fan, L. T., & Friedler, F. (2012). On the equivalence of direct mechanisms and structurally minimal pathways. Journal of Mathematical Chemistry, 50, 1347-1361. doi:10.1007/s10910-012-9974-0

Bellotti, D., Rivarolo, M., Magistri, L. & Massardo, A. F., 2017. Feasibility Study of Methanol Production Plant from Hydrogen and Captured Carbon Dioxide. Journal of CO_2 Utilization, Volume 21, pp. 132-138. doi:10.1016/j.jcou.2017.07.001

Burkhardt, M. & Busch, G., 2013. Methanation of Hydrogen and Carbon Dioxide. Applied Energy, Volume 111, pp. 74-79. doi:10.1016/j.apenergy.2013.04.080

Burkhardt, M., Koschack, T. & Busch, G., 2015. Biocatalytic methanation of hydrogen and carbon dioxide in an anaerobic three-phase system. Bioresource Technology, Issue 178, pp. 330-333. doi:10.1016/j.biortech.2014.08.023

Cabrera, I. M., Granados, M. L., Terreros, P. & Fierro, J. L. G., 1998. CO_2 Hydrogenation over Pd-Modified Methanol Synthesis Catalysts. Catalysis Today, Issue 45, pp. 251-256. doi:10.1016/S0920-5861(98)00224-7

Chan, F. L., Altinkaya, G., Fung, N. & Tanksale, A., 2017. Low temperature hydrogenation of carbon dioxide into formaldehyde in liquid media. Catalysis Today, pp. 1-6. doi:10.1016/j.cattod.2017.06.012

CHEMIK, 2014. Methanol Synthesis from Carbon Dioxide and Hydrogen over CuO/ZnO/ZrO2 promoted catalysts. 1(68), pp. 61-68.

Daramola, M. (2015). Infrastructure for CO_2 Capture from South African Power Generating Plant. 4th South African Centre for Carbon Capture & Storage Conference. Johannesburg.

Diaz-Alvarado, F. A., Carrillo, J., Gracia, F., & Grossmann, I. E. (2018). Search for reaction pathways with P-graphs: Methanation of Carbon Dioxide with Hydrogen. AIChE Journal, 56, 1011-1102. doi:10.1007/s10910-017-0844-7

Fan, L. T., Bertok , B., Friedler, F., & Shafie, S. (2001). Mechanisms of Ammonia-Synthesis Reaction Revisited with the Aid of a Novel Graph-Theoretic Method for Determining Candidate Mechanisms in Deriving the Rate Law of a Catalytic Reaction. Hungarian Journal of Industrial Chemistry, 29, 71-80.

Fan, L. T., & Friedler, F. (1997). Reaction Pathway Analysis by a Network Synthesis Technique. AIChE Annual Meeting. Los Angeles, USA.

Fan, Y. J. & Wu, S. F., 2016. A graphene-supported copper-based catalyst for the hydrogenation of carbon dioxide to form methanol. Journal of CO_2 utilization, Issue 16, pp. 150-156. doi:10.1016/j.jcou.2016.07.001

Fleisch, T. H., Basu, A., & Sills, R. A. (2012). Introduction and advancement of a new clean global fuel: The status of DME developments in China and beyond. Journal of Natural Gas Science and Engineering, 9(November 2012), 94-107. doi: 10.1016/j.jngse.2012.05.012

Fornari, T., Rotstein, E., & Stephanopoulos, G. (1989). Studies on the synthesis of chemical reaction paths—II. reaction schemes with two degrees of freedom. Chemical Engineering Science, 44(7), 1569-1579. doi:10.1016/0009-2509(89)80033-8

Fornari, T., & Stephanopoulos, G. (1994). Synthesis of Chemical Reaction Paths: Economic and Specification Constraints. Chemical Engineering Communications, 129(1), 159-182. doi:10.1080/00986449408936257

Friedler, F., Fan, L. T., & Imreh, B. (1998). Process Network Synthesis: Problem Definition. Networks: An International Journal, 31(2), 119-124. doi:10.1002/(SICI)1097-0037(199803)31:2<119::AID-NET6>3.0.CO;2-K

Gaikwad, R., Bansode, A. & Urakawa, A., 2016. High-Pressures Advantages in Stoichiometric Hydrogenation of Carbon Dioxide to Methanol. Journal of Catalysis, Volume 343, pp. 127-132. doi:10.1016/j.jcat.2016.02.005

Gnanamani, M. K., Jacobs , G., Keogh, R. A., Shafer, W. D., Sparks, D. E., Hopps, S. D., Thomas, G. A., Davis, B. H. (2015). Fischer-Tropsch synthesis: Effect of pretreatment

conditions of cobalt on activity and selectivity for hydrogenation of carbon dioxide. Applied Catalysis A: General, 499, 39-46. doi:10.1016/j.apcata.2015.03.046

Hashimoto, K., Kumagai, N., Izumiya, K., Takano, H., Shinomiya, H., Sasaki, Y., . . . Kato, Z. (2016). The use of renewable energy in the form of methane via electrolytic hydrogen generation using carbon dioxide as the feedstock. Applied Surface Science, 388(B), 608-615. doi:10.1016/j.apsusc.2016.02.130

Hong, S. H. (2013). Catalytic Hydrogenation of Carbon Dioxide. Organic Chemistry Current Research, 2(2), 1. doi:10.4172/2161-0401.1000e119

Hus, M., Dasireddy, V., Stefancic, N. S. & Likozar, B., 2017. Mechanism, kinetics and thermodynamics of carbon dioxide hydrogenation to methanol on CuZnAl2O4 spinel-type heterogeneous catalysts. Applied Catalysis B: Environmental, Issue 207, pp. 267-278.

IHS Chemical. (2015). Methanol into Fuels Applications: New Sources of Growth? Special Report Prospectus. London: IHS Chemical Prospectus.

Jadhav, S. G., Vaidya, P. D., Bhanage, B. M. & Joshi, J. B., 2014. Catalytic carbon dioxide hydrogenation to methanol A review of recent studies. Chemical Engineering Research and Design, Issue 92, pp. 2557-2567. doi:10.1016/j.cherd.2014.03.005

Joo, O.-S., n.d. CAMERE Process for Carbon Dioxide Hydrogenation to Form Methanol. Catalysis Laboratory, Korea Institute of Science and Technology, pp. 686-689.

Jun, K.-W., Lee, S.-J., Choi, M.-J. & Lee, K.-W., n.d. Catalytic Hydrogenation of CO_2 into Hydrocarbons: Support Effects on Fe and Fe-K Catalysts, Korea: Korea Research Institute of chemical Technology - Catalysis Division.

Kar, S., Kothandaraman, J., Goeppert, A. & Prakash, S., 2018. Advances in catalytic homogeneous hydrogenation of carbon dioxide to methanol. Journal of CO_2 Utilization, Volume 23, pp. 212-218. doi:10.1016/j.jcou.2017.10.023

Lakner, R., Bertok, B., & Friedler, F. (2018). Synthesis of Startable Reaction Pathways. Chemical Engineering Transactions, 70, 1129-1134. doi:10.3303/CET1870189

Laurenczy, G. & Dyson, P. J., 2014. Homogeneous Catalytic Dehydrogenation of Formic Acid: Progress Towards a Hydrogen-Based Economy. J Braz Chem Soc, 25(12), pp. 2157-2163. doi:10.5935/0103-5053.20140235

Leonzio, G. (2018). Methanol Synthesis: Optimal Solution for a Better Efficiency of the Process. Processes, 6(20). doi:10.3390/pr6030020

Li, M., Hu, S., Li, Y., & Shen, J. (2000). A Hierarchical Optimization Method for Reaction Path Synthesis. Industrial & Engineering Chemistry Research, 4315-4319. doi:10.1021/ie9904596

Liu, F., Vilaca, P., Rocha, I., & Rocha, M. (2015). Development and application of efficient pathway enumeration algorithms for metabolic engineering applications. Computer methods and programs in biomedicine, 118, 134-146. doi:10.1016/j.cmpb.2014.11.010

Lukhele, K., Premlall, K., Shongwe, M., Mabuza, M. M., & Daramola, M. O. (2017). Effect of SO_2 CO-Feeding on CO_2 Adsorption capacity of South African Coals During CO_2 Sequestration. Petroleum and Coal, 177-186.

Matzen, M. & Demirel, Y., 2016. Methanol and dimethyl ether from renewable hydrogen and carbon dioxide Alternative fuels production and life-cycle assessment. Journal of Cleaner Production , Issue 139, pp. 1068-1077. doi:10.1016/j.jclepro.2016.08.163

Miguel, C. V., Soria, M. A., Mendes, A. & Madeira, L. M., 2015. Direct CO_2 hydrogenation to methane or methanol from post-combustion exhaust streams - A thermodynamic study. Journal of Natural Gas Science and Engineering, Issue 22, pp. 1-8. doi:10.1016/j.jngse.2014.11.010

Ng, W. P., Varbanov, P. S., Klemes, J. J., Hegyhati, M., Bertok, B., Heckl, I., & Lam, H. L. (2013). Waste to Energy for Small Cities: Economics versus Carbon Footprint. Chemical Engineering Transactions, 889-894. doi:10.3303/CET1335148

Olah, G. A. (2005). Beyond Oil and Gas: The Methanol Economy. Angewandte Chemie(44), 2636-2639. doi:10.1002/anie.200462121

Osler, K., Dheda, D., Ngoy, J., Wagner, N., & Daramola, M. O. (2017). Synthesis and evaluation of carbon nanotubes composite adsorbent for CO_2 capture: A comparative study of CO_2 adsorption capacity of single-walled and multi-walled carbon nanotubes. International Journal of Coal Science & Technology, 4(1), 41-49. doi:10.1007/s40789-017-0157-2

Roger, M., Brown, F., Gabrielli, W. & Sargent, F., 2018. Efficient Hydrogen-Dependent Carbon Dioxide Reduction by Escherichia Coli. Current Biology, Issue 28, pp. 104-145. doi:10.1016/j.cub.2017.11.050

Rotstein, E., Resasco, D., & Stephanopoulos, G. (1982). Studies on the synthesis of chemical reaction paths—I: Reaction characteristics in the (ΔG, T) space and a primitive synthesis procedure. Chemical Engineering Science, 37(9), 1337-1352. doi:10.1016/0009-2509(82)85006-9

Seo, D. H., Lee, Y., Park, S., Fan, L. T., Shafie, S., Bertok, B., & Friedler, F. (2001). Graph-Theoretical Identification of Pathways for Biochemical Reactions. Biotechnology Letters, 23, 1551-1557. doi:10.1023/A:1011913225764

Sepiacci, P., & Manca, D. (2015). Economic Assessment of Chemical Plants Supported by Environmental and Social Sustainability. Chemical Engineering Transactions, 43, 2209-2214. doi:10.3303/CET1543369

Tan, R. R., Aviso, K. B., Klemes, J. J., Lam, H. L., Varbanov, P. S., & Friedler, F. (2018). Towards Generalized Process Networks: Prospective New Research Frontiers for the P-graph Framework. Chemical Engineering Transactions, 70, 91-96. doi:10.3303/CET1870016

Tursunov, O., Kustov, L., Kustov, A. & Travyanov, A., 2017. A Brief Review of CO_2 Hydrogenation to Methanol over Cu- And Fe- Based Catalysts. Oil & Gas Science and Technology, 72(5), 1-9. dio:10.2516/ogst/2017027

USAID, 2015. Greenhouse Gas Emissions in South Africa. [Online] Available at: http://www4.unfccc.int/submissions/INDC/Published%20Documents/South%20Africa/1/South%20Africa.pdf. [Accessed 1 February 2018].

Van der Ham, L. G., Van Den Berg, H., Benneker, A., Simmelink, G., Timmer, J., & Van Weerden, S. (2012). Hydrogenation of carbon dioxide for methanol production. Chemical Engineering Transactions, 29, 181-186. doi:10.3303/CET1229031

Vanhove, A., 2015. Improvements on the design of carbon dioxide conversion to methanol process using Aspen Plus® interface, Lisbon: Instituto Superior Técnico.

Varbanov, P., Friedler, F., & Klemes, J. J. (2017). Process Network Design and Optimisation Using P-graph: The Success, the Challenges and Potential Roadmap. Chemical Engineering Transactions, 61, 1549-1554. doi:10.3303/CET1761256

Watari, R., Kayaki, Y., Hirano, S.-i., Matsumoto, N., & Ikariya, T. (2017). Development of Homogeneous Hydrogenation of Carbon Dioxide to Formate Catalyzed by Copper Complexes. Energy Procedia, 114, 7150-7153. doi:10.1016/j.egypro.2017.03.1877

Wesselbaum, S., Hintermair, U., & Leitner, W. (2012). Continuous-Flow Hydrogenation of Carbon Dioxide to Pure Formic Acid using an Integrated $scCO_2$ Process with Immobilized Catalyst and Base. Angewandte Chemie International Edition, 51(34), 8585-8588. doi:10.1002/anie.201203185

Yoro, K. O., & Sekoai, P. T. (2016). The Potential of CO_2 Capture and Storage Technology in South Africa's Coal-Fired Thermal Power Plants. MDPI: Environments, 2(24), 1-20. doi:10.3390/environments3030024

Yoro, K. O., Sekoai, P. T., Isafiade, A. J., & Daramola, M. O. (2019). A review on heat and mass integration techniques for energy and material minimization during CO_2 capture. International Journal of Energy and Environmental Engineering, 10(3), 367-387. doi:10.1007/s40095-019-0304-1

Zamani, A. H. & Abdullah, N. H., 2018. Modeling and optimization of carbon dioxide methanation via in situ hydrogen generated from aluminum foil and alkaline water by Box–Behnken design. Journal of the Taiwan Institute of Chemical Engineers, Issue 82, pp. 156-182. doi:10.1016/j.jtice.2017.11.013

Zargari, N., Jung, E., Lee, J.-H. & Jung, K. W., 2017. Carbon dioxide hydrogenation Efficient catalysis by an NHC-amidate Pd(II) complex. Tetrahedron Letters, Issue 58, pp. 3330-3332. doi:10.1016/j.tetlet.2017.07.040

Zhanghuai, S. & Yuan, K., 2000. Synthesis of Light Hydrocarbons from Carbon Dioxide and Hydrogen over Fe/ZrO2 or Fe/TiO2 Catalysts. Journal of Natural Gas Chemistry, 9(4), pp. 283-292.

Zhao, Y., Qian, X., Zhao, X. & Zhang, Z., 2018. Hydrogenation of Carbon Dioxide under Atmospheric Pressure and Low Temperature. International Journal of Hydrogen Energy, 43(5) pp. 3062-3069. doi:10.1016/j.ijhydene.2017.12.124

Zhenya, Y., Weiping, D., Qinghong, Z. & Ye, W., 2013. Hydrogenation of carbon dioxide to light olefins over non-supported iron catalyst. Chinese Journal of Catalysis, Issue 34, pp. 956-963. doi:10.1016/S1872-2067(12)60559-2

3. Framework Development

The framework developed and explained in this dissertation comprises two main components, i.e. the development of the P-Graph model, and the analysis thereof. This chapter provides a brief explanation of the framework.

In Step 1, a Reaction Pathway Database (RPD) was constructed for the system in question. This RPD comprised all currently known reaction pathways, along with their associated operating conditions, catalysts and conversions. At this stage in the framework, no reaction kinetics were required, as the framework aims to use current literature sources to determine which pathway is viable, and should be looked at in more detail.

In Step 2, a P-Graph model was constructed using the reaction pathways listed in the previously developed RPD. Reactants, intermediates and products are represented by a variation of dots, with the actual reaction and interaction of species being represented by a horizontal bar. Each horizontal bar is used to represent a different reaction, and was labelled in accordance with the paper from which the reaction pathway is extracted. This results in a reaction pathway superstructure, where all reaction pathways are considered together in a network, with the optimum solution being a subset within the P-Graph model.

Due to the vast array of pathway combinations achievable from the database, conditions were implemented into the model to further reduce the search space to a more manageable region. This formed part of Step 3. These conditions included limiting the type and number of products being formed in each combination, and were considered to be simplifying assumptions. The nature of these conditions is dependent on the infrastructure in which this framework is implemented. Chapter 4 of this dissertation provides further detail on these conditions.

Step 4 involved completing a final run of the P-Graph model, after accounting for the aforementioned conditions. When using P-Graph Studio ® various algorithms are available in solving a P-Graph model, as was detailed in Section 2.11. The Solution Structure Generation (SSG) algorithm was able to determine the number of unique reaction pathway combinations achievable, defining each combination as a separate case study. Step 5 involved extracting these case studies, and defining each system, in terms of its reaction pathway and its associated operation conditions, conversion and selectivities. This information was further used in Step 6.

In Step 6, Aspen Plus ® simulations were developed for each case study. This simulation provided a basic plant design for each case study, taking into account the use of pressure-driven unit operations, heat exchangers and separation systems. However, when costing these unit operations in each case study, there exists costing capacity limits, as was determined by Turton et al. (2009). To abide by these limits, certain unit operations were broken down into a series of unit operations, ensuring that each unit abides by the aforementioned limits. This was Step 7 of this framework.

In Step 8, the associated mass and energy balances of each case study, determined through Aspen Plus ®, was extracted from the simulations. This information was utilized in costing the unit operations, as well as the cost and sales potential of the reactants and products, respectively. These economic calculations were Step 9 of the framework.

The viability of a case study was dependent on both its environmental benefit, as well as its ability to yield a profit. Case studies that were unable to meet both these factors are immediately eliminated from the search space. Step 10 involved eliminating case studies using three criteria, which incorporated both environmental and economic benefits.

With the reduced search space being known, Step 11 shifted the focus to accounting for the catalyst required in each case study, as well as its annual replacement. This allowed for the catalyst cost to be easily integrated into the annual profit/loss calculation of the reduced search space. Step 12 used all of the information available on the reduced search space, as well as a performance index, to rank the remaining case studies in order of their viability. This performance index accounted for both the environmental and economic benefits of the case study, finding an effective compromise between the two.

Unfortunately, much of the data utilized in this analysis was economic data, and is highly subject to change. In order to determine the effect that these economic factors would have on the results of the framework, a sensitivity analysis was conducted. This was Step 13 of the framework. This analysis determined the most influential factors in the study, showing the key factors around which, the viability of a pathway is dependent.

Step 14 involved tabulating the reduced search space, which is ranked in order of viability. It is important to note however, that the reduced search space is solely dependent on the RPD, and alterations or additions to this RPD may result in changes in the reduced search space. Figure 5 provides an overview of the systematic framework developed in this dissertation.

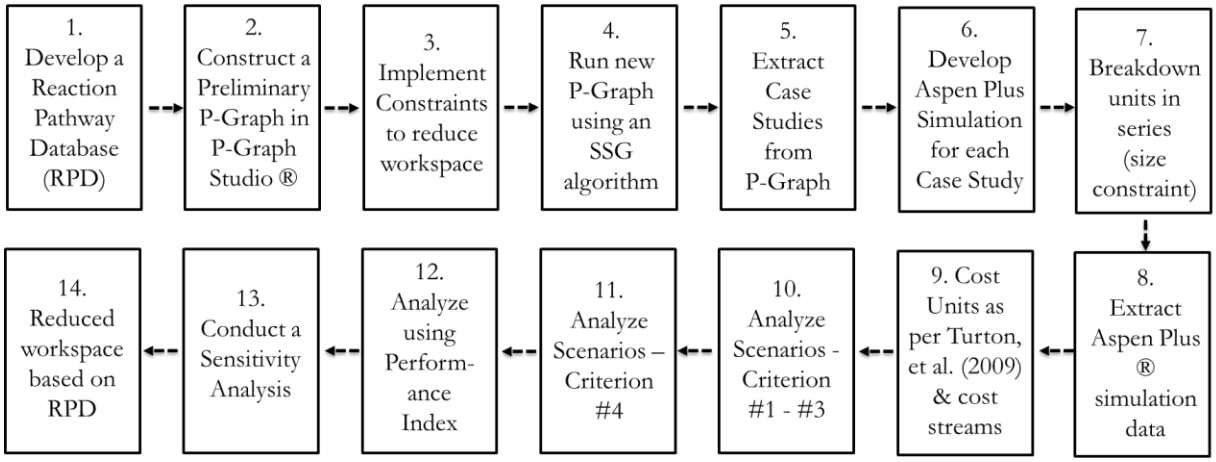

Figure 5: Complete overview of systematic framework developed

Steps 1 through to 5 of the framework deal with the development of a P-Graph model, whereas steps 6 through to 14 deal with the analysis of the P-Graph results.

With the most viable pathway being known at this early stage, the focus can be shifted outside of the framework, to the optimization of the operations conditions, and the design of the plant thereof. The strength in such a framework lies in the fact that it is dependent on an RPD and can be used on any reactive system prior to extensive design procedures. This allows for resources to be better managed and utilized during the early stages of plant development.

4. Model development through P-Graph

With the focus on CO_2 utilization becoming especially prominent in recent years, the search space of reaction pathways is vast. One of the most effective approaches in determining how the reaction pathways can be combined, is based on the P-Graph algorithm. This algorithm generates all possible reaction pathways combinations that are able to convert the reactant, i.e. CO_2, into a final product. A recent study in the P-Graph was able to formally prove that the new P-Graph reaction pathway algorithms, are able to generate a complete set of reaction pathways, identical to those found using linear algebraic approaches (Barany et al., 2012). Therefore, utilizing the P-Graph concept in this dissertation ensures that all unique reaction pathway combinations are considered in this analysis.

This chapter explains the systematic approach followed in developing the P-Graph model, i.e. Steps 1 through to 5 of the Framework Summary (Chapter 3).

4.1. Methodology for P-Graph development

The development of the P-graph that was utilized in this analysis, employed a systematic framework or methodology as explained in the stages below:

1. A literature review was conducted on the possible reaction pathways that contain CO_2 and H_2. These reaction systems were utilized in generating a Reaction Pathway Database (RPD) (Section 4.2), containing the information given in the problem statement in Section 1.3 of this dissertation.
2. Using the RPD, a preliminary P-Graph was developed. At this stage the P-Graph had no constraints, and was color coded depending on the source from which the reaction pathway is extracted. Color coding allows for cross referencing of the pathways upon the analysis of the results.
3. The focus then shifted to the various conditions to be implemented within the P-Graph, in order to reduce the search space. These conditions were sub-divided into three categories. The justification and reasoning behind each of these conditions are detailed in Section 4.4 of this dissertation.

a. Condition 1: The prevention of multiple products being produced from a single pathway.

b. Condition 2: The types of products being produced from the pathways, which is dependent on the infrastructure of the region in which this analysis is conducted.

c. Condition 3: The complexity to which the reaction pathway analyzed was looked into, i.e. the number of sub reactions that occur in order to produce the desired product.

4. The preliminary P-Graph model was adjusted to incorporate these constraints and run using the SSG algorithm, to determine the new, reduced search space. Section 4.5 shows the final P-Graph utilized in this analysis.

4.2. Reaction pathway database

Table 1 shows the reactions utilized in the construction of the reaction pathways superstructure, as well as the relevant information required.

Table 1: Reaction pathway database based on data extracted from various literature sources

Source	Reaction	Temp	Pressure	Catalyst	Product	X_{CO2}	Selectivity
Zhao et al., 2018	$H_2O \rightarrow H^+ + OH^-$ $KBH_4 \rightarrow K^+ + BH_4^-$ $CO_2 + OH^- \rightarrow HCO_3^-$ $BH_4^- + 4HCO_3^- \rightarrow 4HCO_2^- + B(OH)_4^-$	50°C	1 atm	n/a	Formate (HCOO)	50.74%	40.60%
Gaikwad et al., 2016	$CO_2 + 3H_2 \leftrightarrow CH_3OH + H_2O$ $CO_2 + H_2 \leftrightarrow CO + H_2O$ $CO + 2H_2 \leftrightarrow CH_3OH$	260°C to 280°C	Up to 442 bar	$Cu/ZnO/Al_2O_3$	Methanol (CH_3OH)	98.7%	>99.9%
Bellotti et al., 2017	$CO_2 + H_2O \leftrightarrow CH_3OH + H_2O$	240°C	80 bar	$CuO/ZnO/Al_2O_3$	MeOH	96%	-
Chan et al., 2017	$CO_2 + H_2 \leftrightarrow HCOOH$ $HCOOH + H_2 \leftrightarrow HCHO + H_2O$	298 K to 363 K	70 bar	Pt-Cu	Formaldehyde (HCHO)	-	-
	$CO_2 + H_2 \leftrightarrow CO + H_2O$ $CO + H_2 \leftrightarrow HCHO$	298 K to 363 K	70 bar	Pt-Cu	Formaldehyde (HCHO)	-	-
Burkhardt & Busch, 2013	$4H_2 + CO_2 \rightarrow CH_4 + 2H_2O$	37°C	1 atm	Hydrogenotrophic Methanogenic Archaea	Methane (CH_4)	~ 100%	~ 100%

Source	Reaction	Temp	Pressure	Catalyst	Product	X_{CO2}	Selectivity
Hashimoto et al., 2016	$4H_2 + CO_2 \rightarrow CH_4 + 2H_2O$	100°C	Unknown	Ni-40Zr	Methane	Unknown	~100%
CHEMIK, 2014	$CO_2 + 3H_2 \leftrightarrow CH_3OH + H_2O$ $CO_2 + H_2 \leftrightarrow CO + H_2O$	433 K to 513 K	8 MPa	Cu/Zn/Zr	MeOH	6% to 14%	65% to 80%
Jun et al., n.d.	$2CO_2 + 3H_2 \leftrightarrow C_2H_6 + 2O_2$ $3CO_2 + 4H_2 \leftrightarrow C_3H_8 + 3O_2$	573 K	1 atm	Fe/TiO_2 or Fe/Al_2O_3	C2+ Hydrocarbons	Unknown	Unknown
Miguel et al., 2015	$CO_2 + 4H_2 \leftrightarrow CH_4 + 2H_2O$	100°C	1 atm	Ru-based or Cu-based or Ni-based	Methane	~100%	~100%
Zhenya et al., 2013	$4H_2 + CO_2 \rightarrow CH_4 + 2H_2O$ $CO_2 + H_2 \leftrightarrow CO + H_2O$ $2CO_2 + 3H_2 \leftrightarrow C_2H_6 + 2O_2$ $3CO_2 + 4H_2 \leftrightarrow C_3H_8 + 3O_2$	673 K	2 MPa	Li, Na, K, Rb, Cs with Fe based	Olefins (Alkenes)	42%	37%
Ando, 2016	$2CO_2 + 6H_2 \rightarrow C_2H_4 + 4H_2O$	623 K	5 MPa	Li, Na, K, Cs, Ca and La with Fe-Cu	Alkenes (C2)	42%	0.72%
	$3CO_2 + 9H_2 \rightarrow C_3H_6 + 6H_2O$	623 K	5 MPa	Li, Na, K, Cs, Ca and La with Fe-Cu	Alkenes (C3)	42%	3.8%
Zamani & Abdullah, 2018	$Al + 3H_2O \xrightarrow[NaOH]{} Al(OH)_3(l) + 1.5\ H_2$	Ambient	Ambient	NaOH	1-gram Al generates 1.2 litres H_2		
	$CO_2 + 4H_2 \rightarrow CH_4 + 2H_2O$	276.6°C	Unknown	AZH-CM	Methane	97.5%	Unknown

Source	Reaction	Temp	Pressure	Catalyst	Product	X_{CO2}	Selectivity
Matzen & Demirel, 2016	$2CH_3OH \rightarrow CH_3OCH_3 + H_2O$	250°C to 400°C	25 bar	Alumina based	DME	87.2%	99.5%
Fan & Wu, 2016	$CO_2 + 3H_2 \leftrightarrow CH_3OH + H_2O$	473 K to 553 K	10 to 20 bar	CZZA/rGO	MeOH	20.7%	85.0%
Hus et al., 2017	$CO_2 + 3H_2 \leftrightarrow CH_3OH + H_2O$	200°C to 400°C	20 bar	Cu/Zn/Al	MeOH	10%	~100%
Alitalo et al., 2015	$CO_2 + 4H_2 \rightarrow CH_4 + 2H_2O$	53°C to 55°C	Unknown	Methanogenic Archaea	Methane	~100%	Unknown
Burkhardt et al., 2015	$CO_2 + 4H_2 \rightarrow CH_4 + 2H_2O$	36.5°C to 37.7°C	1 atm	Methanobacterium Thermoautotro-phicum	Methane	100%	~100%
Zargari et al., 2017	$CO_2 + H_2 \leftrightarrow HCOOH$	200°C	130 atm	NHC-Amidate Pd(II) complex	Formic Acid	Unknown	Unknown
Tursunov et al., 2017	$CO_2 + 3H_2 \leftrightarrow CH_3OH + H_2O$ $CO_2 + H_2 \leftrightarrow CO + H_2O$ $CO + 2H_2 \leftrightarrow CH_3OH$	250°C	15 bar	Cu/Zn/rGO	MeOH	26%	51%
Cabrera et al., 1998	$CO_2 + 3H_2 \leftrightarrow CH_3OH + H_2O$ $CO_2 + H_2 \leftrightarrow CO + H_2O$	433 K to 473 K	40 bar	CZA-Pd Modified	MeOH	Increased - Unknown	Increased - Unknown

Source	Reaction	Temp	Pressure	Catalyst	Product	X_{CO2}	Selectivity
Vanhove, 2015	$CO_2 + 3H_2 \leftrightarrow CH_3OH + H_2O$ $CO_2 + H_2 \leftrightarrow CO + H_2O$ $CO + 2H_2 \leftrightarrow CH_3OH$	260°C	330 bar	Fe-Cu	MeOH	95.3%	98.2%
Jadhav et al., 2014	$CH_4 + H_2O \leftrightarrow CO + 3H_2$ $CH_4 + 2H_2O \leftrightarrow CO_2 + 4H_2$ $CO_2 + 3H_2 \leftrightarrow CH_3OH + H_2O$ $CO_2 + H_2 \leftrightarrow CO + H_2O$ $CO + 2H_2 \leftrightarrow CH_3OH$	250°C to 300°C	5 MPa to 10 MPa	CuO/ZnO/Al_2O_3	MeOH	Not stated	Not stated
Roger et al., 2018	$CO_2 + H_2 \leftrightarrow HCOOH$	25°C	10 bar	Escherichia Coli FHL enzyme	Formate Ion and Formic Acid	103%	Unknown
Zhanghuai & Yuan, 2000	$CO_2 + H_2 \leftrightarrow CO + H_2O$ $CO_2 + 4H_2 \rightarrow CH_4 + 2H_2O$ $4CO_2 + 6H_2O \leftrightarrow 2C_2H_6 + 7O_2$ $3CO_2 + 4H_2O \leftrightarrow C_3H_8 + 5O_2$	723 K	1.5 MPa	Fe/ZrO_2 and Fe/TiO_2	Hydrocarbons	20%	69%
Gnanamani et al., 2015	$4H_2 + CO_2 \leftrightarrow CH_4 + 2H_2O$ $3H_2 + CO_2 \leftrightarrow CH_3OH + H_2O$ $CO_2 + H_2 \leftrightarrow CO + H_2O$	220°C	1.89 MPa	1% Na/ 20% Co-SiO_2	Hydrocarbons and Alcohols	23.5%	15.3% Methane 73.2% HC

Source	Reaction	Temp	Pressure	Catalyst	Product	X_{CO2}	Selectivity
Van der Ham et al., 2012	$CO_2 + 3H_2 \leftrightarrow CH_3OH + H_2O$ $CO_2 + H_2 \leftrightarrow CO + H_2O$ $CO + 2H_2 \leftrightarrow CH_3OH$	4498 K to 548 K	5 MPa	$Cu/ZnO/Al_2O_3$	MeOH	12%	36%
	$CO_2 + 3H_2 \leftrightarrow CH_3OH + H_2O$ $CO_2 + H_2 \leftrightarrow CO + H_2O$ $CO + 2H_2 \leftrightarrow CH_3OH$	443 K	3 MPa	$Cu/ZnO/Al_2O_3$	MeOH	26%	73%
	$CO_2 + 3H_2 \leftrightarrow CH_3OH + H_2O$ $CO_2 + H_2 \leftrightarrow CO + H_2O$ $CO + 2H_2 \leftrightarrow CH_3OH$	523 K to 543 K	2 MPa	Cu-Ga/ZnO	MeOH	5%	85%

4.3. Initial P-Graph model

Based on the RPD in Section 4.2, a preliminary P-Graph model was constructed using P-Graph Studio ® Software. Figure 6 shows the preliminary P-Graph model. It is important to note that the different colors are used in differentiating between the reaction pathways, and are color-coded according to the paper from which they were extracted.

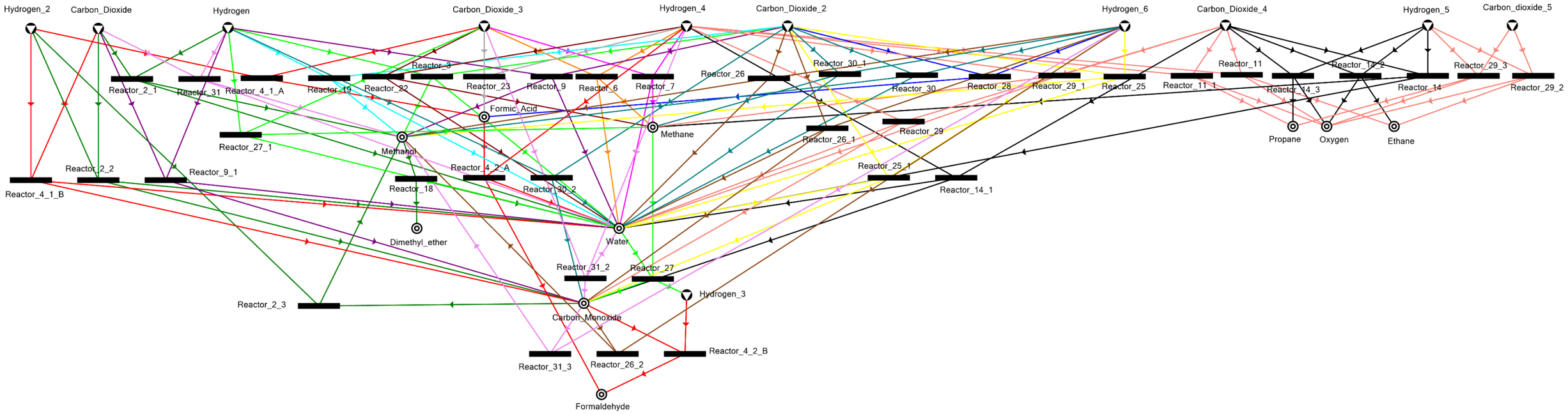

Figure 6: Preliminary P-Graph based on the reaction pathway database before implementing conditions

The reactor numbers, in Figure 6, are associated with a specific source. Below is a key to illustrate this link.

Number	Source	Number	Source	Number	Source	Number	Source	Number	Source
2	Gaikwad et al., 2016	9	CHEMIK, 2014	17	Zamani & Abdullah, 2018	22	Burkhardt et al., 2015	27	Jadhav et al., 2014
3	Bellotti et al., 2017	11	Jun et al., n.d.	18	Matzen & Demirel, 2016	23	Zargari et al., 2017	28	Roger et al., 2018
4	Chan et al., 2017	13	Miguel et al., 2015	19	Fan & Wu, 2016	24	Tursunov et al., 2017	29	Zhanghuai & Yuan, 2000
6	Burkhardt & Busch, 2013	14	Zhenya et al., 2013	20	Hus et al., 2017	25	Cabrera et al., 1998	30	Gnanamani et al., 2015
7	Hashimoto et al., 2016	16	Ando, 2016	21	Alitalo et al., 2015	26	Vanhove, 2015	31	Van der Ham et al., 2012

This P-Graph was constructed on version 5.2.1.14 of P-Graph Studio ®. Using the Solution Structure Generation (SSG) algorithm, the total number of possible reaction pathway combinations were determined. However, prior to running the model, it was important to note the limitations of the P-Graph Studio ® software. These limitations are:

- P-Graph Studio ® is only able to display a maximum of 100,000 solutions.
- P-Graph Studio ® can read up to a maximum of 4,194,000 solutions.

Unfortunately, P-Graph Studio ® was unable to handle the preliminary run of this P-Graph model. Table 2 shows the results for this preliminary run.

Table 2: Preliminary P-Graph results before the addition of conditions

Factor	Value
Algorithm	Solution Structure Generation (SSG)
Number of Solutions	4,194,000 (terminated due to insufficient memory in the software)
Computational Time	7 min 41.09 seconds

This search space is rather large, and is impractical to work with. Furthermore, Table 2 indicates that the solutions were terminated due to insufficient memory in the software, thereby indicating an incomplete search space. In order to reduce the search space, conditions were added to the model.

4.4. P-Graph conditions

This chapter details the conditions employed in the P-Graph model, to reduce the search space.

4.4.1. Condition 1

The first condition implemented, involved the use of the mutual exclusion principle. This condition ensured that each reaction pathway system only produced a single product. For example, when a single reaction was involved in the production of MeOH, all other MeOH pathways and other economically valuable product pathways, such as methane and DME, were

not in operation simultaneously. This condition was implemented due to the nature of this research being to find the most effective pathway by which to utilize CO_2 and H_2 to form a carbon negative fuel source, thereby implying a single product. Table 3 shows the mutual exclusions that were implemented in the P-Graph model.

Table 3: List of mutual exclusions applied to the preliminary P-Graph

No.	Purpose of Mutual Exclusion	Reactor Unit Operations Involved
1	Production of MeOH from CO_2	Reactor_2_1; Reactor_3; Reactor_9; Reactor_19; Reactor_25; Reactor_26; Reactor_30; Reactor_31
2	RWGS Reaction	Reactor_2_2; Reactor_4_1_B; Reactor_9_1; Reactor _14_1; Reactor_26_1; Reactor_29; Reactor_30_2; Reactor_31_2; Reactor_25_1
3	Production of MeOH from CO	Reactor_2_3; Reactor_26_2; Reactor_31_3
4	Production of Methane from CO_2	Reactor_6; Reactor_7; Reactor_14; Reactor_22; Reactor_27_1; Reactor_29_1; Reactor_30_1
5	Production of Formic Acid	Reactor_4_1_A; Reactor_23; Reactor_28
6	Production of Ethane	Reactor_11; Reactor_14_2; Reactor_29_2
7	Production of Propane	Reactor_11_1; Reactor_14_3; Reactor_29_3
8	Production of Formaldehyde	Reactor_4_2_A; Reactor_4_2_B
9	Prevent more than one product being formed simultaneously	Reactor_4_1_A; Reactor_4_2_A; Reactor_4_2_B; Reactor_6; Reactor_7; Reactor_11; Reactor_11_1; Reactor_14; Reactor_14_2; Reactor_14_3; Reactor_22; Reactor_23; Reactor_27; Reactor_27_1; Reactor_28; Reactor_29_1; Reactor_29_2; Reactor_29_3; Reactor_30_1; Reactor_2_1; Reactor_3; Reactor_9; Reactor_19; Reactor_25; Reactor_26; Reactor_30; Reactor_31; Reactor_2_2; Reactor_4_1_B; Reactor_9_1; Reactor_14_1; Reactor_26_1; Reactor_29; Reactor_30_2; Reactor_31_2; Reactor_25_1

These mutual exclusions were able to reduce the number of possible pathway combinations, from 4,194,000 to 96 pathways, a much more realistic search space. This search space, however, was further reduced through the implementation of Condition 2 and Condition 3.

4.4.2. Condition 2

This condition deals with the types of products that are produced from the pathways, and is dependent on the infrastructure of the region in which this analysis is conducted. This analysis was conducted using the South African infrastructure as the basis. Much of the carbon negative investigations that is being conducted at research institutions in South Africa focuses on the production of MeOH, DME and higher hydrocarbons. As a result, this condition limited the pathways considered to those involved in the production of propane, butane, MeOH and DME.

4.4.3. Condition 3

This condition deals with the complexity of the reaction pathway systems, i.e. the number of sub-reactions that occur when producing the desired product. For the sake of this dissertation a maximum of three sub-reactions were utilized. The reason for choosing three sub-reactions lies in maintaining a single product pathway, as per Condition 1, whilst also considering the possibility of certain products being intermediates in their reactive systems.

The production of butane occurs by means of the following reaction system (Inui et al., 1998):

$$CO_2 + H_2 \leftrightarrow CH_3OH + H_2O \quad (28)$$

$$2CH_3OH \leftrightarrow CH_3OCH_3 + H_2O \quad (29)$$

$$CH_3OCH_3 \leftrightarrow C_2H_4 + H_2O \quad (30)$$

$$3C_2H_4 \leftrightarrow 2C_3H_6 \quad (31)$$

$$2C_3H_6 + 2CH_3OH \leftrightarrow 2C_4H_{10} + O_2 \quad (32)$$

The production of butane has a high complexity, containing five sub-reactions in its reactive system. This eliminates butane from the search space.

4.5. Revised P-Graph model

Figure 7 shows the revised P-Graph that was constructed, after taking into account the conditions that are detailed in Section 4.4. This P-Graph was constructed using P-Graph studio ®. It is important to note that arrows entering the reactor unit operations imply reactants, whereas the arrows leaving a reactor unit operation show a product.

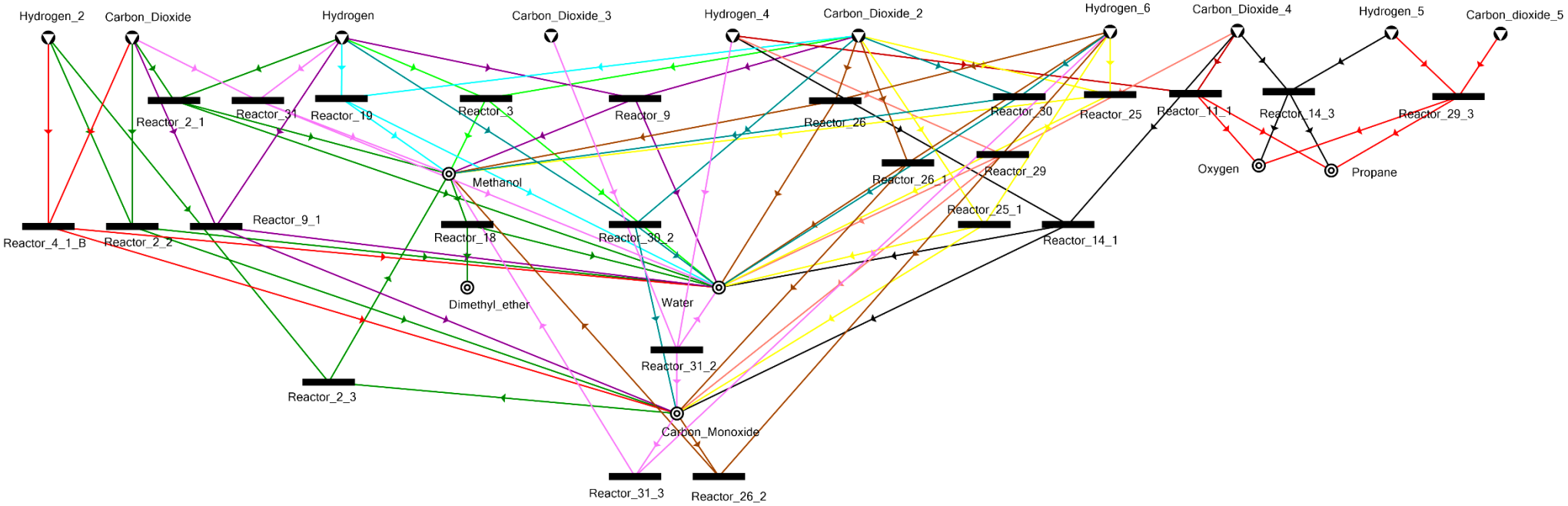

Figure 7: Final revised P-Graph after the implementation of the conditions

Table 4 shows the results after the conditions are implemented into the P-Graph.

Table 4: P-Graph results after all conditions were implemented

Factor	Value
Algorithm	Solution Structure Generation (SSG)
Number of Solutions	85
Computational Time	0.13 seconds

This computation time is based on a Dell Intel® Core™ i5-2520M CPU @ 2.50 GHz with 8.00 GB Installed Ram (7.88 GB usable). It is likely that the computation time will change depending on the operating system used. However, the result of having 85 possible solutions, or number of different combinations, is a very practical search space. From this point forward, each of these combinations were treated as individual case studies. All 85 case studies are given in Appendix A.

4.6. References

Alitalo, A., Niskanen, M., & Aura, E. (2015). Biocatalytic methanation of hydrogen and carbon dioxide in a fixed bed bioreactor. Bioresource Technology, Issue 196, 600-605. doi:10.1016/j.biortech.2015.08.021

Ando, H., 2016. Selective Alkene Production by the Hydrogenation of Carbon Dioxide over Fe-Cu Catalyst. ScienceDirect - Energy Procedia, Issue 89, pp. 421-427. doi:10.1016/j.egypro.2016.05.056

Barany, M., Bertok, B., Imreh, C., Fan, L. T., & Friedler, F. (2012). On the equivalence of direct mechanisms and structurally minimal pathways. Journal of Mathematical Chemistry, 50, 1347-1361. doi:10.1007/s10910-012-9974-0

Bellotti, D., Rivarolo, M., Magistri, L. & Massardo, A. F., 2017. Feasibility Study of Methanol Production Plant from Hydrogen and Captured Carbon Dioxide. Journal of CO_2 Utilization, Volume 21, pp. 132-138. doi:10.1016/j.jcou.2017.07.001

Burkhardt, M. & Busch, G., 2013. Methanation of Hydrogen and Carbon Dioxide. Applied Energy, Volume 111, pp. 74-79. doi:10.1016/j.apenergy.2013.04.080

Burkhardt, M., Koschack, T. & Busch, G., 2015. Biocatalytic methanation of hydrogen and carbon dioxide in an anaerobic three-phase system. Bioresource Technology, Issue 178, pp. 330-333. doi:10.1016/j.biortech.2014.08.023

Cabrera, I. M., Granados, M. L., Terreros, P. & Fierro, J. L. G., 1998. CO_2 Hydrogenation over Pd-Modified Methanol Synthesis Catalysts. Catalysis Today, Issue 45, pp. 251-256. doi:10.1016/S0920-5861(98)00224-7

Chan, F. L., Altinkaya, G., Fung, N. & Tanksale, A., 2017. Low temperature hydrogenation of carbon dioxide into formaldehyde in liquid media. Catalysis Today, pp. 1-6. doi:10.1016/j.cattod.2017.06.012

CHEMIK, 2014. Methanol Synthesis from Carbon Dioxide and Hydrogen over CuO/ZnO/ZrO2 promoted catalysts. 1(68), pp. 61-68.

Fan, Y. J. & Wu, S. F., 2016. A graphene-supported copper-based catalyst for the hydrogenation of carbon dioxide to form methanol. Journal of CO_2 utilization, Issue 16, pp. 150-156. doi:10.1016/j.jcou.2016.07.001

Gaikwad, R., Bansode, A. & Urakawa, A., 2016. High-Pressures Advantages in Stoichiometric Hydrogenation of Carbon Dioxide to Methanol. Journal of Catalysis, Volume 343, pp. 127-132. doi:10.1016/j.jcat.2016.02.005

Gnanamani, M. K., Jacobs , G., Keogh, R. A., Shafer, W. D., Sparks, D. E., Hopps, S. D., Thomas, G. A., Davis, B. H. (2015). Fischer-Tropsch synthesis: Effect of pretreatment conditions of cobalt on activity and selectivity for hydrogenation of carbon dioxide. Applied Catalysis A: General, 499, 39-46. doi:10.1016/j.apcata.2015.03.046

Hashimoto, K., Kumagai, N., Izumiya, K., Takano, H., Shinomiya, H., Sasaki, Y., . . . Kato, Z. (2016). The use of renewable energy in the form of methane via electrolytic hydrogen generation using carbon dioxide as the feedstock. Applied Surface Science, 388(B), 608-615. doi:10.1016/j.apsusc.2016.02.130

Hus, M., Dasireddy, V., Stefancic, N. S. & Likozar, B., 2017. Mechanism, kinetics and thermodynamics of carbon dioxide hydrogenation to methanol on CuZnAl2O4 spinel-type heterogeneous catalysts. Applied Catalysis B: Environmental, Issue 207, pp. 267-278.

Inui, T., Anpo, M., Izui, K., Yanagida, S., & Yamaguchi, T. (1998). Advances in Chemical Conversions for Mitigating Carbon Dioxide (1st ed.). United States of America: Elsevier.

Jadhav, S. G., Vaidya, P. D., Bhanage, B. M. & Joshi, J. B., 2014. Catalytic carbon dioxide hydrogenation to methanol A review of recent studies. Chemical Engineering Research and Design, Issue 92, pp. 2557-2567. doi:10.1016/j.cherd.2014.03.005

Jun, K.-W., Lee, S.-J., Choi, M.-J. & Lee, K.-W., n.d. Catalytic Hydrogenation of CO_2 into Hydrocarbons: Support Effects on Fe and Fe-K Catalysts, Korea: Korea Research Institute of chemical Technology - Catalysis Division.

Matzen, M. & Demirel, Y., 2016. Methanol and dimethyl ether from renewable hydrogen and carbon dioxide Alternative fuels production and life-cycle assessment. Journal of Cleaner Production , Issue 139, pp. 1068-1077. doi:10.1016/j.jclepro.2016.08.163

Miguel, C. V., Soria, M. A., Mendes, A. & Madeira, L. M., 2015. Direct CO_2 hydrogenation to methane or methanol from post-combustion exhaust streams - A thermodynamic study. Journal of Natural Gas Science and Engineering, Issue 22, pp. 1-8. doi:10.1016/j.jngse.2014.11.010

P-Graph Studio ® v 5.2.1.14 (n.d.). Pannonia: Department of Computer Science and Systems Technology, University of Pannonia.

Roger, M., Brown, F., Gabrielli, W. & Sargent, F., 2018. Efficient Hydrogen-Dependent Carbon Dioxide Reduction by Escherichia Coli. Current Biology, Issue 28, pp. 104-145. doi:10.1016/j.cub.2017.11.050

Tursunov, O., Kustov, L., Kustov, A. & Travyanov, A., 2017. A Brief Review of CO_2 Hydrogenation to Methanol over Cu- And Fe- Based Catalysts. Oil & Gas Science and Technology, 72(5), 1-9. dio:10.2516/ogst/2017027

Van der Ham, L. G., Van Den Berg, H., Benneker, A., Simmelink, G., Timmer, J., & Van Weerden, S. (2012). Hydrogenation of carbon dioxide for methanol production. Chemical Engineering Transactions, 29, 181-186. doi:10.3303/CET1229031

Vanhove, A., 2015. Improvements on the design of carbon dioxide conversion to methanol process using Aspen Plus® interface, Lisbon: Instituto Superior Técnico.

Zamani, A. H. & Abdullah, N. H., 2018. Modeling and optimization of carbon dioxide methanation via in situ hydrogen generated from aluminum foil and alkaline water by Box–Behnken design. Journal of the Taiwan Institute of Chemical Engineers, Issue 82, pp. 156-182. doi:10.1016/j.jtice.2017.11.013

Zargari, N., Jung, E., Lee, J.-H. & Jung, K. W., 2017. Carbon dioxide hydrogenation Efficient catalysis by an NHC-amidate Pd(II) complex. Tetrahedron Letters, Issue 58, pp. 3330-3332. doi:10.1016/j.tetlet.2017.07.040

Zhanghuai, S. & Yuan, K., 2000. Synthesis of Light Hydrocarbons from Carbon Dioxide and Hydrogen over Fe/ZrO2 or Fe/TiO2 Catalysts. Journal of Natural Gas Chemistry, 9(4), pp. 283-292.

Zhao, Y., Qian, X., Zhao, X. & Zhang, Z., 2018. Hydrogenation of Carbon Dioxide under Atmospheric Pressure and Low Temperature. International Journal of Hydrogen Energy, 43(5) pp. 3062-3069. doi:10.1016/j.ijhydene.2017.12.124

Zhenya, Y., Weiping, D., Qinghong, Z. & Ye, W., 2013. Hydrogenation of carbon dioxide to light olefins over non-supported iron catalyst. Chinese Journal of Catalysis, Issue 34, pp. 956-963. doi:10.1016/S1872-2067(12)60559-2.

5. P-Graph analysis

The model required to analyze the aforementioned case studies can be subdivided into data around which the model is built, the costing procedure required for the economic analysis, the constraints and equations associated in the analysis procedure, as well as the criterion required for reducing the search space.

5.1. The development of Aspen Plus ® Simulations

Before developing the model required to analyze the aforementioned 85 case studies, additional data was required. This data was found through the use of Aspen Plus ® Simulation software, and involved developing a separate simulation for each of the case studies derived in the P-Graph. In order to maintain consistency across all 85 case studies, a generic flowsheet structure was followed for all of the sub-reactions in each case study. This implied that if a case study contained three sub-reactions within the reaction system, the generic flowsheet structure was repeated three times. Figure 8 shows the generic flowsheet structure.

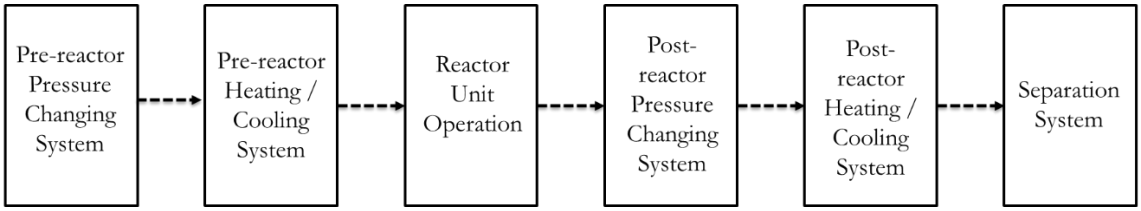

Figure 8: Generic flowsheet structure of Aspen Plus ® Simulations

However, in any simulation environment, there is a certain degree of uncertainty that exists within the model. This uncertainty is brought about by a lack of information that is available. In order to overcome such a challenge, assumptions are introduced and implemented into the model, to provide a basis on which the model can be built. This was also the case in developing each model on the Aspen Plus ® software. These assumptions included:

- All reactors utilized were RStoich reactors, as the reactions, and their associated conversions, are directly extracted from literature.

- Pressure-driven and heat transfer unit operations were broken up in series, to keep the energy usages and heat transfer areas of each individual unit within the ranges established in the design of similar unit operations (Turton et al., 2009). These limitations are detailed in Section 5.2.2, which deal with the costing constraints.
- All pressure-driven unit operations had a mechanical efficiency of 72% (U.S. Department of Energy: Industrial Technologies Program, 2006).
- The recycle to purge ratio in all simulations was set at a 90/10 split, respectively.
- Where no reaction conversion was found in literature, a Gibbs Free Reactor was used in Aspen Plus ® to obtain an estimation of the conversion expected under the specified conditions.

Paired with the assumptions detailed above, the following data were extracted from Aspen Plus ® for each case study:

The Mass Balance

- The flow rates of all outlet streams, including waste, intermediates and products
- The purity of the product streams
- The amount of CO_2 and H_2 fed into the plant
- The amount of unreacted CO_2 and H_2 in the waste stream

The Energy Balance

- The type of material for the construction of the unit operations
- The capacity (kW) of all the pressure-driven unit operations
- The heat transfer area for all heat exchanger unit operations
- Heat released or taken in by heat exchangers, reactors and separation unit operations
- Physical sizing of heat exchanger unit operations and all separation unit operations

5.2. The costing of unit operations

The procedure utilized in the costing of unit operations was developed by Turton et al. (2009). The following subsections detail the costing procedure, as well as the constraints associated with this procedure.

5.2.1. Costing procedure

The procedure to cost equipment unit operations, including heat exchangers, compressors, turbines, process vessels and towers, were as follows (Turton et al., 2009). All of the constants required, tables and graphs can be found in Appendix C.

- *Step 1:* Calculate the C_p^o value based on Equation (33).

$$log_{10}C_p^o = K_1 + K_2 log_{10}(A) + K_3\big(log_{10}(A)\big)^2 \quad (33)$$

Equation (33) calculates the purchased ambient cost at standard conditions (C_p^o) using the capacity of the unit operation (A) and the purchased cost constants (K_1, K_2 and K_3).

- *Step 2:* Calculate the pressure factor of the unit operation using Equation (34). This step did not occur for the compressors, pumps and turbines.

$$log_{10}F_p = C_1 + C_2 log_{10}P + C_3(log_{10}P)^2 \quad (34)$$

Equation (34) calculates the pressure factor (F_p) using the operation pressure of the unit operation (P) and the pressure factor constants (C_1, C_2 and C_3).

For process vessels, and towers, the pressure factor is calculated by means of Equation (35). However, if the pressure within the process vessel is less than 0.5 barg, the pressure factor (F_p) is 1.25.

$$F_p = \frac{\dfrac{(P+1)*D}{2\big(850 - 0.6(P+1)\big)} + 0.00315}{0.0063} \quad (35)$$

Equation (35) calculates the pressure factor (F_p) of a process vessel using the operating pressure of the unit (P) and the diameter (D).

- *Step 3:* The material factor (F_M) was dependent on the material of construction for the unit operation (Turton et al., 2009). The material factor identification numbers and the associated graph is depicted in Appendix C of this dissertation.

- *Step 4:* The costing equation developed by Turton et al. (2009) costs all unit operations as per the year 2001. This cost was termed the bare module cost, and was used as a cost basis when accounting for inflation. The bare module cost as per 2001 can be calculated

using Equation (36). Unit operations that do not require the calculation of a pressure factor, i.e. compressors, pumps and turbines, are costed using Equation (37).

$$C_{BM} = C_p^o(B_1 + B_2F_MF_P) \quad (36)$$

$$C_{BM} = C_p^oF_{BM} \quad (37)$$

Equation (36) and (37) calculated the bare module costs of the unit operations (C_{BM}) using the purchased cost at ambient conditions (C_p^o), the material factor (F_M), the pressure factor (F_p), the bare module factor (F_{BM}) and the bare module cost constants (B_1 and B_2).

- *Step 5:* With the bare module cost as per 2001 having been calculated, the effect of inflation on the unit operation cost needs to be accounted for. The Chemical Engineering Cost Price Index (CEPCI) accounts for inflation.

$$Cost\ in\ 2018 = Cost\ in\ 2001 * \frac{CEPCI_{2018}}{CEPCI_{2001}} \quad (38)$$

Trays are utilized in distillation columns, and are able to provide liquid holdup, thereby achieving the vapor-liquid mass transfer that is required for separation in the distillation column. The costing of the trays however, were slightly different from the other unit operations, as the number of trays also needs to be taken into account. For this costing procedure, steps 1 and 5 remain the same however, steps 2, 3 and 4 are as follows:

- *Step 2 for trays:* The quantity factor (F_q) for the trays was calculated using Equation (39). This equation only applies when the number of trays (N) is less than 20. If the number of trays exceeds 20, the quantity factor is 1.

$$log_{10}F_q = 0.4771 + 0.08516log_{10}N - 0.3473(log_{10}N)^2 \quad (39)$$

- *Step 3 for trays:* The bare module factor (F_{BM}) was dependent on the material of construction for the unit operation (Turton et al., 2009). The bare module factors are given in Appendix C of this dissertation.

- *Step 4 for trays:* The bare module cost is calculated using Equation (40).

$$C_{BM} = C_p^o * N * F_{BM} * F_q \quad (40)$$

This costing was completed by means of a MATLAB code. The MATLAB codes that are utilized in the costing of the unit operations are given in Appendix D.

5.2.2. Costing capacity limits

The costing limits specifically focus on the size and capacity of the various unit operations within each case study. Each Aspen Plus ® Simulation was altered to abide by these constraints. All equations detailed in Section 5.2.1 were subject to these constraints, and must be adhered to, for the costing equations to provide accurate results. Table 5 details the unit operations as well as their associated capacity limits (Turton et al., 2009).

Table 5: Unit operation capacity limits associated with the costing procedure and equations

Unit Operation	Type	Capacity Units	Min Size	Max Size
Compressors	Centrifugal, Axial and Reciprocating	Fluid power, kW	450	3,000
	Rotary	Fluid power, kW	18	950
Heat Exchangers	Scraped Wall	Area, m^2	2	20
	Teflon Tube	Area, m^2	1	10
	Bayonet	Area, m^2	10	1,000
	Floating Head	Area, m^2	10	1,000
	Fixed Tube	Area, m^2	10	1,000
	U-Tube	Area, m^2	10	1,000
	Kettle Reboiler	Area, m^2	10	100
	Double Pipe	Area, m^2	1	10
	Multiple Pipe	Area, m^2	10	100
	Flat Plate	Area, m^2	10	1,000
	Spiral Plate	Area, m^2	1	100
	Air Cooler	Area, m^2	10	10,000
	Spiral Tube	Area, m^2	1	100

Process Vessels	Horizontal	Volume, m^3	0.1	628
	Vertical	Volume, m^3	0.3	520
Pumps	Reciprocating	Shaft power, kW	0.1	200
	Positive Displacement	Shaft power, kW	1	100
	Centrifugal	Shaft power, kW	1	300
Towers	Tray and Packed	Volume, m^3	0.3	520
Trays	Sieve	Area, m^2	0.07	12.30
	Valve	Area, m^2	0.70	10.50
	Demisters	Area, m^2	0.70	10.50
Turbines	Axial Gas Turbines	Fluid power, kW	100	4,000
	Radial Gas/Liquid Expanders	Fluid power, kW	100	1,500

5.2.3. Breakdown of unit operations

In order to abide by the capacity limits detailed in Section 5.2.2, many of the unit operations lying outside of these ranges were broken down into a series of unit operations. By doing so, this reduces the energy capacity of each unit operation, thereby allowing for each individual unit operation to lie within the allotted ranges. For example, a single compressor unit operation going from 1 bar to 300 bar requires a lot of energy, and can be deemed to be impractical. This compressor can be broken up into a series of compressor unit operations with incremental pressure changes. This can be represented diagrammatically in Figure 9.

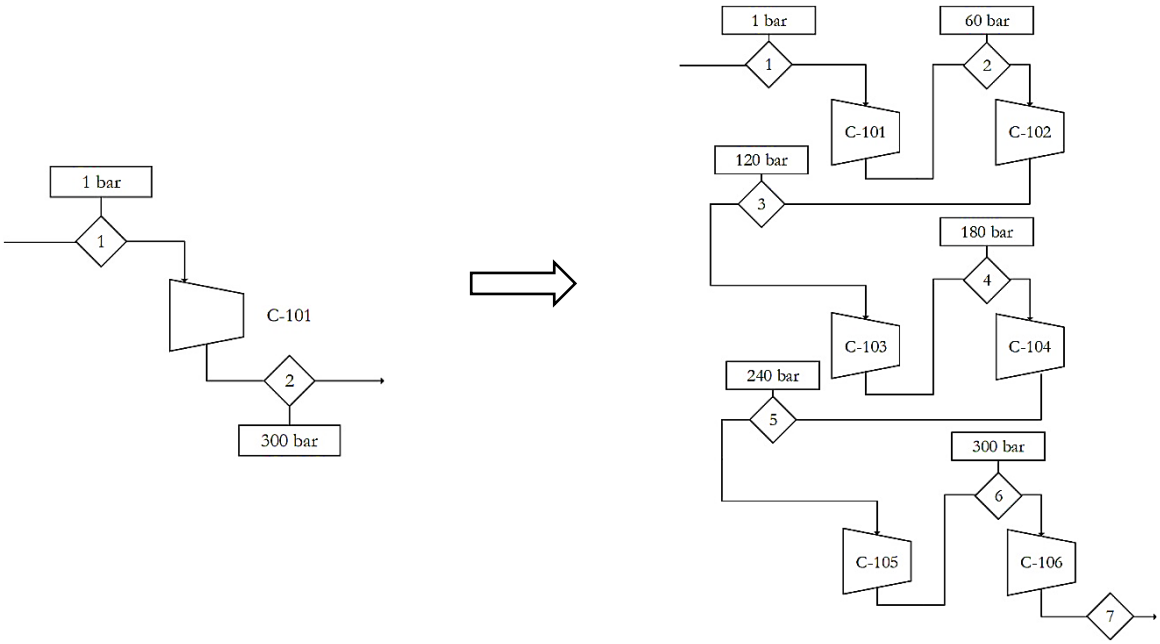

Figure 9: Diagrammatic representation of the breakdown of unit operations

5.3. Model constraints

Based on the data that has been extracted from the Aspen Plus ® Simulations and the costing procedure detailed in Section 5.2, additional equations were required in the analysis. One of the most important factors to be considered in the construction of any process, is the economic investment needed. In order to calculate the total capital cost, excluding reactor unit operations, required for each individual case study, the total cost of the unit operations needs to be calculated. This was done by means of the following mathematical equations:

$$HE_{Total} = \sum_{i_{HE}=1}^{n_{HE}} C_{i_{HE}} \tag{41}$$

$$P_{Total} = \sum_{i_P=1}^{n_P} C_{i_P} \tag{42}$$

$$S_{Total} = \sum_{i_S=1}^{n_S} C_{i_S} \tag{43}$$

$$C_{Total} = HE_{Total} + P_{Total} + S_{Total} \tag{44}$$

Equations (41), (42) and (43) show that the total cost of heat exchanger unit operations (HE_{Total}), pressure-driven unit operations (P_{Total}) and separation unit operations (S_{Total}) were calculated as the summation of the individual unit operations within the case study, i.e. $C_{i_{HE}}$, C_{i_P} and C_{i_S}, respectively. Equation (44) states that the total unit operation cost (C_{Total}) was calculated by summing all of the total costs calculated from Equation (41), (42) and (43).

Energy can be subdivided into either heat energy (Q) or work (W). Before considering how these energy requirements should be met, the total energy required to operate all unit operations needed to be calculated. This was done by means of the following mathematical equations:

$$Q_{Total} = \sum_{i=1}^{n} Q_i \tag{45}$$

$$W_{Total} = \sum_{j=1}^{m} W_j \tag{46}$$

$$E_{Total} = Q_{Total} + W_{Total} \tag{47}$$

Equations (45) and (46) show that the total heat (Q_{Total}) and work (W_{Total}) required in a process was calculated as the summation of the heat and work done by each unit operation, i.e. Q_i and W_j, respectively. The total energy requirements of the plant (E_{Total}) was calculated as the summation of the total heat and work energy.

With the total energy requirements of the plant in each case study, being known, the amount and cost of NG required to power such a plant can be calculated. Unfortunately, when utilizing NG to meet energy requirements, CO_2 is also produced. This is discussed more extensively in Section 5.4.2. The following mathematical equations deal with calculating the values associated with the utilization of NG:

$$m_{NG} = \frac{E_{Total}}{HV_{NG}} \tag{48}$$

$$m_{CO_2\ Produced} = \frac{m_{NG}}{M_{CH_4}} * M_{CO_2} \tag{49}$$

$$C_{Total\ NG} = C_{NG} * E_{Total} \tag{50}$$

Equation (48) calculates the mass of NG (m_{NG}) required to power all of the unit operations, by dividing the total energy requirements of the plant by the heating value of NG (HV_{NG}). Equation (49), on the other hand, uses the stoichiometric ratio of NG to CO_2 during the combustion of methane, to calculate the mass of CO_2 produced ($m_{CO_2\ Produced}$) from the NG combustion. This calculation utilizes the molar mass for both methane (M_{CH_4}) and CO_2 (M_{CO_2}). Equation (50) calculates the total cost of NG required ($C_{Total\ NG}$), by utilizing the cost of NG per energy unit (C_{NG}), and the total energy requirement of the plant.

The annual profit or loss of a plant was determined by taking into account the inlet and outlets streams of the plant, i.e. drawing a comparison between the expected sales revenue and the cost of reactants required. This also provided an estimation as to the payback period of the initial capital investment of the plant, assuming no external cost factors such as labor. In order to perform such calculations, the following mathematical equations were utilized:

$$m_{CO_2\ Purchased} = m_{CO_2\ Fed} - m_{CO_2\ Produced} \tag{51}$$

$$C_{RM} = \sum_{k=1}^{a} (m_k * C_k) \tag{52}$$

$$SP_{Products} = \sum_{l=1}^{b} (m_l * SP_l) \tag{53}$$

$$Profit = SP_{Products} - (C_{RM} + C_{Total\ NG}) \tag{54}$$

$$PBP = \frac{C_{Total}}{Profit} \tag{55}$$

Equation (51) calculated the net CO_2 benefit of the plant ($m_{CO_2\ Benefit}$) as the difference in the mass of CO_2 being fed into the plant ($m_{CO_2\ Fed}$) and the mass of CO_2 produced ($m_{CO_2\ Produced}$) from NG combustion. Equations (52) and (53) calculated the annual feed cost (C_{RM}) and sales potential ($SP_{Products}$) of the plant. These calculations utilize the mass flow rate of feed (m_k) or product (m_l), along with its associated cost (C_k) or sales potential (SP_l). Equation (54) was utilized in calculating the profit of each plant as the difference between the annual sales potential of the products, and the annual cost of the feed and NG utility. The payback period (*PBP*) was calculated by means of Equation (55), which shows the time taken to pay off all unit operations (C_{Total}) based on the annual profit from Equation (54).

In order to account for the annual cost of owning the unit operations, as well as maintaining these assets, the equivalent annualized cost was required. This formula is generally utilized as a capital budgeting tool, and compares projects that have different lifespan (Smith, 2005). This value was important in ranking each of the case studies over the duration of 1 year. The following mathematical equations were involved in these calculations:

$$CRF = \frac{r}{1-(1+r)^{-n}} \tag{56}$$

$$ACC = CRF * C_{Total} \tag{57}$$

$$Operational\ Cost\ per\ Annum = C_{RM} + C_{Total\ NG} \tag{58}$$

$$Performance\ Index\ (Z) = \frac{m_{CO_2\ Purchased}}{ACC + Operational\ Cost\ per\ Annum} \tag{59}$$

Equation (56) calculates the capital recovery factor (*CRF*) by utilizing the annual discount rate (r) and the lifespan of the plant (n). This factor was utilized in the calculation of the annualized capital cost (*ACC*), as per Equation (57). The total feed operational cost per annum was a summation of the raw material cost (C_{RM}) and the NG cost ($C_{Total\ NG}$). Equation (59) shows the performance index that was utilized in ranking the reduced workspace. This performance index is explained in Section 5.4.4.

5.4. Analysis criteria

Each case study was analyzed individually, before being compared to another. This section details the criteria that were utilized whilst reducing the search space derived from the P-Graph.

5.4.1. Criterion 1: Economic viability

The main aim behind the development and analysis of the P-Graph, was to find the pathway that is most geared towards both environmental and economic benefits. This first criterion focuses solely on the economic standpoint of the analysis, whilst also taking into account the energy required to meet the operating conditions of each reaction pathway. As per Equation (55) above, the lowest possible payback period was found by dividing the total equipment cost, excluding the reactors, by the annual profit. It was within this annual profit calculation

(Equation (54)) that the energy requirements were taken into account, with the cost of NG utility being dependent on the mass of NG required to produce the energy requirements of each case study.

Furthermore, when looking at the remaining two terms of Equation (54), the complexity of the equation becomes evident. The sales potential of the product takes into account the separation system required to achieve the necessary market purity. The annual cost of the reactant gas takes into account the cost required to scrub the CO_2, assuming an impure CO_2 feed stream, as well as the cost required to produce H_2 by means of an electrolyzer unit.

It is important to note, however, that the payback period calculated in Equation (55) only incorporated part of the cost factors required during the operation of the plant. Other factors that were not factored into the payback period included labor, land, transportation and maintenance (Smith, 2005).

When the annual profit calculation yields a negative value, this implies that the sales potential is lower than the cost of the reactants and utilities, indicating a loss. When such a scenario occurs, this immediately shows that the plant will not be able to be sustained financially. Such case studies were deemed infeasible. The reasoning here was that only basic input/output costs were factored into the payback period. During the construction and operation of a plant, many additional costs are incurred. As a result, this will only further increase the loss of the plant, reaffirming the fact that the plant will not be able to be sustained financially.

5.4.2. Criterion 2: Environmental impact

This criterion analyzed the case studies from an environmental perspective. Although the economic standpoint was extremely important, equal attention needs to be paid to the environmental benefits that each scenario provided. Although there are many environmentally friendly ways in which to produce energy, such as solar power, wind power and hydroelectric power, this dissertation employed the use of NG as the primary energy source. The reasoning behind this choice was in the low efficiencies that were noted in renewable energy sources. Furthermore, the use of NG reduced the need of the plant to rely on the current electricity grid, which is primarily coal powered.

Assuming that the NG is primarily composed of methane, the combustion of the NG produces water and CO_2 by means of the following equation:

$$CH_4 + 2O_2 \rightarrow CO_2 + H_2O \quad (60)$$

The CO_2 produced was compared to the CO_2 fed into the plant. Should this value be higher than that being fed into the plant, it would imply that the net effect of the plant will involve the production of CO_2, thus adding to the environmental concerns being faced.

Therefore, in order for a case study to be deemed environmentally beneficial, the CO_2 produced should be less than that fed into the process. This could then be deemed as a carbon negative process. Such a scenario would result in both environmental and economic benefits, including:

- A portion of the current atmospheric CO_2 emissions were being taken into the plant, thereby resulting in an environmental benefit.
- The CO_2 produced in the combustion of methane, could be recycled and fed directly into the plant once the process is operating at steady state conditions. This lowers the amount of CO_2 that needs to be purchased, thereby becoming an economic benefit.

5.4.3. Criterion 3: Analysis of the payback period

One of the most important factors surrounding an economic analysis, is the investment opportunities of the project. Potential investors pay special attention to the return they can expect to see on their investment, and how long it would take for them to see this return. This time period is dictated by the payback period of the plant. The payback period is dependent on various factors including the industry, the size of the investment, plant and equipment life, and the cost of capital. The plants presented in the case studies produce over 200,000 tons of product per annum.

Due to this production rate, these case studies were classified as being medium to large production plant, which should ideally have a payback period of between 2 and 10 years (leanmanufacture.net, 2009), for the project to be deemed a feasible investment.

5.4.4. Criterion 4: Catalyst cost and performance index

The reduced search space was further analyzed by accounting for the catalyst that was required in each scenario, as well as using a performance index in order to rank each scenario from the most viable to the least viable option.

The economic value of the catalysts was looked into from a broad approach. In order to conduct this economic analysis, there were four major catalyst assumptions that were made:

i. There was no deactivation function for the catalysts. All catalysts were assumed to operate at a consistent efficiency throughout their lifespan. This was a simplifying assumption, as many deactivation functions were not available in literature for the required catalyst compositions.
ii. The catalysts are replaced on an annual basis, allowing for the catalyst cost to be easily integrated into the annual profit or loss calculations.
iii. All catalysts are costed per tonnage.
iv. There were no conversion costs associated with these catalysts. The conversion costs refer to the cost incurred in order to convert the catalyst from its components to its useful state for the reaction to take place.

The main aim of this systematic framework was to determine the most efficient pathway, whilst remaining environmentally and economically beneficial. When approaching this problem from a mathematical perspective, the performance index can be used to quantify both these benefits, thus making it easier to find the case study that has the best draw off between the two factors in question. This also allows for the remaining case studies to be ranked from the most viable to the least viable option.

The performance index (Z) is given by Equation (59) in Section 5.3, and is the ratio of CO_2 intake of the process to the annual costs associated with the scenario. In order to achieve the best possible performance from a given scenario, this ratio was maximized. Maximizing this relationship implied finding a draw off between the environmental and economic benefits of the case study. A high intake in CO_2 is an environmental benefit, whereas a low cost is an economic benefit.

5.5. References

Aspen Plus V10 (2018), USA, Aspen Technology, Inc.

leanmanufacture.net. (2009). Payback Period. (leanmanufacture.net) Retrieved September 3, 2018, from http://www.leanmanufacture.net/kpi/paybackperiod.aspx

Smith, R. (2005). Chemical Process design and Integration. West Sussex, England: John Wiley & Sons Ltd.

Turton, R., Bailie, R. C., Whiting, W. B., & Shaelwitz, J. A. (2009). Analysis, Synthesis and Design of Chemical Processes. United States of America: Pearson Education Inc.

U.S. Department of Energy: Industrial Technologies Program . (2006). Improving Pumping System Performance: A Sourcebook for Industry. Washington, DC: Energy Efficiency and Renewable Energy (EERE).

6. Application of systematic framework

The systematic framework developed and explained in this dissertation was applied to the CO_2/H_2 RPD created during the development of the P-Graph model. This RPD is given in Section 4.2. The application of this framework was subdivided into two main components, namely the constants used in the application and the results thereof.

6.1. Data utilized in analysis

The following subsections detail the data required for the P-Graph to be analyzed from an economic perspective.

6.1.1. Cost of reactants and utilities

There were 3 main feed streams required for these case studies, which were divided into two categories i.e. the reactants, CO_2 and H_2, and the Natural Gas (NG) utility. The energy required for operation of the plant was met and produced using NG. This design decision was solely based on an environmental perspective. NG has proven to have a lower carbon footprint in comparison to coal (Liang et al., 2012). Furthermore, NG was chosen in order to alleviate some of the strain that is being placed on the current electricity grid. Table 6 gives the cost data that was utilized for the feed streams that are entering the process.

Table 6: Cost of raw materials or reactants required for the case studies and the utility required

Feed	Cost	Units	Reference
CO_2	100.00	$/ton	(Keith et al., 2018)
H_2	1,000.00	$/ton	(Kayfeci et al., 2019)
NG	3.02	$/MMBtu	(Motiang & Nembahe, 2018)

It was expected that the cost of CO_2 would be zero, or perhaps even a negative cost, i.e. implying a revenue, due to the fact that this compound is considered a waste product. However,

in many of these cases, the CO_2 would also contain impurities, as is the case with flue gas. The cost of CO_2 provided in Table 6 was the cost of purchasing pure CO_2, i.e. with no impurities. This study worked from a worst-case scenario perspective in determining economic feasibility. Therefore, should the case arise where the cost of CO_2 was reduced to zero or a negative cost, the profitability of the feasible scenarios would increase substantially.

6.1.2. Cost of catalysts

Due to the fact that many of the catalysts required in the RPD could not be purchased with the compositions that were required for the reactions, the catalysts components were first costed, and then the catalyst cost was found using the compositions given in literature. Table 7 gives the component costs that are associated with the catalysts.

Table 7: Cost of each individual component required for the catalysts needed in each case study

Catalyst Comp	Cost ($/ton)	Reference
Copper	6,613.87	(Bernhardt & Reilly, 2019)
Zinc	3,196.71	(Bernhardt & Reilly, 2019)
Aluminium	2,535.32	(Bernhardt & Reilly, 2019)
Cobalt	83,775.73	(Bernhardt & Reilly, 2019)
Graphite	1,480.00	(Bernhardt & Reilly, 2019)
Silicon Metal	3,042.38	(Bernhardt & Reilly, 2019)
Palladium	28,875,033.00	(Bernhardt & Reilly, 2019)
Oxygen	40.00	(Dorris et al., 2016)
Hydrogen	1,000.00	(Kayfeci et al., 2019)
Zirconium	1,500.00	(Bernhardt & Reilly, 2019)

Using these component costs, the cost of each individual catalyst was calculated. Table 8 gives all of the catalyst combinations that were required during the analysis procedure, and their associated costs. The catalyst composition was extracted from the RPD and the sources from which the reaction was extracted.

Table 8: Catalyst costs with their respective mass compositions

Catalyst	Mass Composition	Cost ($/ton)
Palladium Oxide (PdO)	0.87 : 0.13	25,101,071.41
Zinc Oxide	0.80 : 0.20	2,576.10
Aluminium Oxide	0.53 : 0.47	1,360.52
Copper Oxide	0.80 : 0.20	5,291.86
Silicon Dioxide	0.47 : 0.53	1,443.31
Zirconium Dioxide	0.74 : 0.26	1,120.84
Hydrogen Peroxide	0.06 : 0.94	37.63
Cobalt Silicon Dioxide	0.50 : 0.50	32,668.97

6.1.3. Sales potential of products

Although each of the simulations were restricted to focus on a single product being produced, it is important to note that some of the unreacted intermediates may also be potentially sold to generate additional revenue, thereby increasing the profitability of that scenario. For example, when considering the production of DME from MeOH, the DME would be considered to be the primary product, however, the unreacted MeOH could also be sold as an additional 'product' stream, but in smaller quantities. In order for this to occur, however, the unreacted MeOH needs to be of a sufficiently high purity, allowing it to be sold in the current MeOH market. This required additional separation unit operations when developing the Aspen Plus ® simulations. Table 9 gives the sales potential of the products and intermediates that were produced in each scenario.

Table 9: Sales potential of products that are produced via the various case studies

Product	Sales Potential	Units	References
MeOH	470.00	$/ton	(Jasper & El-Halwagi, 2015)
DME	720	$/ton	Price explained below
Propane	580.00	$/ton	(Argus, 2018)
Water	3.28	$/ton	(Department of Water and Sanitation, 2017)

The price of DME ranges from $450 per ton (Memon et al., 2017) to $990 per ton (Otaraku & Onyekaonwu, 2018), and was dependent on the purity of the compound. For the sake of this

research a sales potential lying in the middle of this range is assumed, i.e. $720 per ton. This allows the sales potential in this study to be competitive with the current market.

6.1.4. Additional data utilized

In addition to the economic data given above, there were also additional parameters that were required. Table 10 shows the additional data that was required for this analysis.

Table 10: Other factors that are required for the case studies to be analysed

Parameter	Value	Units	Date	Reference
CEPCI	576.40	-	Jan 2018	(Fichani & Masialeti, 2019)
Heat Value of NG	0.055	GJ/kg	-	(Beedu & Modi, 2014)
Loan Interest Rate	10.25	%	Jan 2019	(Matebeni et al., 2019)

Additionally, a plant lifespan of 10 years was assumed when calculating the annualized capital cost. This is the upper limit of the payback period in Criterion 3 (Section 5.4.3), and therefore it is assumed that the plant will run for this duration.

6.2. Application of reduction criteria 1 to 3

As per the P-Graph model developed in Chapter 4, there were 85 case studies that were to be analyzed using the systematic framework developed and detailed in this dissertation. The application of the first three criteria results in the following reduction in the search space:

- Criterion #1 – The economic viability criterion was able to reduce the search space to 13 possible case studies, all dealing with the production of MeOH and DME from the direct approach. These remaining 13 possible pathways were case studies 5, 6, 7, 8, 9, 11, 12, 13, 14, 15, 16, 17 and 19.
- Criterion #2 – The environmental impact criterion was able to reduce the remaining search space to a mere 9 case studies. The remaining 9 case studies were case studies 6, 7, 8, 9, 12, 14, 15, 16 and 17.

- Criterion #3 – Upon further analysis of the payback period, 3 case studies had payback periods outside of the range given in this criterion, thereby reducing the search space to 6 case studies.

6.3. Application of reduction criterion 4

Of the 6 remaining case studies, three were involved in the production of MeOH, i.e. Case Studies 6, 7 and 8, whilst the remaining three dealt with the production of DME, i.e. Case Studies 14, 15 and 16. This section elaborates on the application of the fourth criterion, whilst also providing an analysis on the remaining six case studies. The purpose of this discussion is to compare the analysis with the performance index, thereby validating the ranking of the final, reduced search space.

6.3.1. Costing of the catalysts

Table 11 shows the catalyst specifications required for the MeOH production scenarios.

Table 11: Catalysts and compositions required for the production of MeOH from the reduced case study workspace

Case Study	6	7	8
Catalyst	CZA-PdO	$Cu/ZnO/Al_2O_3$	$CuO/ZnO/Al_2O_3$
Mass Composition	27:15:3:5	16:21:13	26:15:9
Cost ($/ton)	2,514,777.02	3,569.66	3,776.89

Table 12 shows the case study number and the catalysts required for the DME production pathways, with catalyst #1 being that which was required for the MeOH production and catalyst #2 being the one needed for MeOH dehydration to DME. The reaction system was a combination of Equations (6) and (13).

Table 12: Catalysts and compositions required for the production of DME from the reduced case study workspace

Case Study	14	15	16
Catalyst #1	CZA-PdO	$Cu/ZnO/Al_2O_3$	$CuO/ZnO/Al_2O_3$
Mass Composition #1	27:15:3:5	16:21:13	26:15:9
Cost #1 ($/ton)	2,514,777.02	3,569.66	3,776.89
Catalyst #2	Al/Si	Al/Si	Al/Si
Mass Composition #2	9:91	9:91	9:91
Cost #2 ($/ton)	2,998.37	2,998.37	2,998.37

6.3.2. Analysis of the methanol production pathways

Based on the data gathered from previous stages in this systematic framework, Table 13 gives the information relevant to the MeOH production case studies.

Table 13: Important data for final MeOH production workspace

Case Study	6	7	8
Total Unit Operation Cost ($x10^6$) (USD)	12.94	26.69	12.93
MeOH Production Rates ($x10^4$) (tons/annum)	2.35	2.46	2.50
CO_2 Purchased ($x10^3$) (tons/annum)	16.55	4.41	16.70
Annual Profit ($x10^6$) (USD)	3.62	4.67	4.34
Payback Period Before Catalyst Cost (years)	3.57	5.68	2.98
Payback Period After Catalyst Cost (years)	11.65	5.69	2.98
Performance Index ($x10^{-3}$)	1.72	0.39	1.73

Looking at this data from an analytical perspective, Table 13 shows that Case Study 6 had the greatest change in payback period after accounting for the annual replacement of the catalyst. Table 11 shows that Case study 6 had highest costing catalyst, due to the presence of palladium. Palladium is a rare transition metal, and ideally is not viable to use in large scale production plants due to its cost and lack of availability. Furthermore, Case study 6 had the lowest production rate of MeOH per annum. This showed that the extra cost incurred, due to the catalyst, was not offset by the production rate and as a result, was not as viable in comparison to the other two case studies presented. Furthermore, the cost of the catalyst in Case Study 6

had a major impact on the payback period, with the payback period increasing from 3.49 years to 11.99 years. As per Criterion 3, this payback period was outside of the feasible range (leanmanufacture.net, 2009).

When comparing Case Studies 7 and 8, it was seen that the production rate and profits yielded in both scenarios were very similar, with almost no significant distinguishing differences. As a result, the comparison factors for these two scenarios were dependent on the additional CO_2 required for the process, and the payback period after the catalyst had been considered. Case Study 8 takes in almost 4 times more CO_2 than Case Study 7, and had a payback period almost half that of Case Study 7. This shows that Case Study 8 had a greater environmental benefit, whilst also maintaining a good economic standpoint.

Looking at the performance index value for these three case studies, it was noted than the performance index aligns with the final outcome of the analysis, showing that Case study 8 was the most favorable of the three scenarios. However, Case Study 6, which was analytically deemed to be the least viable of the three options, was in fact more feasible than Case Study 7. This was due to the operating conditions of Case Study 6 being a lot lower than that which was necessary for Case Study 7. Case Study 6 operated at a pressure of 40 bar, whereas Case Study 7 operated at 330 bar. This resulted in Case study 7 being much more energy intensive, thereby reducing its feasibility.

Therefore, the ranking of the MeOH production pathways, in order from most to least viable option, was Case Study 8, Case study 6 and Case Study 7.

6.3.3. Analysis of the DME production pathways

The same analysis technique in section 6.3.2 was conducted for the DME production pathways. Table 14 gives the important data regarding the three DME pathways remaining after search space reduction.

Table 14: Important data for final DME production workspace

Case Study	14	15	16
Total Unit Operation Cost ($x10^6$) (USD)	15.22	29.01	15.26
DME Production Rates ($x10^4$) (tons/annum)	1.63	1.71	1.73
CO_2 Purchased ($x10^3$) (tons/annum)	15.02	2.80	15.06
Annual Profit ($x10^6$) (USD)	4.49	5.60	5.27
Payback Period Before Catalyst Cost (years)	3.39	5.18	2.89
Payback Period After Catalyst Cost (years)	7.70	5.18	2.90
Performance Index ($x10^{-3}$)	1.51	0.24	1.52

Looking at the data in Tables 12 and 14 from an analytical perspective, Case Study 14 had the highest catalyst cost with the lowest production rate, and the longest payback time after accounting for the catalyst. As with Case Study 6 in the MeOH production pathways, this case study utilized a palladium catalyst.

For Case Studies 15 and 16, the deciding factors were the CO_2 required to be fed into the plant, and the payback periods, due to the close proximity of the values noted in the production rates and the annual profits. These two factors accounted for both the environmental and economic standpoints, respectively.

Table 14 shows that the payback period of Case study 16 was almost half that of Case Study 15, and utilized over five times more CO_2, leading to a better economic and environmental benefit being obtained from Case Study 16. Therefore, this case study was chosen as being the most viable option by which to produce DME.

When analyzing all of the scenarios by means of the performance index, Case Study 16 was the most viable option. However, Case Study 14, which was analytically deemed to be the least feasible option, was in fact the second most viable option to produce DME. As with the MeOH production case studies, this was due to the operating conditions of Case Study 15 being much higher than Case Study 14, thereby having a higher energy requirement to operate the plant.

The ranking of the DME production plants in order of most viable to least viable option was Case Study 16, Case Study 14 and Case Study 15.

6.4. Final ranking of reduced search space

Based on the analysis conducted, the search space of reaction pathways was able to be reduced from 85 possible case studies, to a mere 6 possible scenarios, all of which were deemed feasible options. This was a 93% reduction in the original search space. Table 15 gives the ranking of the 6 remaining case studies from most viable option to the least viable option, along with their associated reactions, operating conditions, catalysts, conversions noted in literature, and their respective performance index (Z), as is given by Equation (59) and detailed in Section 5.4.4.

Table 15: Final ranking of the reduced workspace in order of viability

Rank	CS	Reaction	Temp (°C)	Press (bar)	Catalyst	X_{CO2} (%)	Z
#1	8	$CO_2 + 3H_2 \leftrightarrow CH_3OH + H_2O$	240	80	$CuO/ZnO/Al_2O_3$	96.00	1.73
#2	6	$CO_2 + 3H_2 \leftrightarrow CH_3OH + H_2O$	200	40	CZA-PdO	61.54	1.72
#3	16	$CO_2 + 3H_2 \leftrightarrow CH_3OH + H_2O$	240	80	$CuO/ZnO/Al_2O_3$	96.00	1.52
		$2CH_3OH \rightarrow CH_3OCH_3 + H_2O$	400	25	Al/Si	86.76	
#4	14	$CO_2 + 3H_2 \leftrightarrow CH_3OH + H_2O$	200	40	CZA-PdO	61.54	1.51
		$2CH_3OH \rightarrow CH_3OCH_3 + H_2O$	400	25	Al/Si	86.76	
#5	7	$CO_2 + 3H_2 \leftrightarrow CH_3OH + H_2O$	260	330	Fe-Cu	93.59	0.39
#6	15	$CO_2 + 3H_2 \leftrightarrow CH_3OH + H_2O$	260	330	Fe-Cu	93.59	0.24
		$2CH_3OH \rightarrow CH_3OCH_3 + H_2O$	400	25	Al/Si	86.76	

Table 15 shows that the production of MeOH was deemed more environmentally and economically beneficial than the production of DME. This was clearly evident in the methanol case studies exhibiting a higher objective function. This agrees with the work conducted by Matzen and Demirel (2016), who also concluded that MeOH producing plants are more viable than DME producing plants.

6.5. References

Argus. (2018). Daily International LPG Prices and Market Commentary. Argus International LPG (18-22), 1-16.

Beedu, R., & Modi, P. (2014). Design of Bio Gas Generation Plant Based on Food Waste. International Journal of Current Engineering and Technology (2), 417-420.

Bernhardt, D., & Reilly, J. F. (2019). Mineral Commodity Summaries 2019. U.S. Geological Survey. Virginia: U.S. Department of the Interior. ISBN:978-1-4113-4283-5

Department of Water and Sanitation. (2017). Annual Report for 2017/18 Financial Year. Pretoria. ISBN:978-0-621-46731-4

Dorris, C. C., Lu, E., Park, S., & Toro, F. H. (2016). High-Purity Oxygen Production Using Mixed Ionic-Electronic Conducting Sorbents. Senior Design Reports, Paper 78.

Fichani, K., & Masialeti, M. (2019). Prospects for value addition in copper in the emerging Kalahari Copper Belt of Botswana. Journal of the Southern African Institute of Mining and Metallurgy, 119(10), 825-831. doi:10.17159/2411-9717/570/2019.

Jasper, S., & El-Halwagi, M. M. (2015). A Techno-Economic Comparison between Two Methanol-to-Propylene Processes. Processes, 3, 684-698. doi:10.3390/pr3030684

Kayfeci, M., Kecebas, A., & Bayat, M. (2019). Chapter 3 - Hydrogen production in Solar Hydrogen Production (pp. 45-83). Academic Press. ISBN:978-0-12-814853-2

Keith, D. W., Holmes, G., Angelo, D. S., & Heidel, K. (2018). A Process for Capturing CO_2 from the Atmosphere. CellPress Joule, 1573-1594. doi:10.1016/j.joule.2018.05.006

Liang, F.-Y., Ryvak, M., Sayeed, S., & Zhao, N. (2012). The role of natural gas as a primary fuel in the near future, including comparisons of acquisition, transmission and waste handling costs of as with competitive alternatives. Chemistry Central Journal, 6 (Suppl 1), 1-24. doi:10.1186/1752-153X-6-S1-S4

leanmanufacture.net. (2009). Payback Period. (leanmanufacture.net) Retrieved September 3, 2018, from http://www.leanmanufacture.net/kpi/paybackperiod.aspx

Matebeni, F., Dempers, C., & Verwey, R. (2019). Economic Growth and other Indicators - September 2019. Markets and Economic research Center - Macroeconomic Digest. Pretoria: National Agricultural Marketing Council (NAMC).

Memon, A. A., Sheikh, S., Siddique, M., Ishtiyaque, S., Jatoi, A. S., & Mushtaq, F. (2017). Di-Methyl Ether (DME) Prospective in Terms of Conventional Fuels in Pakistan from Gasification of Aboriginal Coal. Journal of Applied and Emerging Sciences, 7(2).

Motiang, M., & Nembahe, R. (2018). Energy Price Report. Pretoria: Department of Energy.

Otaraku, I., & Onyekaonwu, C. (2018). Process Design of Associated Natural Gas to Dimethyl Ether Production Via Direct Synthesis. International Journal of Chemical and Process Engineering, 5(1), 1-7. doi:10.18488/journal.65.2018.51.1.7

7. Limitations of framework

Much of the information utilized during this analysis, is subject to change, and depends on the time at which the analysis is being conducted. In order to determine the reliability of the information used in this analysis, as well as its effect should changes occur, a sensitivity analysis was conducted.

This analysis looked at the fluctuations in various factors, over the duration of two years. The minimum and maximum value within this duration were noted and their effect on the payback period of the most viable scenario, i.e. Case Study 8, was monitored.

7.1. Data subject to change

Table 16 shows the factors for which this sensitivity analysis was conducted, as well as the minimum and maximum values associated with each factor. All values are given in $/ton, with the exception of the CEPCI, which is dimensionless, and the Natural Gas (NG) price, which is given in $/MMBtU.

Table 16: Factors that are subject to change during this analysis

Factor	Min	Max	Reference
CEPCI	567.5	603.1	(Okoro & Sun, 2019)
NG Price	2.91	6.27	(Motiang & Nembahe, 2018)
CO_2 Cost	15	120	(Luckow et al., 2015)
CO_2 Cost (Source)	94	232	(Keith et al., 2018)
H_2 Cost (Electrolyzer)	1,000	5,640	(Meier, 2014)
H_2 Cost (GGE)	3,800	6,700	(Singh, Moore, & Shadis, 2005)
MeOH Selling Price	390	600	(Jasper & El-Halwagi, 2015)
Copper Cost	4,863.40	7,323.91	(Bernhardt & Reilly, 2020)
Zinc Cost	1,931.25	3,196.71	(Bernhardt & Reilly, 2020)
Aluminium Cost	1,772.52	2,535.32	(Bernhardt & Reilly, 2020)

7.2. Effect on most viable pathway

Using the ranges given in Table 16, the effect of these factors were monitored against the payback period of the most feasible pathway. This could be represented using a tornado diagram as per Figure 10, below.

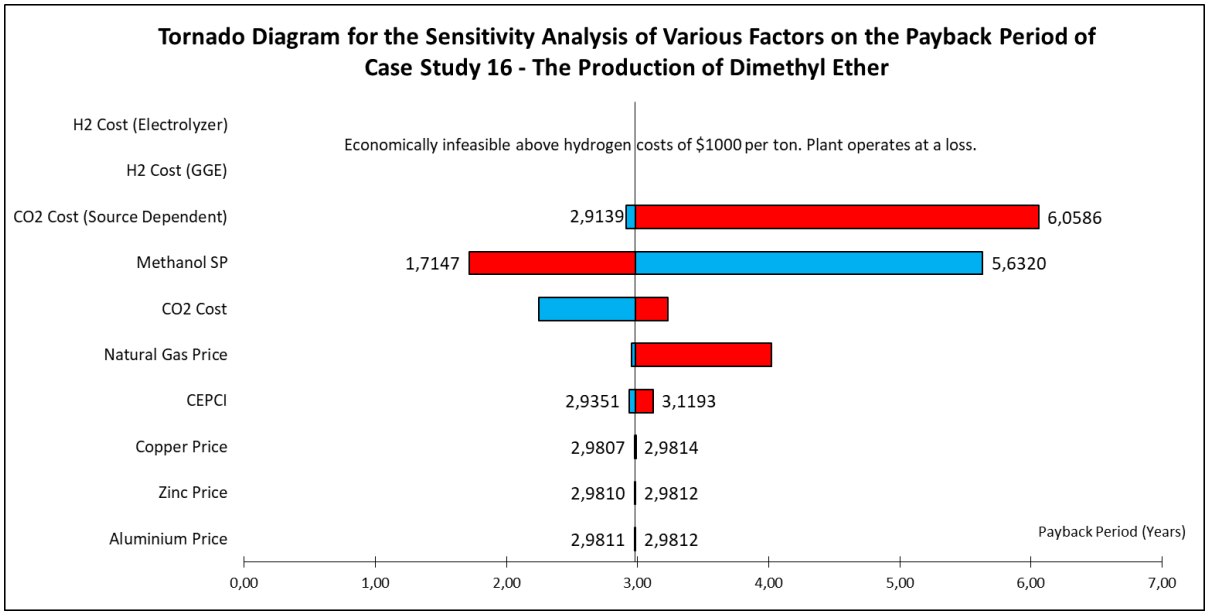

Figure 10: Tornado diagram showing the effect of various factors on the payback period of the most viable pathway (Case study 8)

Figure 10 shows that the hydrogen cost, had the greatest impact on the results noted in this dissertation. At values above $1000 per ton of hydrogen gas, Case study 8 became economically infeasible, i.e. the plant operates at a loss. As a result, no payback period could be calculated within these ranges. Other factors that had a significant impact on the results of this dissertation, aiding in determining under which economic conditions these results hold, were the sales potential of MeOH, and the cost of CO_2 and natural gas. All other factors had little impact on the payback periods, showing that changes in those factors did not alter the results of this systematic framework significantly.

This tornado diagram shows that the most influential factors were the sales potential of the products and the cost of the reactants. These economic factors were necessary in determining the annual profit expected from each scenario.

7.3. References

Bernhardt, D., & Reilly, J. F. (2020). Mineral Commodity Summaries 2020. U.S. Geological Survey. Virginia: U.S. Department of the Interior. ISBN:978-1-4113-4362-7

Jasper, S., & El-Halwagi, M. M. (2015). A Techno-Economic Comparison between Two Methanol-to-Propylene Processes. Processes, 3, 684-698. doi:10.3390/pr3030684

Keith, D. W., Holmes, G., Angelo, D. S., & Heidel, K. (2018). A Process for Capturing CO_2 from the Atmosphere. CellPress Joule, 1573-1594. doi:10.1016/j.joule.2018.05.006

Luckow, P., Stanton, E. A., Fields, S., Biewald, B., Jackson, S., Fisher, J., & Wilson, R. (2015). 2015 Carbon Dioxide Price Forecast . Massachusetts: Synapse: Energy Economics, Inc.

Meier, K. (2014). Hydrogen production with sea water electrolysis using Norwegian offshore wind energy potentials. International Journal of Energy and Environmental Engineering, 5(2), 1-12.

Motiang, M., & Nembahe, R. (2018). Energy Price Report. Pretoria: Department of Energy.

Okoro, O. V., & Sun, Z. (2019). Desulphurisation of Biogas: A Systematic Qualitative and Economic-Based Quantitative Review of Alternative Strategies. ChemEngineering , 3(3), 76. doi:10.3390/chemengineering3030076

Singh, M., Moore, J. & Shadis, W., 2005. Hydrogen Demand, Production, and Cost by Region to 2050, Argonne: U.S. Department of Energy.

8. Optimization of most viable reaction pathway

With the ranking of the reduced search space now being known, the focus shifted to the optimization of the most viable pathway. This chapter details the optimization components considered for the most viable reaction pathway, i.e. Case Study 8.

8.1. Reactor operating conditions

This subsection details the approach that was followed for optimizing the reactor unit operation, in terms of its operating temperature and pressure.

8.1.1. Reaction kinetics and reaction constants

Based on the systematic framework developed and presented in this dissertation, the most viable pathway was found to be the production of MeOH via the direct hydrogenation of CO_2. As per Section 6.4, this occurred over a $CuO/ZnO/Al_2O_3$ (CZA) catalyst with a molar composition of 55:30:15, respectively (Bellotti et al., 2017). In order to optimize the operating conditions of this reaction – in terms of the temperature and pressure – the kinetics for this reaction was required, at the aforementioned catalyst composition.

The work conducted by Ledakowicz et al. (2013) looked at the hydrogenation of CO_2 to MeOH over various catalysts, and derived kinetics for each scenario. This direct hydrogenation occurs by means of the following chemical reaction:

$$CO_2 + 3H_2 \leftrightarrow CH_3OH + H_2O \quad (61)$$

The catalyst that matched with that utilized in Case Study 8, i.e. the most viable pathway, was referred to as a TMC-3/1 Industrial ZA Tarnow catalyst. The characteristics of the TMC-3/1 catalyst is given in Table 17 (Ledakowicz et al., 2013).

Table 17: Characteristics of the TMC-3/1 catalyst utilized in reaction kinetics derivation

Factor	Value
Specific surface area	75 – 80 m^2/g
Active Cu surface area	7.0 – 7.5 m^2/g
Pore volume	0.20 – 0.25 cm^3/g
Apparent density	2.15 g/cm^3
Bulk density	1.30 kg/dm^3
Crushing strength	4,400 – 550 daN/cm^2

The reaction kinetics that are associated with Equation (61), over the TMC-3/1 catalyst, is as follows (Ledakowicz et al., 2013):

$$r_m = \frac{k_d P_{CO_2} P_{H_2} \left(1 - \frac{1}{K_1^*} \frac{P_{H_2O} P_{CH_3OH}}{P_{H_2}^3 P_{CO_2}}\right)}{\left(1 + k_c \frac{P_{H_2O}}{P_{H_2}} + k_a \sqrt{P_{H_2}} + k_b P_{H_2O}\right)^3} \tag{62}$$

All of the kinetic parameters given in Equation (62) are a function of temperature and can be represented by the following general equation (Ledakowicz et al., 2013):

$$k_i = A_i \, exp\left(-\frac{E_i}{RT}\right), i = a, b, c, d \tag{63}$$

The constants required for each of the kinetic parameters are shown in Table 18 (Ledakowicz et al., 2013).

Table 18: Kinetic parameter constants

Parameter	A_i Value	E_i Value
k_a	0.499 bar $^{-0.5}$	- 17,197 kJ/mol
k_b	6.62 x 10 $^{-11}$ bar $^{-1}$	-124,119 kJ/mol
k_c	3,453.80	n/a
k_d (TMC-3)	0.29 mol/(g.hr.bar ^{2})	-46.20 kJ/mol

Unfortunately, work conducted by Ledakowicz et al. (2013) did not look into the equilibrium constant kinetic parameter, denoted by K_1^*. For this equilibrium constant, the expression derived by Bussche and Froment in 1996 was utilized (Bussche & Froment, 1996).

$$log_{10}K_1^* = \frac{3066}{T} - 10.592 \quad (64)$$

Bussche and Froment noted that the RWGS reaction occurred over a CZA catalyst, and must be accounted for when considering the production of MeOH (Bussche & Froment, 1996). However, the work conducted by Ledakowicz et al. (2013) proved otherwise, stating that the CO/H_2 mixture was dry and does not react. As a result, the only meaningful reaction to account for in this system would be the direct hydrogenation of CO_2 to MeOH (Ledakowicz et al., 2013).

The CZA catalyst is highly subjective to temperature and pressure, and only promotes MeOH production within certain operating ranges. Operating at conditions outside of this range may result in unwanted by-products, such as methane, being formed, or the breakdown of the catalyst. This range was determined in 1996 by Bussche and Froment and utilized during the research conducted in 2013. Therefore, this optimization model also utilized these operating condition constraints, both of which are shown in Table 19 (Bussche & Froment, 1996).

Table 19: CZA catalyst operating conditions constraints

Factor	Minimum Value	Maximum Value
Temperature	180°C	280°C
Pressure	15 bar	51 bar

8.1.2. Initial pre-reactor optimization basis

As a basis for the optimization procedure, a preliminary flowsheet containing the unit operations involved in the reactor's operating conditions was required. The following unit operations were required in the pre-reactor system:

- Mixer – This allowed for the CO_2 and H_2 feed streams to be mixed together into a single stream, to be pressurized and heated, before being fed into the reactor.
- Compressor – This unit was required to change the pressure of the feed stream.
- Heat exchanger – This unit operation was involved in the heating or cooling of the feed stream, to the desired operating temperature of the reactor.

At this point, the order of the compressor and heat exchanger unit operations was used as a basis, and is investigated further in Section 8.2 (Compressor/Heat Exchanger Configuration).

Figure 11 shows the preliminary flowsheet utilized in the optimization of the reactor operating conditions.

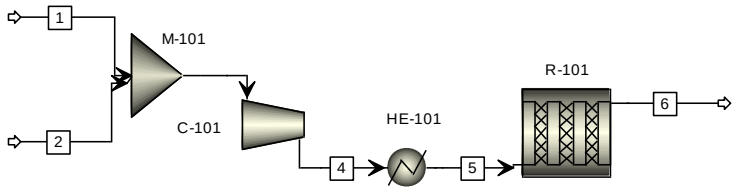

Figure 11: Preliminary flowsheet utilized in the optimization of the reactor operating conditions

The initial feed stream conditions were set at:

- Temperature = 25°C
- Pressure = 1 bar
- Feed ratio = 1:3 (w.r.t CO_2 to H_2)

8.1.3. Aspen Plus ® reaction kinetic parameters

In order for kinetics to be inputted into the Aspen Plus ® software, all of the kinetic parameters were required to be of the following form (Aspen Plus V10, 2018):

$$ln(k_i) = ln(A_i) - \frac{E_i}{RT} \tag{65}$$

Equation (65) is separated and termed by means of an A and B coefficient, with each coefficient being calculated by means of Equation (66) and (67) (Aspen Plus V10, 2018).

$$A = ln(A_i) \tag{66}$$

$$B = \frac{E_i}{R} \tag{67}$$

Applying this general formula to the kinetic parameters in Section 8.1.2, Table 20 shows the kinetic data required as per the Aspen Plus ® reactor formulations.

Table 20: Kinetic parameters required for Aspen Plus ® reactor modelling

Kinetic Parameter	Co-Eff A	Co-Eff B
K_1^*	24.39	-7,059.73
k_a	0.70	-2,068.44
k_b	23.44	-14,928.92
k_c	8.15	0
k_d	-1.24	-5.56

8.1.4. Optimization model specifications in Aspen Plus ®

When conducting optimization on the Aspen Plus ® platform, various factors were required to be defined whilst building the optimization model, including (Aspen Plus V10, 2018):

- The variables that were to be monitored, i.e. the dependent variables
- The variables that were changed, i.e. the independent variables
- The constants involved in the calculations
- The step sizes of the independent variables in the model
- The constraints of the optimization model
- The objective function

Any additional code that was required in the Aspen Plus ® Optimization model was included in the Fortran tab (Aspen Plus V10, 2018).

In the Aspen Plus ® optimization model for the operating conditions of the reactor, Table 21 shows the variables, along with their relevant step sizes.

Table 21: Optimization variables with their step sizes

Variable (Independent Variable)	Step Size
Temperature	1^oC
Pressure	1 bar

Table 22 shows the constraints that were implemented for the optimization model.

Table 22: Optimization constraints for reactor operating conditions

Factor	Minimum	Maximum
Temperature	180°C	280°C
Pressure	15 bar	51 bar
Compressor Size	18 kW	3,000 kW
Heat Exchanger Area	1 m^2	100 m^2

The temperature and pressure constraints were based on the operating range of the catalyst. The compressor size and heat exchanger area constraints were noted as per the constraints of the costing formula developed by Turton et al. (2009) (Chapter 5), with the type of heat exchanger and compressor being dependent on the size of the unit operation.

The factors monitored in this optimization model, i.e. the dependent variables, were as follows:

- The hourly production rate of MeOH
- The conversion of CO_2
- The capacity of the compressors required in achieving the reactor pressure
- Heat exchanger area required to achieve the reactor temperature

By using the Fortran option in Aspen Plus ® additional codings were achieved. This code utilized the variables to calculate additional data. The following data were calculated using the Fortran tab:

- Annual MeOH production, assuming a 24-hour plant operation over 330 days per annum
- Cost of the compressor system required
- Cost of the heat exchanger system required
- Total capital cost for the pre-reactor system

In order to calculate the cost of the compressor system, heat exchanger system and the total capital cost of the pre-reactor system, the costing formula developed by Turton et al. (2009) was utilized. This costing procedure was detailed in Section 5.2.

8.1.5. Objective function

The objective function utilized in this optimization is as follows:

$$max(Y_1) = \frac{Annual\ Production\ Rate\ of\ MeOH}{Total\ Capital\ Cost\ Required} \quad (68)$$

Where Y_1 is used to denote the first objective function that is used in the optimization model.

As per Equation (68), the objective function (Y_1) was maximized. Maximizing this ratio implies a draw off between the environmental and economic benefits. A high MeOH production rate implies a greater product sales potential, as well as a low amount of CO_2 that is left unreacted. Furthermore, a low capital cost also shows an economic benefit, lowering the initial capital investment required for the pre-reactor system.

8.1.6. Optimization model – Observations and results

Figure 12 shows the production of MeOH over the specified temperature and pressure range. The production of MeOH increased steadily as the temperature rose, until the region of approximately 200°C to 220°C – after which the production rate begins to decrease significantly. This was expected for the MeOH production reaction, as it is an exothermic reaction, which is promoted at lower temperatures. Furthermore, the increase in temperature results in unwanted by-products being formed, thereby reducing the production of MeOH. Figure 12 also shows that at lower pressures and specific temperature ranges, the catalyst was unable to operate and therefore no MeOH production rate was noted.

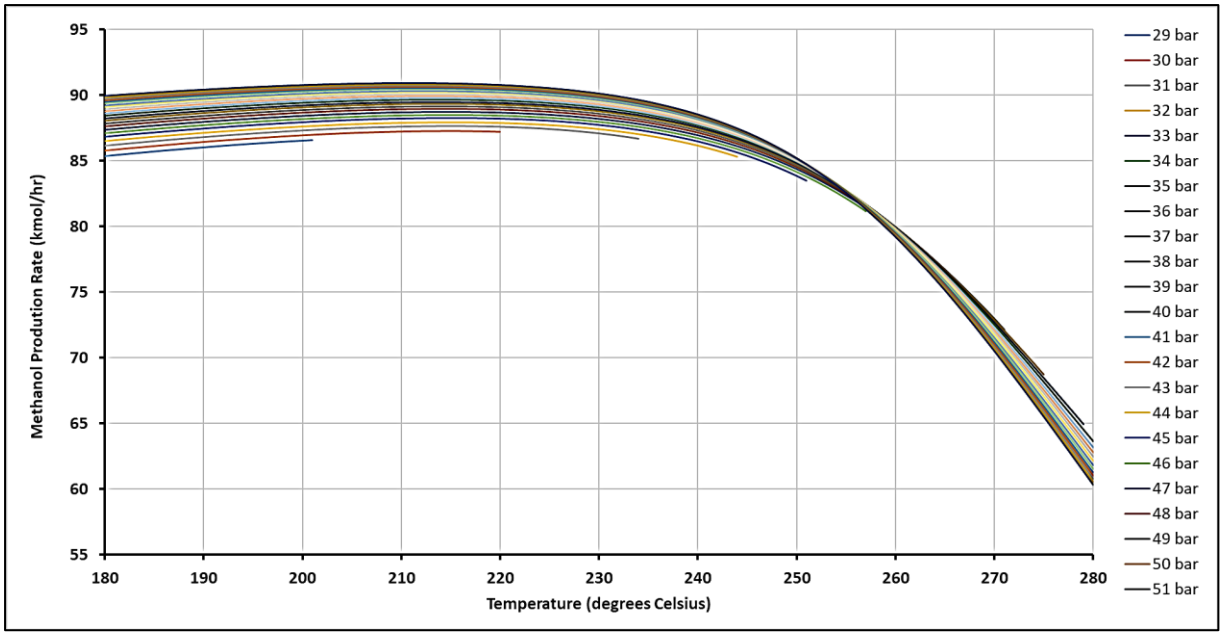

Figure 12: Line graph showing the effect of temperature and pressure on the hourly production of MeOH

Table 23 details the pressure and temperature ranges for which Aspen Plus ® deemed that the catalyst is not in operation.

Table 23: Pressure and temperature ranges for which the catalyst is not in operation within the predetermined constraints

Pressure Range (bar)	Temperature Range (°C)
15 - 28	180 – 280
29	202 – 280
30	221 – 280
31	235 – 280
32	245 – 280
33	252 – 280
34	258 – 280
35	263 – 280
36	267 – 280
37	272 – 280
38	276 – 280
39	280

Figure 13 shows the effect of temperature and pressure on the objective function.

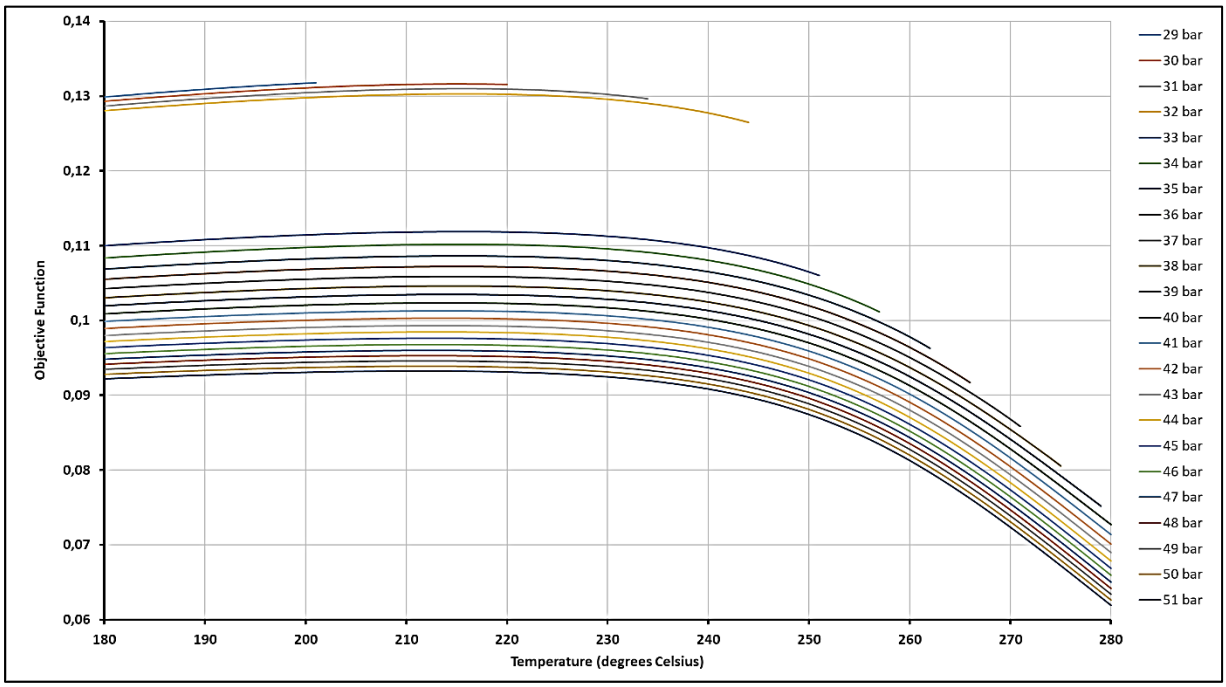

Figure 13: Line Graph showing the effect of temperature and pressure on the objective function

Figure 14 is a 3D surface representation that combines the data shown in Figure 12 and Figure 13. It is seen that the objective function decreased as the pressure and temperature begins to increase. This decrease in the objective function was noted more explicitly in the increase of the operating pressure, rather than the increase of the temperature. This was due to the fact that the cost of compressors was much higher than the cost of heat exchangers. Therefore, an increase in pressure was proven to be much more costly, than an increase in temperature.

Based on the optimization model and the objective function defined previously (Section 8.1.5), the most feasible operating point for the reactor would be 29 bar and 201°C, as this pressure and temperature combination yields the highest objective function value.

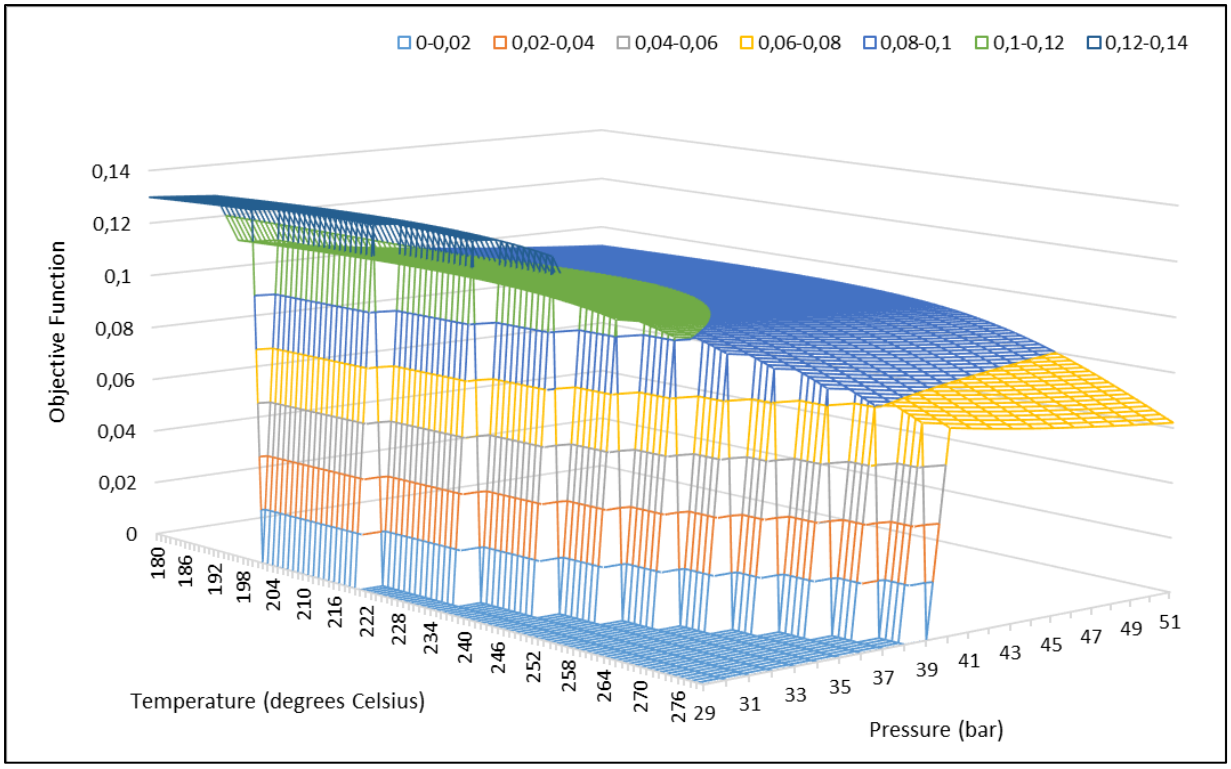

Figure 14: 3D Surface plot showing the effect of temperature and pressure on the objective function of the pre-reactor system

8.2. Compressor/Heat exchanger configuration

With the optimum operating conditions having been determined, the focus shifted to the optimum configuration of the pre-reactor compressor/heat exchanger unit operations. This optimization was conducted using a superstructure approach, as is shown in Section 8.2.1.

8.2.1. Pre-reactor configuration superstructure

The most effective method in to determine the optimum configuration of the pre-reactor system was through the use of a superstructure that encompasses all possible combinations. This superstructure comprised of the following unit operations:

- 2 splitters
- 2 mixers
- 6 heat exchangers
- 2 compressors

Figure 15 shows the pre-reactor superstructure configuration utilized in this optimization model.

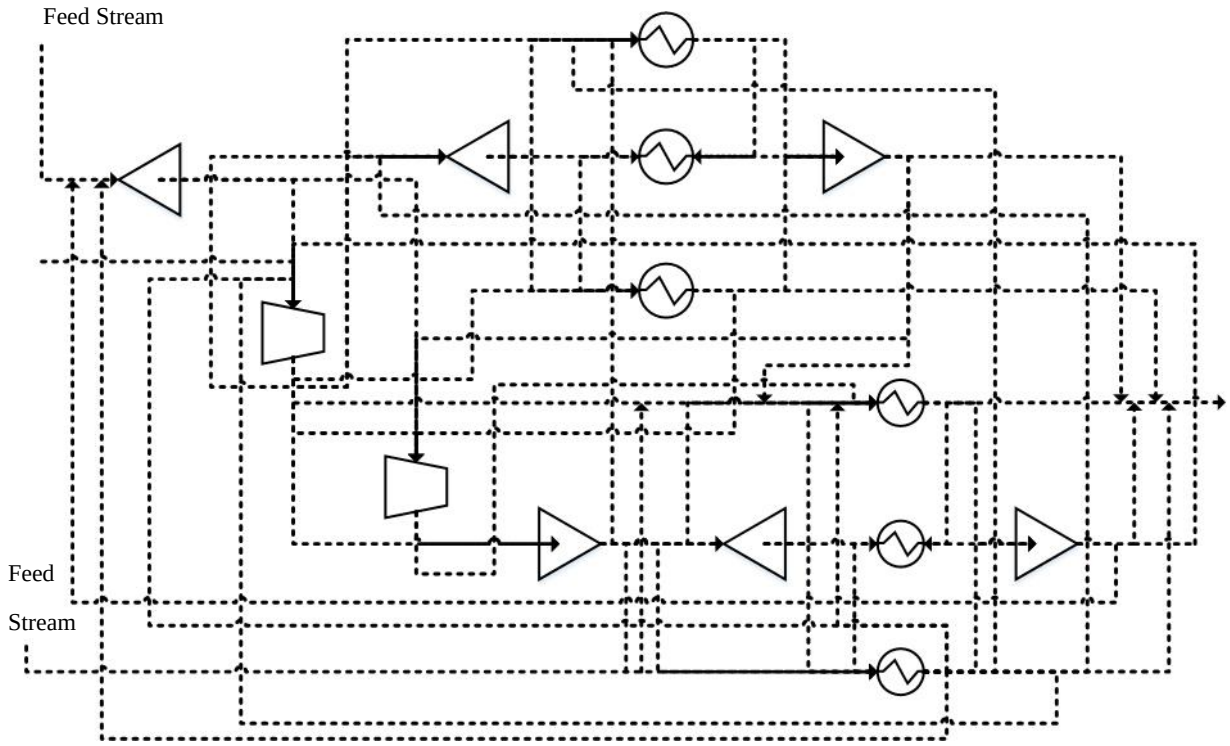

Figure 15: Pre-reactor compressor/heat exchanger superstructure

8.2.2. Superstructure analysis and scenario description

Through the analysis of this superstructure by means of Aspen Plus ® software, there were a total of 20 configurations that were possible, with each of these configurations being referred to as a new scenario (Aspen Plus V10, 2018). Table 24 shows the 20 possible options obtained from the superstructure, as well as a brief description of each configuration's physical set up.

Table 24: List of all possible compressor/heat exchanger configurations based on the superstructure

Scenario	Configuration	Description
1 (Base Case)	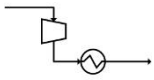	Single compressor with a single heat exchanger (C/HE system)
2	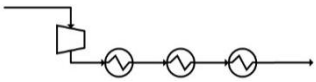	Single compressor with a series heat exchanger system of 3 units (C/HE system)
3	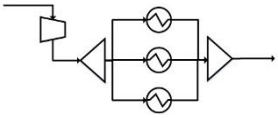	Single compressor with a parallel heat exchanger system of 3 units (C/HE system)
4	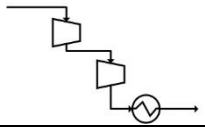	2 compressors in series with a single heat exchanger (C/HE system)
5	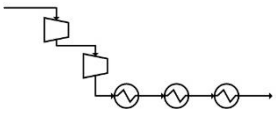	2 compressors in series with a series heat exchanger system of 3 units (C/HE system)
6	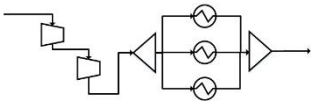	2 compressors in series with a parallel heat exchanger system of 3 units (C/HE system)
7	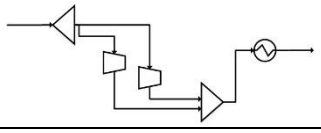	2 compressors in parallel with a single heat exchanger (C/HE system)
8	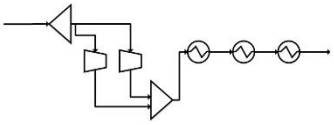	2 compressors in parallel with a series heat exchanger system of 3 units (C/HE system)
9	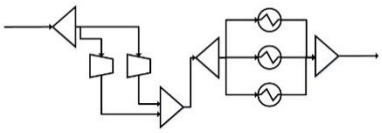	2 compressors in parallel with a parallel heat exchanger system of 3 units (C/HE system)
10	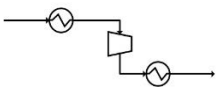	1 pre-compressor heat exchanger, with a single compressor & a single post-compressor heat exchanger (HE/C/HE system)

11	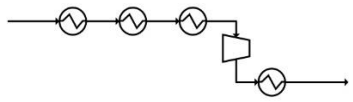	3 pre-compressor heat exchangers in series, with a single compressor & a single post-compressor heat exchanger (HE/C/HE system)
12	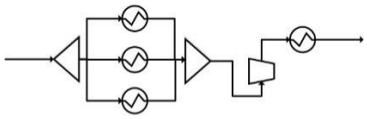	3 pre-compressor heat exchangers in parallel, with a single compressor & a single post-compressor heat exchanger (HE/C/HE system)
13	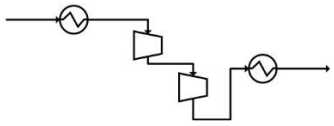	1 pre-compressor heat exchanger, with 2 compressors in series & a single post-compressor heat exchanger (HE/C/HE system)
14	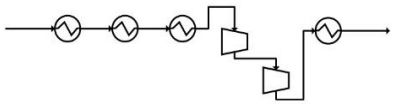	3 pre-compressor heat exchangers in series, with 2 compressors in series & a single post-compressor heat exchanger (HE/C/HE system)
15	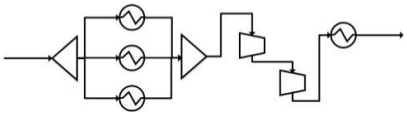	3 pre-compressor heat exchangers in parallel, with 2 compressors in series & a single post-compressor heat exchanger (HE/C/HE system)
16	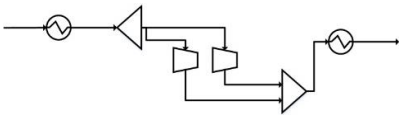	1 pre-compressor heat exchanger, with 2 compressors in parallel & a single post-compressor heat exchanger (HE/C/HE system)
17	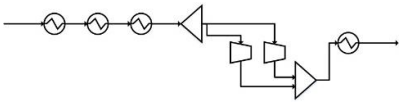	3 pre-compressor heat exchangers in series, with 2 compressors in parallel & a single post-compressor heat exchanger (HE/C/HE system)
18	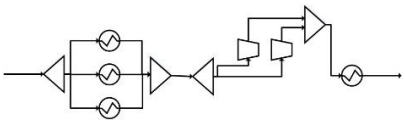	3 pre-compressor heat exchangers in parallel, with 2 compressors in parallel & a single post-compressor heat exchanger (HE/C/HE system)

19	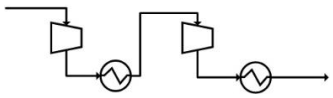	2 compressors in series with an intermittent cooling system of a single heat exchanger after each compressor (C/HE/C/HE system)
20	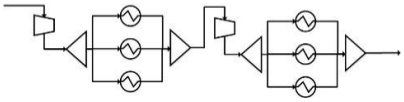	2 compressors in series with an intermittent cooling system of 3 heat exchangers in parallel after each compressor (C/HE/C/HE system)

8.2.3. Optimization model specifications in Aspen Plus ®

Using the superstructure developed in Section 8.2.1, and all of the scenarios in Section 8.2.2, an optimization model was built to determine the best configuration to obtain the operating conditions required in the reactor. As per Section 8.1.4, various information was required in Aspen Plus ® when building an optimization model (Aspen Plus V10, 2018). First and foremost were the variables involved in the optimization model, with the variable, in this case, being the type of configuration, i.e. the scenario.

The values monitored and tracked throughout each scenario were as follows:

- The capacity of the compressor unit operations in kilowatts (kW)
- Size of the heat exchangers required in the scenario in m^2

By using the Fortran tab in Aspen Plus ®, the following additional data were calculated:

- The total capacity of the compressor system required
- Percentage energy reduction in compressor system capacity. The comparison was done in relation to the base case scenario, i.e. Scenario #1.
- Total heat exchanger size required
- Percentage reduction in heat exchanger size, in relation to the base case scenario
- Cost of the heat exchanger and compressor system required, as per the costing formula developed by Turton et al. (2009).

8.2.4. Objective function

When developing the objective function for this optimization model, various factors were accounted for. One such factor was the cost of the compressors and heat exchangers relative to one another. Compressor unit operations are much more costly than heat exchangers (Turton et al., 2009), and therefore the objective function must account for this difference. This showed that a reduction in compressor size was more feasible than a reduction in heat exchanger size.

In order to incorporate this importance into the objective function, a weighting factor was utilized. This weighting factor allowed for the compressor savings to hold more value than the heat exchanger savings, and was calculated as the percentage cost of each unit operation, in relation to the total capital cost experienced in the base case scenario.

The compressor weighting factor is denoted by C_f and is calculated as shown in Equation (69).

$$C_f = \frac{Initial\ Compressor\ Cost}{Initial\ Capital\ Cost} \tag{69}$$

The heat exchanger weighting factor is denoted by HE_f and was calculated as shown in Equation (70).

$$HE_f = \frac{Initial\ HE\ Cost}{Initial\ Capital\ Cost} \tag{70}$$

Using the base case scenario, the compressor and heat exchanger weighting factors were calculated to be 0.993 and 0.007, respectively, thereby showing the minimal effect of heat exchangers on the cost of a process. Heat exchangers are much cheaper than compressors and therefore there is more flexibility with the number of heat exchanger unit operations.

The second optimization objective function (Y_2) is represented by means of the following equation:

$$max(Y_2) = \left(C_f * \frac{\%\ Energy\ Savings}{Compressor\ System\ Cost} + HF_f * \frac{\%\ Size\ Reduction}{HE\ System\ Cost}\right) * 10^7 \tag{71}$$

By maximizing the above objective function, a draw off is found between the scenarios that contains the best saving in energy usage or size reduction, with respect to the cost required to achieve such a scenario. A scale factor of 10^7 was used to increase the values of the objective function, thereby allowing them to be registered in the Aspen Plus ® software.

8.2.5. Observations and results

Based on the optimization model configured in Aspen Plus ®, Table 25 shows the results obtained for each of the scenarios detailed in Section 8.2.2.

Table 25: Data for the various scenario evaluated in the optimization of the unit operation configuration

Scenario	Compressor Capacity Reduction (%)	Heat Exchanger Size Reduction (%)	Objective Function
1	0.000	0.000	0.000
2	0.000	0.481	0.007
3	0.000	0.000	0.000
4	-4.915	-4.179	-0.148
5	-4.915	-3.621	-0.129
6	-4.915	-4.179	-0.137
7	-9.614	-8.013	-0.275
8	-9.614	-7.376	-0.247
9	0.000	0.000	0.000
10	-54.979	-576.858	-2.489
11	-54.979	-703.206	-2.498
12	-54.979	-576.858	-2.433
13	-62.129	-580.431	-2.394
14	-81.947	-834.183	-2.611
15	-81.947	-591.224	-2.505
16	-54.979	-576.858	-2.313
17	-54.979	-819.817	-2.367
18	-54.979	-576.858	-2.257
19	9.970	-83.520	-0.662
20	9.970	-83.520	-0.545

Using the objective function in Equation (71), the maximum value in Table 25 was noted for scenario 2, implying the optimum configuration. This scenario was a single compressor unit operation with multiple heat exchangers in series.

Table 25 shows that much of the scenarios yielded a negative value for the percentage capacity reduction of the compressor or the percentage size reduction of the heat exchanger unit operations. This shows an increase in size, subsequentially increasing the cost of the pre-reactor compressor/heat exchanger system.

The case studies that do yield positive reduction values are scenarios 2, 19 and 20. In scenario 2, there was a reduction in heat exchanger size, whereas in scenarios 19 and 20, there was a reduction in compressor capacity. Although the reduction in compressor size was deemed to be more feasible, due to the expensive nature of a compressor, the objective function still yielded a negative result. The capacity of the compressor system required was less than that initially shown in the base case scenario, i.e. scenario #1, however, the cost to add two compressor unit operations drastically increases the capital cost of the compressor system, thereby outweighing the effect of the reduced compressor capacity. Heat exchangers, on the other hand, are much cheaper than compressors. Therefore, adding multiple heat exchangers was not as impactful on the capital cost.

8.3. Number of pre-reactor unit operations

This section details the procedure followed in determining the optimum number of unit operations in the pre-reactor system.

8.3.1. Optimization model specifications in Aspen Plus ®

In order to determine the optimum number of unit operations that were required in the pre-reactor configuration, the focus was limited specifically to the heat exchangers. This was done as the optimum configuration, from Section 8.2, proved to be a single compressor with multiple heat exchangers in series. In order to build the Aspen Plus ® optimization model, the variable was set as being the number of heat exchangers unit in series, assuming an equal temperature drop across each heat exchanger.

The following values were monitored in this model:

- The total heat exchanger area of the new system

By employing the Fortran option on Aspen Plus ® additional equations were coded into the model. This allowed for two additional values to be calculated, namely:

- The percentage reduction in the heat exchanger size, in comparison to the base case scenario, which is a single compressor and a single heat exchanger.
- The cost of the new heat exchanger system required.

The constraints of the model were initially set in relation to the number of heat exchanger unit operations to be tested in the model – and was set at a maximum of 10. This was an initial constraint basis, and would need to be revised if a solution was not found. However, this constraint proved to be adequate for the model.

8.3.2. Objective function

The objective function that was developed for this optimization problem needed to find the best draw off between the reduction in the heat exchanger size and the cost of the heat exchanger system. Therefore, the objective function utilized in this optimization model is given by Equation (72).

$$max(Y_3) = \frac{\%\ Size\ Reduction}{Cost\ of\ HE\ system} * 10^5 \qquad (72)$$

The objective function, denoted by Y_3, was maximized, thereby implying a draw off between one of two possibilities, namely:

- The size of the heat exchanger system was reduced as much as possible
- The cost of the heat exchanger system was as low as possible

It is important to note, that this objective function uses a scaling factor of 10^5. This scaling factor does not play a role in the objective function but rather serves to increase the values obtained, so that they may be registered by the Aspen Plus ® software.

8.3.3. Optimization model – Observations and results

Table 26 shows the results obtained from Aspen Plus ®.

Table 26: Results obtained from the optimization model on Aspen Plus ®

No. of Heat Exchangers	Heat Exchanger System Area (m^2)	Cost of Heat Exchanger System ($)	% Reduction in Heat Exchanger Area	Objective Function
1	10.0801	35,808.89	0.0000	0.0000
2	10.0397	39,183.79	0.4008	1.0229
3	10.0316	41,999.10	0.4815	1.1464
4	10.0286	44,435.11	0.5107	1.1493
5	10.0272	46,608.48	0.5244	1.1252
6	10.0265	48,588.30	0.5320	1.0949
7	10.0260	50,418.50	0.5365	1.0642
8	10.0257	52,128.85	0.5395	1.0350
9	10.0255	53,740.52	0.5416	1.0077
10	10.0254	55,269.19	0.5430	0.9825

Table 26 shows that an increase in the number of heat exchangers caused a reduction in the total size of the heat exchanger system. However, the difference in area was minor, especially at higher heat exchanger numbers. Furthermore, an increase in the number of heat exchangers increased the cost of the heat exchanger system.

Figure 16 shows the change in the objective function as the number of heat exchangers increased. Based on this graph, and the optimization model, the optimum number of heat exchangers to utilize in this configuration was 4. Therefore, the final configuration of the pre-reactor system would be a single compressor followed by 4 heat exchanger units in series.

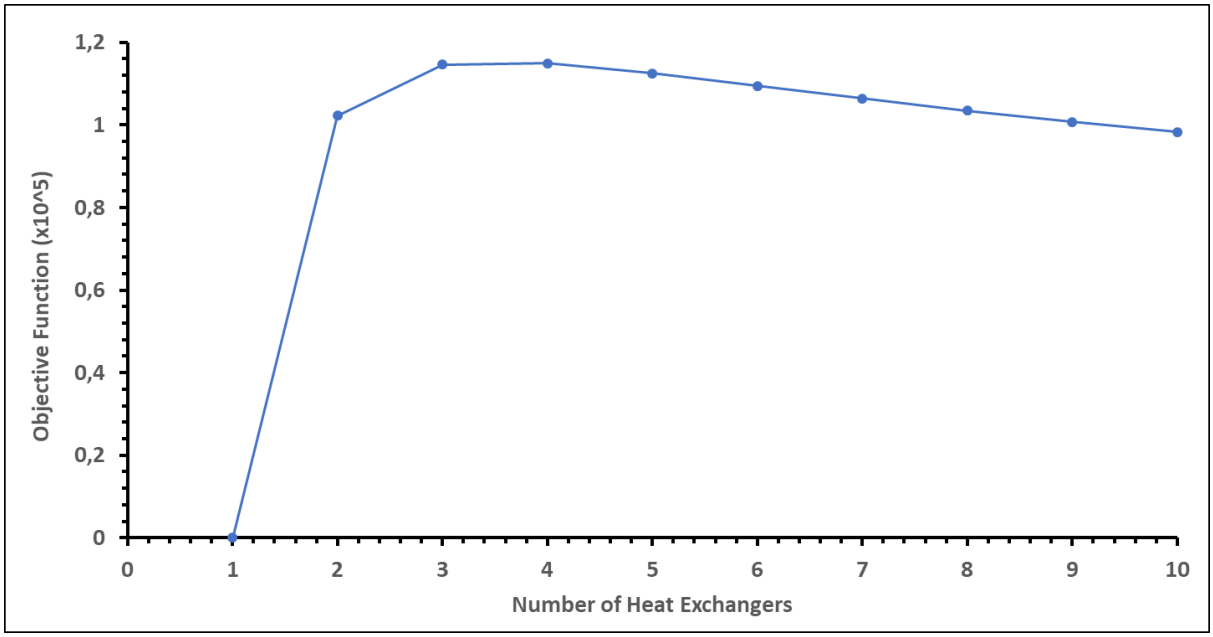

Figure 16: Line graph showing the change in the objective function as the number of heat exchangers increase

8.4. CO_2/H_2 feed ratio

This section details the procedure followed in determining the optimum feed ratio of CO_2 and H_2.

8.4.1. Optimization model specification in Aspen Plus ®

In order to optimize on the feed ratio, the variable was the hydrogen flow rate entering the system, with the flow rate of CO_2 remaining constant at 100 kmol/hr. The constraint set on the H_2 flow rate was between 200 and 400 kmol/hr with a step size of 1.

The constants or parameters of this optimization model were as follows:

- The input flow rate of CO_2
- The economic data - in terms of selling prices of products and costs of reactants

Throughout the optimization process, the following values were monitored:

- The amount of unreacted CO_2
- The conversion of CO_2 to MeOH

- The production rate of MeOH

Using the Fortran code, the following values were calculated:

- The hourly cost of CO_2
- The hourly cost of H_2
- The hourly sales potential of MeOH

8.4.2. Objective function

The objective function that was used to determine the optimum feed ratio, was from an economic standpoint. As the flow rate of hydrogen increases, so will the conversion of CO_2, due to the surplus of unreacted H_2 gas in the feed mixture. However, this increased H_2 flow rate will increase the hourly cost of H_2 required, thereby reducing the profit margin of the process. Equation (73) shows the profit calculation that is used as the objective function in this optimization problem.

$$max(Y_4) = Sales\ Potential\ of\ MeOH - Cost\ of\ Reactants \quad (73)$$

This objective function (Y_4) represents the hourly profit noted in the process and was maximized to achieve the best economic performance possible.

8.4.3. Optimization model – Observations and results

Figure 17 shows the change in hourly profit in relation to the change in H_2 flowrate that was entering the plant.

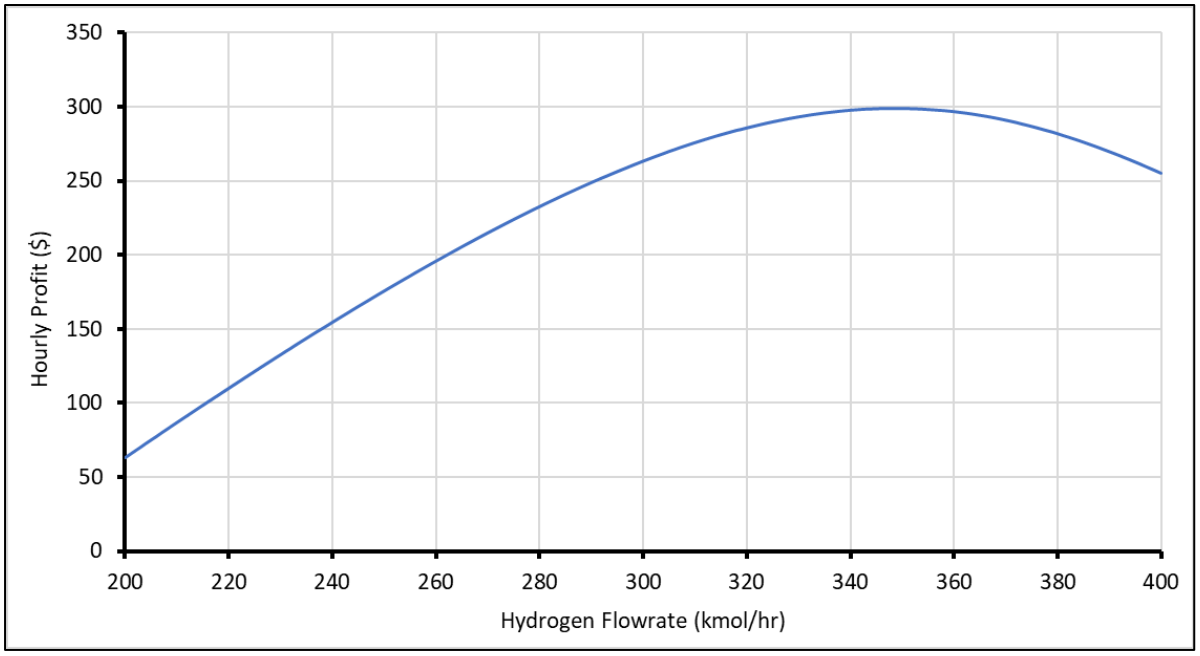

Figure 17: Line graph showing the effect that the hydrogen flow rate has on the hourly profit

The initial increase in hydrogen flowrate drastically increased the profit. This was the point at which the hydrogen was causing increased MeOH production, and therefore the sales potential was much higher than the cost of the reactants. However, as the flow rate of hydrogen begins to increase, the hourly profit reached a maximum before starting to decrease steadily.

This decrease was caused by the surplus hydrogen being outweighed by the minor changes in MeOH production. As per the objective function detailed in Section 8.4.2, the aim of this optimization model was to find the highest hourly profit. This maximum was noted at 349 kmol/hr.

Therefore, the optimal CO_2 to H_2 ratio was deemed to be 1:3.49, resulting in a CO_2 conversion of 97.6879%.

8.5. Post-reactor flash drum conditions

This section deals with the optimization of the flash drum unit operation, to obtain maximum recovery of the unreacted gases.

8.5.1. Optimization model specifications in Aspen Plus ®

In order to determine the optimum operating conditions of the post-reactor flash drum, for maximum recovery of MeOH during the separation process, an optimization model was built around the flash drum unit operation. This flash drum, however, must be accompanied by the necessary turbine and heat exchanger, in order to bring the product stream to the desired conditions required for separation.

The variables that were considered in this optimization model, with their associated constraints, are as follows:

- Pressure, constrained to between 1 bar and 29 bar
- Temperature, constrained to between 10°C and 200°C

These constraints were chosen as they do not exceed the exit conditions of the product stream leaving the reactor. As a result, cooling down/lowering the pressure of the product stream would be a much cheaper mechanism to facilitate the separation process. Furthermore, the water and MeOH mixture needed to be separated from the unreacted gas. At high temperatures the water and MeOH mixture becomes a vapor, thus increasing the difficulty, and in turn the cost, of the separation process.

The following factors were monitored in this optimization model:

- The hourly flow rate of MeOH leaving the bottom of the flash drum, i.e. the liquid stream
- The capacity of the turbine required to achieve the desired pressure in kilowatts
- The size of the heat exchanger required in m^2
- The dimensions of the flash drum required, w.r.t the length and the diameter

As in previous optimization models, the Fortran tab in Aspen Plus ® was utilized to code additional equations. The following were calculated using the Fortran function:

- The volume of the flash drum unit operation in m^3
- The cost of the turbine, heat exchanger and flash drum unit operations required, as per the formula developed by Turton et al. (2009)
- The annual flash drum recovery of MeOH
- The total capital cost of the turbine/heat exchanger/flash drum system

8.5.2. Objective function

The objective function in this model is denoted by Y_5, and is shown in Equation (74).

$$max(Y_5) = \frac{Annual\ MeOH\ recovery\ of\ flash\ drum}{Total\ capital\ cost\ of\ post\ reactor\ system} \quad (74)$$

By maximizing the objective function Y_5, a draw-off between the MeOH recovery rate of the flash drum, and the capital cost required to achieve such a recovery, was achieved.

8.5.3. Optimization model – Observations and results

Based on the optimization model, there were various operating conditions at which there was no MeOH recovery. Therefore, the flash drum becomes inoperable under these conditions and serves no purpose. Table 27 shows the temperature and pressure ranges for which the flash drum is inoperable.

Table 27: Temperature showing the pressure and temperatures for which the flash drum is inoperable

Pressure (bar)	Temperature Range (°C)	Pressure (bar)	Temperature Range (°C)
1	80 – 200	16	170 – 200
2	100 – 200	17	170 – 200
3	110 – 200	18	175 – 200
4	120 – 200	19	175 – 200
5	125 – 200	20	175 – 200
6	130 – 200	21	180 – 200
7	135 – 200	22	180 – 200
8	140 – 200	23	185 – 200
9	145 – 200	24	185 – 200
10	150 – 200	25	185 – 200
11	155 – 200	26	190 – 200
12	155 – 200	27	190 – 200
13	160 – 200	28	190 – 200
14	165 – 200	29	190 – 200
15	165 – 200		

Figure 18 shows the change in the objective function with respect to temperature and pressure. The effect of pressure on the objective function was much larger than that experienced by temperature. This became evident by the increasing value of the objective value as the pressure increased. Due to the reactor operating at 29 bar, an increase in the post-reactor pressure would lower the work of the turbine, thereby resulting in a cheaper post reactor system.

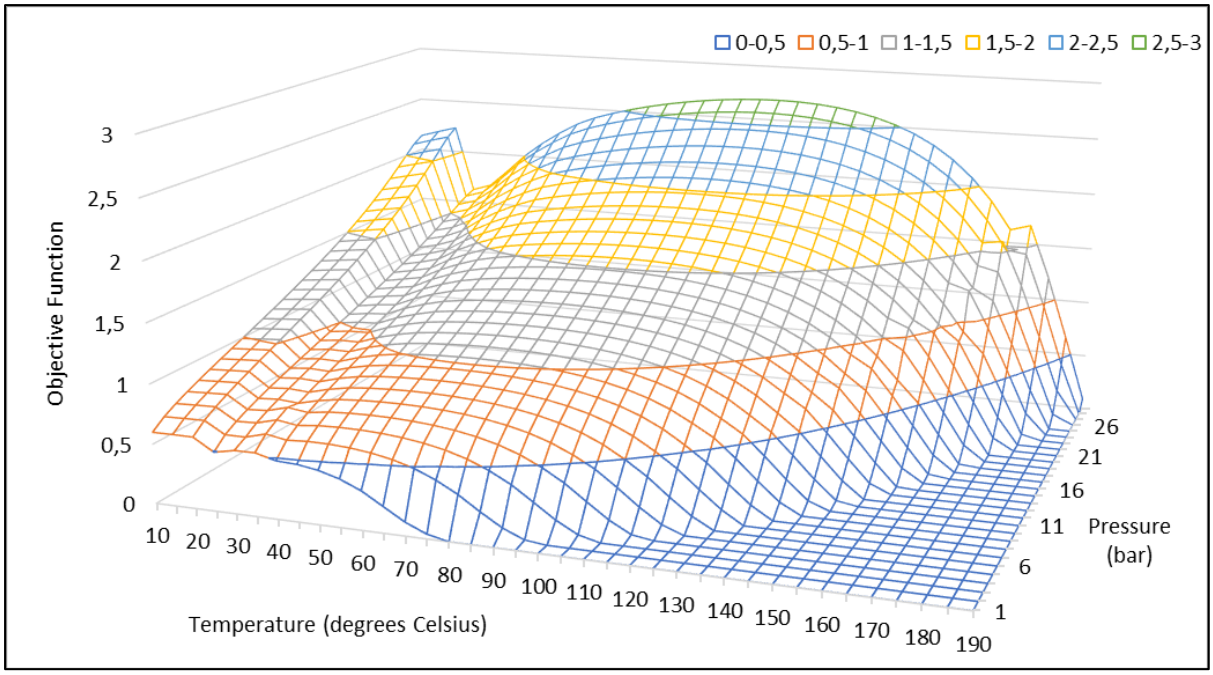

Figure 18: 3D Surface plot showing the effect of temperature and pressure on the objective function of the post-reactor system

The optimum operating conditions for the flash drum unit operation was 29 bar and 110°C.

8.6. The recycle structure

With the optimization of the flash drum completed, the unreacted gas can be recycled back into the process, in order to reduce the amount of purged gas, i.e. waste. Recycling the gas would also prove to be economically beneficial to the process, as it would result in a lower amount of reactant feed being purchased, thereby increasing the hourly profit margin of the plant. However, the point at which the unreacted gas is recycled, or reintroduced into the process, can affect the unit operations involved.

8.6.1. Optimization model specifications in Aspen Plus ®

Based on the optimum configuration previously determined, there were a total of one compressor and four heat exchanger unit operations in the pre-reactor system. The recycled gas could be introduced at any point along these pre-reactor unit operations. The following five options show the possible recycle structures:

- Option 1: Before the compressor unit operation
- Option 2: After the compressor but before heat exchanger 1
- Option 3: Between heat exchanger 1 and 2
- Option 4: Between heat exchanger 2 and 3
- Option 5: Between heat exchanger 3 and 4

The variable in this optimization model was the recycle structure, and the position that it holds upon re-entering the system. The values to be monitored were simply the individual sizes of the 4 heat exchangers involved and the total heat exchanger system size.

8.6.2. Objective function

The objective function (Y_6) utilized in this optimization model looked solely at the total size of the heat exchanger system. Therefore, this is represented by means of Equation (75).

$$min(Y_6) = \sum_{i=1}^{4} (HE\ Area)_i \tag{75}$$

This objective function did not incorporate the cost of the heat exchanger system, as the costing formula developed by Turton et al. (2009) showed that the cost of the heat exchangers was directly proportional to the size of the heat exchangers. Therefore, a decrease in the overall area of the heat exchanger system resulted in a decrease in the heat exchanger system cost.

8.6.3. Optimization model – Observations and results

Figure 19 shows the summation of the heat exchanger areas noted for each option. As can be seen by this graph, Option 2, i.e. the recycling of the unreacted gas between the compressor and first heat exchanger, proved to be the least feasible option, with the total heat exchanger system area being in excess of 250 m^2. The most feasible scenario was Option 4, i.e. the recycle of the unreacted gas to between heat exchangers 3 and 4. This option was able to provide a total heat exchanger area of 7.9 m^2, which is a 26.4% reduction in the area of the base case scenario, i.e. Option 1.

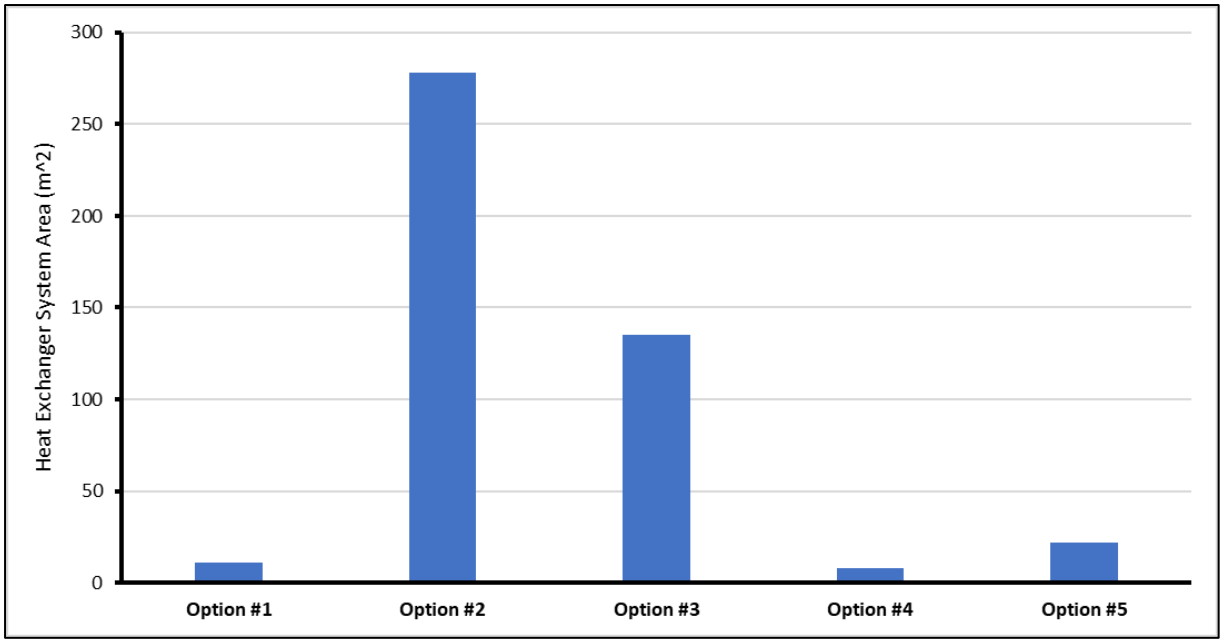

Figure 19: Bar graph of the total sizes of the heat exchanger areas for the various possible recycle structure options

8.7. The distillation column

Due to the close proximity between the boiling points of MeOH and water, a distillation column was required for the separation process. Using Aspen Plus ® software a basic distillation column was designed. The specifications of this distillation column are shown in Table 28.

Table 28: Specifications of the distillation column required in the separation of the MeOH /water mixture

Name	**S-102**
Property method	PENG-ROB
Water solubility method	3
Number of stages	23
Light key component recovery	0.9999
Heavy key component recovery	0.0001
Distillate vapor fraction	1
Minimum reflux ratio	0.66
Actual reflux ratio	1.44
Minimum number of stages	14.99
Number of actual stages	23
Feed stage	16.21
Number of actual stages above feed	15.21
Distillate temperature [^{o}C]	110.01
Bottom temperature [^{o}C]	152.79
Distillate to feed fraction	0.49
Total CO_2 emission flow [kg/hr]	7.19×10^{-8}
Net stream CO_2 emission production [kg/hr]	0

The physical dimensions of the distillation column are shown in Table 29.

Table 29: Physical specification of the distillation column required

User tag number	**S-102**
Diameter Bottom section [meter]	0.61
Bottom tangent to tangent height [meter]	22.56
Design gauge pressure Bottom [barg]	31.43
Design temperature Bottom [C]	180.57
Operating temperature Bottom [C]	152.79
Number of trays Bottom section	31
Bottom Tray type	SIEVE
Bottom Tray spacing [meter]	0.61
Molecular Wt Overhead Prod.	31.99

Based on Tables 28 and 29, it is seen that the distillation column designed and simulated, was able to yield a 99.9% recovery of MeOH in the top stream of the column. Furthermore, the low CO_2 values in the distillation column attest to the efficiency of the flash drum previously optimized.

8.8. Energy saving analysis and heat integration

This section deals with the possibility of energy savings in the newly optimized process, through the implementation of heat integration.

8.8.1. Final process flow diagram before heat integration

Figure 20 employs all of the optimization components detailed in the previous sections of this dissertation.

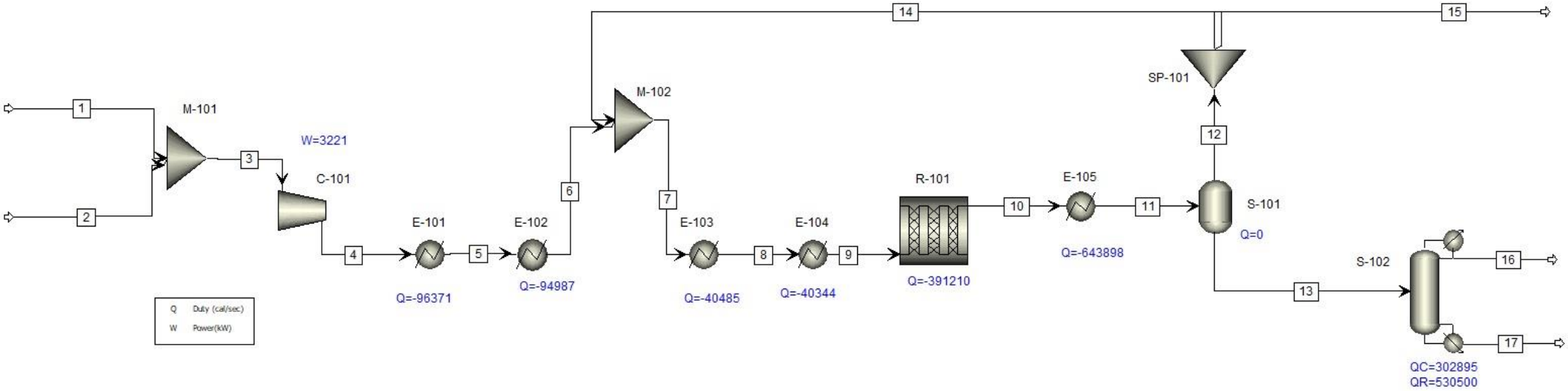

Figure 20: Final process flow diagram before heat integration

8.8.2. Possible solutions and design changes

In order to perform heat integration on a plant, all of the existing heat exchanger data must be known. Table 30 details the current heat exchanger systems in the process, as shown in Section 8.8.1.

Table 30: Current heat exchanger data for the process depicted in Section 8.8.1

Heat Exchanger	Type	Base Duty [cal/sec]	Recoverable Duty [cal/sec]	Hot Inlet Temp [C]	Hot Outlet Temp [C]	Cold Inlet Temp [C]	Cold Outlet Temp [C]	Hot Side Fluid	Cold Side Fluid
E-101	Cooler	9.64×10^{4}	9.64×10^{4}	585.9	491.5	249.0	250.0	4_To_6	HP Steam
E-102	Cooler	9.50×10^{4}	9.50×10^{4}	491.5	398.4	249.0	250.0	4_To_6	HP Steam
E-105	Cooler	6.44×10^{5}	8.61×10^{4}	209.0	110.0	30.0	35.0	10_To_11	Air
E-103	Cooler	4.05×10^{4}	4.05×10^{4}	247.9	228.4	174.0	175.0	7_To_9	MP Steam
E-104	Cooler	4.03×10^{4}	4.03×10^{4}	228.4	209.0	174.0	175.0	7_To_9	MP Steam
Condenser@S-102	Cooler	3.03×10^{5}	0.0	110.5	110.0	30.0	35.0	Condenser@S-102_to_16	Air
Reboiler@S-102	Heater	5.31×10^{5}	0.0	175.0	174.0	152.3	152.8	MP Steam	Reboiler@S-102_to_17
R-101	Heater	3.91×10^{5}	0.0	250.0	249.0	209.0	209.5	HP Steam	R-101_heat

Table 31 shows the total utilities required, along with potential savings.

Table 31: Potential savings of the process based on Aspen Energy Analyzer ®

	Actual	Target	Savings	% of Actual
Total Utilities [cal/sec]	2.14×10^{6}	1.42×10^{6}	7.17×10^{5}	33.48
Heating Utilities [cal/sec]	9.22×10^{5}	5.63×10^{5}	3.58×10^{5}	38.87
Cooling Utilities [cal/sec]	1.22×10^{6}	8.61×10^{5}	3.58×10^{5}	29.39

Table 31 was further analysed to determine the type of hot and cold utilities that were required in the process. Table 32 shows the detailed data associated with the hot and cold utilities, as was determined using Aspen Energy Analyzer ®. The negative energy cost savings indicate that the utility would increase the energy requirements of the system, i.e. an unfeasible option.

Table 32: Detailed analysis of the hot and cold utilities required for the process

	Current [cal/sec]	Target [cal/sec]	Savings [cal/sec]	Energy Cost Savings [$/Yr]	Energy Cost Savings [%]	ΔTmin [C]
MP Steam	5.31×10^{5}	4.24×10^{5}	1.07×10^{5}	31,084	20.16	10
HP Steam	3.91×10^{5}	1.40×10^{5}	2.51×10^{5}	83,032	64.26	10
Total Hot Utilities	9.22×10^{5}	5.63×10^{5}	3.58×10^{5}	114,115	40.26	
Air	9.47×10^{5}	8.61×10^{5}	8.61×10^{4}	11	9.10	10
HP Steam Generation	1.91×10^{5}	0.00	1.91×10^{5}	-62,955	-100.00	10
MP Steam Generation	8.08×10^{4}	0.00	8.08×10^{4}	-23,388	-100.00	10
Total Cold Utilities	1.22×10^{6}	8.61×10^{5}	3.58×10^{5}	-86,332	-100.13	

Unfortunately, due to the fact that all of the heat exchangers are coolers, with the exception of the reboiler and the reactor, there were no opportunities for heat integration. Aspen Energy Analyzer, however, was able to find potential savings through the addition of a heat exchanger unit operation. Table 33 details the possible heat exchanger addition solutions.

Table 33: Possible solutions in order to reduce the energy consumption of the current plant

Solution	Energy Saving	Payback	New Area	Cost	Cost Saving	Location of the new heat exchanger	
	[%]	[year]	[sqm]	[$]	[$/Yr]	Hot Side Fluid	Cold Side Fluid
1	8.02	1.88	119.9000	46,823	24,975	Upstream to E-105	Upstream to Reboiler@S-102
2	0.09	8023	0.0944	10,121	1	Upstream to E-101	Upstream to R-101
3	0.09	8047	0.1248	10,151	1	Upstream to E-102	Upstream to R-101

From these three possible solutions, solutions 2 and 3 were immediately eliminated and deemed as infeasible options. Both of these solutions result in 0.09% energy savings, with the saving-investment, i.e. the additional heat exchanger, only being paid off within 8,000 years. This was highly infeasible and did not promote any investment opportunities into the plant. Solution 1, however, was extremely practical. In solution 1, the addition of a single heat exchanger unit, costing approximately $47,000, would result in an 8.02% energy savings. This savings equates to $25,000 per annum, resulting in a payback period of just under 2 years. Table 34 shows the data change that occurs in the existing heat exchanger infrastructure, after employing solution 1 to the existing plant.

Table 34: Changes to the heat exchanger network by employing Solution 1

Heat Exchanger	Type	Required Area [sqm]	Existing Area [sqm]	New Area [sqm]	Extra Shells	Capital Cost [$]	Hot Side Approach Temp [C]	Cold Side Approach Temp [C]	Design Load [cal/sec]	Base Load [cal/sec]	LMTD Correction Factor
E-100	Process	119.9	0.0	119.9	1	46,823	56.7	10.1	8.59×10^{4}	0	0.9990
E-105	Cooler	221.0	252.1	0.0	0	0	127.4	80.0	5.58×10^{5}	6.44×10^{5}	0.9957
Reboiler	Heater	438.9	522.7	0.0	0	0	22.2	21.6	4.45×10^{5}	5.31×10^{5}	0.9999

8.8.3. Final process flow sheet with heat integration and utilities

Figure 21 shows the final process flow sheet, after accounting for heat integration in the plant.

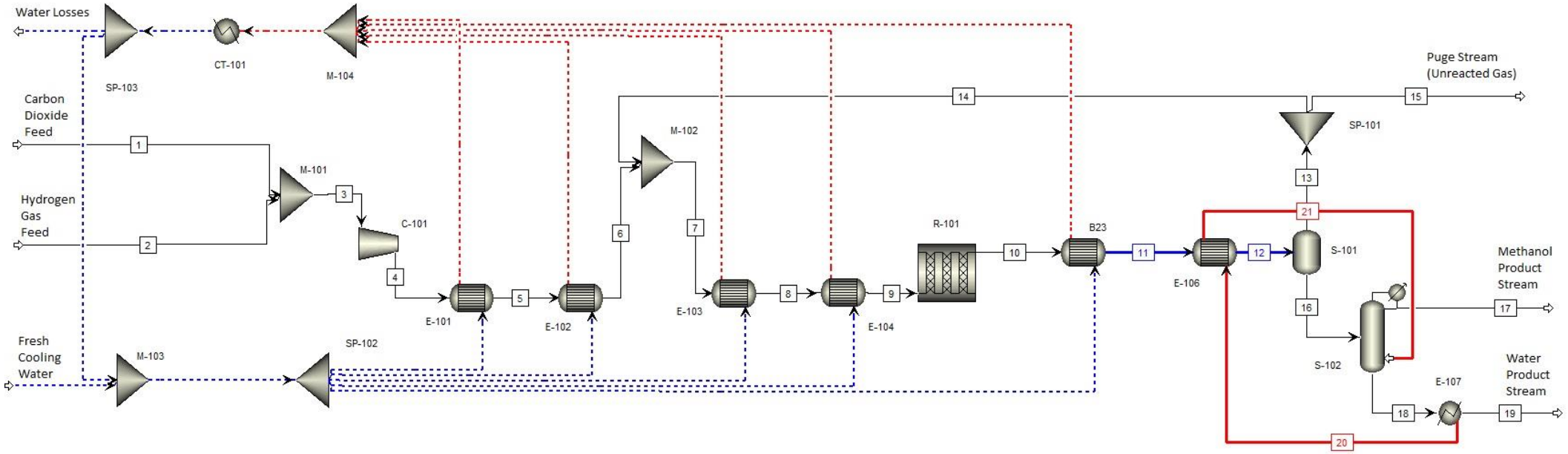

Figure 21: Final process flowsheet after heat integration (colour coded with utility streams)

8.9. Summary of optimization results

Table 35 shows a summary of the optimization results achieved from Section 8.1 through to Section 8.8:

Table 35: Final design summary based on all optimization models

Factor Optimized	Final Value
Reactor operating temperature	201°C
Reactor operating pressure	29 bar
CO_2 conversion to MeOH	97.69 %
Compressor/Heat Exchanger Configuration	Option 2
Description of Option	Single compressor followed by multiple heat exchangers in series
Number of compressors in configuration	1
Number of heat exchangers in configuration	4
Optimum CO_2 to H_2 ratio in the feed	1 : 3.49
Optimum flash drum temperature	110°C
Optimum flash drum pressure	29 bar
Optimum Recycle Position	Between HE 2 and 3
Energy Savings Analysis	Add 1 HE after reactor – Reroute reboiler

8.10. References

Aspen Plus V10 (2018), USA, Aspen Technology, Inc.

Bellotti, D., Rivarolo, M., Magistri, L., & Massardo, A. F. (2017). Feasibility Study of Methanol Production Plant from Hydrogen and Captured Carbon Dioxide. Journal of CO_2 Utilization, 21, 132-138. doi:10.1016/j.jcou.2017.07.001

Bussche, K. V., & Froment, G. F. (1996). A Steady-State Kinetic Model for Methanol Synthesis and the Water Gas Shift Reaction on a Commercial Cu/ZnO/Al2O3 Catalyst. Journal of Catalysis, 1-10. doi:10.1006/jcat.1996.0156

Ledakowicz, S., Nowicki, L., Petera, J., Niziol, J., Kowalik, P., & Golebiowski, A. (2013). Kinetic Characteristics of Catalysts for Methanol Synthesis. Chemical and Process Engineering, 34(4), 497-506. doi:10.2478/cpe-2013-0040

Microsoft Visio 2016: professional edition. Seattle, WA: Visio Corp.,

Turton, R., Bailie, R. C., Whiting, W. B., & Shaelwitz, J. A. (2009). Analysis, Synthesis and Design of Chemical Processes. United States of America: Pearson Education Inc.

9. Conclusion

In conclusion, the systematic framework developed and presented in this dissertation, was able to reduce the possible case studies from 85 to 6 feasible options, all of which dealt with the production of energy sources that could potentially decrease the current strain on non-renewable energy sources. This is a 93% reduction in the search space. This analysis was conducted by employing the P-Graph concept, in order to develop a reaction pathway superstructure, and analyzing the reaction pathway combinations using established criteria. The ranking of this reduced search space was then determined using a performance index, accounting for both economic and environmental aspects. Based on the Reaction Pathway Database (RPD), the most viable pathway to utilize CO_2 and H_2 is through the production of MeOH via the direct approach over a $CuO/ZnO/Al_2O_3$ catalyst at 240^oC and 80 bar pressure. The most viable DME production scenario, on the other hand, is to produce MeOH over the aforementioned catalyst, and then further dehydrate the MeOH over an Al/Si catalyst at 400^oC and 25 bar pressure. The production of MeOH was deemed more feasible than DME production, due to excessive heating requirements in the DME production system.

Upon optimizing the MeOH production pathway using reaction kinetics, the optimized operating conditions were found to be 201^oC and 29 bar pressure. This optimized MeOH synthesis pathway was able to achieve a CO_2 conversion of 97.69%. The optimum pre-reactor configuration was a single compressor unit operation, followed by 4 heat exchanger unit operations in series. The optimum feed ratio of CO_2 to H_2 was 1:3.49, with the optimal recycle point of the unreacted gas being fed between heat exchangers 2 and 3. The results presented in this dissertation, however, are highly subject to the cost of the reactants and the sales potential of the products.

The strength of this framework lies in the fact that the entire process is a stepwise procedure that is entirely dependent on the RPD initially developed. Therefore, the RPD can easily be changed in order to incorporate other reactive species, thereby not limiting this framework to only CO_2 and H_2 systems. Furthermore, the reduction in the reaction pathway search space, allows for resources to be more efficiently utilized, with the most efficient and viable pathway being known at an early stage, i.e. prior to extensive design and optimization procedures.

The shortcomings of this work lie in the complexity of the framework and the software platforms required. This work utilized 4 software platforms, namely P-Graph Studio ®, Aspen Plus ®, MATLAB ® and Microsoft Excel ®, with the results from each platform being manually extracted and inputted into the next software. This requires access to all four software platforms. Furthermore, the manual extraction and input of results into subsequent platforms is time consuming and increases the possibility of human error. This reduces the practicality and usability of the framework. Furthermore, the RPD should be accompanied by experimental data, thereby confirming the conversions and operating extracted from literature.

Future work in this field could involve addressing these shortcomings by automating the framework into a single software platform. This will eliminate both the need for multiple software platforms, whilst also eliminating the need for results to be manually extracted between subsequent steps. Additionally, the framework could be expanded to incorporate systems that utilize other reactants, thereby broadening the industrial application of this work.

10. Appendices

10.1. Appendix A – Case studies evaluated

This section details all of the possible case studies extracted from the P-Graph presented in Section 4.5. The case study numbers of the reaction pathway systems are referenced as such in this dissertation, in order to simulate and evaluate each possibility. All temperatures and pressures extracted in the RPD are converted to Kelvin and bar pressure respectively, in order to maintain consistency in Table 36.

Some of the pathways that were extracted and presented in Section 4.2, did not contain explicit values for the conversions in certain sub reactions. In these cases, a Gibbs Free Reactor is utilized in its associated simulation. This allows for an estimation of the conversion to be seen, based on the reaction's operating conditions. These reaction pathways are represented as having a CO_2 conversion that is dependent on RGibbs – the name of the symbol that is utilized for a Gibbs Free Reactor in the Aspen Plus ® Simulation Software.

Table 36: Case studies to be evaluated based on the P-Graph developed

Case Study	Reaction	Temp (Kelvin)	Pressure (bar)	Catalyst	X_{CO2}	CO_2 : H_2 Ratio
# 1.1	$3CO_2 + 4H_2 \leftrightarrow C_3H_8 + 3O_2$	573	1.01325	Fe / TiO_2	26.407 %	3:4
# 1.2	$3CO_2 + 4H_2 \leftrightarrow C_3H_8 + 3O_2$	573	1.01325	Fe / Al_2O_3	22.675 %	3:4
# 2	$3CO_2 + 4H_2 \leftrightarrow C_3H_8 + 3O_2$	673	20	Li, Na, K, Rb, Cs (Fe based)	10.8188 %	3:4
# 3.1	$3CO_2 + 4H_2O \leftrightarrow C_3H_8 + 5O_2$	723	15	Fe / ZrO_2	10.719 %	1:2
# 3.2	$3CO_2 + 4H_2O \leftrightarrow C_3H_8 + 5O_2$	773	15	Fe / TiO_2	9.5691 %	1:2
# 4	$CO_2 + 3H_2 \leftrightarrow CH_3OH + H_2O$	513	20	CZZA / rGO	11.6 %	1:2
# 5	$CO_2 + 3H_2 \leftrightarrow CH_3OH + H_2O$	553.15	442	Cu / ZnO / Al_2O_3	85.5 %	1:3

Case Study	Reaction	Temp (Kelvin)	Pressure (bar)	Catalyst	X_{CO2}	$CO_2 : H_2$ Ratio
# 6	$CO_2 + 3H_2 \leftrightarrow CH_3OH + H_2O$	474	40	CZA – Pd modified	61.54 %	1:3
# 7	$CO_2 + 3H_2 \leftrightarrow CH_3OH + H_2O$	533.15	330	Fe - Cu	93.5846 %	1:3
# 8	$CO_2 + 3H_2 \leftrightarrow CH_3OH + H_2O$	513.15	80	CuO / ZnO / Al_2O_3	96 %	1:3
# 9	$CO_2 + 3H_2 \leftrightarrow CH_3OH + H_2O$	493.15	18.9	1 % Na / 20 % Co-SiO_2	17.202 %	1:3
# 10	$CO_2 + 3H_2 \leftrightarrow CH_3OH + H_2O$	523 - 543	20	Cu-Ga / ZnO	5 %	1:3
# 11	$CO_2 + 3H_2 \leftrightarrow CH_3OH + H_2O$	493	80	Cu / Zn / Zr / Cr	18 %	1:3
# 12	$CO_2 + 3H_2 \leftrightarrow CH_3OH + H_2O$	513	20	CZZA / rGO	11.6 %	1:3
	$2CH_3OH \leftrightarrow CH_3OCH_3 + H_2O$	673.15	25	Alumina Based	86.764 %	n/a
# 13	$CO_2 + 3H_2 \leftrightarrow CH_3OH + H_2O$	553.15	442	Cu / ZnO / Al_2O_3	85.5 %	1:3
	$2CH_3OH \leftrightarrow CH_3OCH_3 + H_2O$	673.15	25	Alumina Based	86.764 %	n/a
# 14	$CO_2 + 3H_2 \leftrightarrow CH_3OH + H_2O$	474	40	CZA – Pd modified	61.54 %	1:3
	$2CH_3OH \leftrightarrow CH_3OCH_3 + H_2O$	673.15	25	Alumina Based	86.764 %	n/a
# 15	$CO_2 + 3H_2 \leftrightarrow CH_3OH + H_2O$	533.15	330	Fe - Cu	93.5846 %	1:3
	$2CH_3OH \leftrightarrow CH_3OCH_3 + H_2O$	673.15	25	Alumina Based	86.764 %	n/a
# 16	$CO_2 + 3H_2 \leftrightarrow CH_3OH + H_2O$	513.15	80	CuO / ZnO / Al_2O_3	96 %	1:3
	$2CH_3OH \leftrightarrow CH_3OCH_3 + H_2O$	673.15	25	Alumina Based	86.764 %	n/a
# 17	$CO_2 + 3H_2 \leftrightarrow CH_3OH + H_2O$	493.15	18.9	1 % Na / 20 % Co-SiO_2	17.202 %	1:3
	$2CH_3OH \leftrightarrow CH_3OCH_3 + H_2O$	673.15	25	Alumina Based	86.764 %	n/a
# 18	$CO_2 + 3H_2 \leftrightarrow CH_3OH + H_2O$	523 - 543	20	Cu-Ga / ZnO	5 %	1:3
	$2CH_3OH \leftrightarrow CH_3OCH_3 + H_2O$	673.15	25	Alumina Based	86.764 %	n/a

Case Study	Reaction	Temp (Kelvin)	Pressure (bar)	Catalyst	X_{CO2}	$CO_2 : H_2$ Ratio
# 19	$CO_2 + 3H_2 \leftrightarrow CH_3OH + H_2O$	493	80	Cu / Zn / Zr / Cr	18 %	1:3
	$2CH_3OH \leftrightarrow CH_3OCH_3 + H_2O$	673.15	25	Alumina Based	86.764 %	n/a
# 20	$CO_2 + H_2 \leftrightarrow CO + H_2O$	613	20	Li, Na, K, Rb, Cs (Fe based)	2.774 %	1:1
# 21	$CO_2 + H_2 \leftrightarrow CO + H_2O$	613	20	Li, Na, K, Rb, Cs (Fe based)	2.774 %	1:1
	$CO + 2H_2 \leftrightarrow CH_3OH$	553.15	442	Cu / ZnO / Al_2O_3	RGibbs	n/a
# 22	$CO_2 + H_2 \leftrightarrow CO + H_2O$	613	20	Li, Na, K, Rb, Cs (Fe based)	2.774 %	1:1
	$CO + 2H_2 \leftrightarrow CH_3OH$	533.15	330	Fe - Cu	RGibbs	n/a
# 23	$CO_2 + H_2 \leftrightarrow CO + H_2O$	613	20	Li, Na, K, Rb, Cs (Fe based)	2.774 %	1:1
	$CO + 2H_2 \leftrightarrow CH_3OH$	523 - 543	20	Cu – Ga / ZnO	RGibbs	n/a
# 24	$CO_2 + H_2 \leftrightarrow CO + H_2O$	613	20	Li, Na, K, Rb, Cs (Fe based)	2.774 %	1:1
	$CO + 2H_2 \leftrightarrow CH_3OH$	553.15	442	Cu / ZnO / Al_2O_3	RGibbs	n/a
	$2CH_3OH \leftrightarrow CH_3OCH_3 + H_2O$	523.15 - 673.15	25	Alumina Based	87.2 %	n/a
# 25	$CO_2 + H_2 \leftrightarrow CO + H_2O$	613	20	Li, Na, K, Rb, Cs (Fe based)	2.774 %	1:1
	$CO + 2H_2 \leftrightarrow CH_3OH$	533.15	330	Fe - Cu	RGibbs	n/a
	$2CH_3OH \leftrightarrow CH_3OCH_3 + H_2O$	523.15 - 673.15	25	Alumina Based	87.2 %	n/a
# 26	$CO_2 + H_2 \leftrightarrow CO + H_2O$	613	20	Li, Na, K, Rb, Cs (Fe based)	2.774 %	1:1
	$CO + 2H_2 \leftrightarrow CH_3OH$	523 - 543	20	Cu – Ga / ZnO	RGibbs	n/a
	$2CH_3OH \leftrightarrow CH_3OCH_3 + H_2O$	523.15 - 673.15	25	Alumina Based	87.2 %	n/a
# 27	$CO_2 + H_2 \leftrightarrow CO + H_2O$	533.15 - 553.15	442	Cu / ZnO / Al_2O_3	4.5 %	1:1
# 28	$CO_2 + H_2 \leftrightarrow CO + H_2O$	533.15 - 553.15	442	Cu / ZnO / Al_2O_3	4.5 %	1:1
	$CO + 2H_2 \leftrightarrow CH_3OH$	553.15	442	Cu / ZnO / Al_2O_3	RGibbs	n/a

Case Study	Reaction	Temp (Kelvin)	Pressure (bar)	Catalyst	X_{CO2}	$CO_2 : H_2$ Ratio
# 29	$CO_2 + H_2 \leftrightarrow CO + H_2O$	533.15 - 553.15	442	Cu / ZnO / Al_2O_3	4.5 %	1:1
	$CO + 2H_2 \leftrightarrow CH_3OH$	533.15	330	Fe - Cu	RGibbs	n/a
# 30	$CO_2 + H_2 \leftrightarrow CO + H_2O$	533.15 - 553.15	442	Cu / ZnO / Al_2O_3	4.5 %	1:1
	$CO + 2H_2 \leftrightarrow CH_3OH$	523 - 543	20	Cu – Ga / ZnO	RGibbs	n/a
# 31	$CO_2 + H_2 \leftrightarrow CO + H_2O$	533.15 - 553.15	442	Cu / ZnO / Al_2O_3	4.5 %	1:1
	$CO + 2H_2 \leftrightarrow CH_3OH$	553.15	442	Cu / ZnO / Al_2O_3	RGibbs	1:2
	$2CH_3OH \leftrightarrow CH_3OCH_3 + H_2O$	523.15 - 673.15	25	Alumina Based	87.2 %	n/a
# 32	$CO_2 + H_2 \leftrightarrow CO + H_2O$	533.15 - 553.15	442	Cu / ZnO / Al_2O_3	4.5 %	1:1
	$CO + 2H_2 \leftrightarrow CH_3OH$	533.15	330	Fe - Cu	RGibbs	1:2
	$2CH_3OH \leftrightarrow CH_3OCH_3 + H_2O$	523.15 - 673.15	25	Alumina Based	87.2 %	n/a
33	$CO_2 + H_2 \leftrightarrow CO + H_2O$	533.15 - 553.15	442	Cu / ZnO / Al_2O_3	4.5 %	1:1
	$CO + 2H_2 \leftrightarrow CH_3OH$	523 - 543	20	Cu – Ga / ZnO	RGibbs	1:2
	$2CH_3OH \leftrightarrow CH_3OCH_3 + H_2O$	523.15 - 673.15	25	Alumina Based	87.2 %	n/a
# 34	$CO_2 + H_2 \leftrightarrow CO + H_2O$	474	40	CZA – Pd modified	34.375 %	1:1
# 35	$CO_2 + H_2 \leftrightarrow CO + H_2O$	474	40	CZA – Pd modified	34.375 %	1:1
	$CO + 2H_2 \leftrightarrow CH_3OH$	553.15	442	Cu / ZnO / Al_2O_3	RGibbs	1:2
# 36	$CO_2 + H_2 \leftrightarrow CO + H_2O$	474	40	CZA – Pd modified	34.375 %	1:1
	$CO + 2H_2 \leftrightarrow CH_3OH$	533.15	330	Fe - Cu	RGibbs	1:2
# 37	$CO_2 + H_2 \leftrightarrow CO + H_2O$	474	40	CZA – Pd modified	34.375 %	1:1
	$CO + 2H_2 \leftrightarrow CH_3OH$	523 - 543	20	Cu – Ga / ZnO	RGibbs	1:2

Case Study	Reaction	Temp (Kelvin)	Pressure (bar)	Catalyst	X_{CO2}	$CO_2 : H_2$ Ratio
# 38	$CO_2 + H_2 \leftrightarrow CO + H_2O$	474	40	CZA – Pd modified	34.375 %	1:1
	$CO + 2H_2 \leftrightarrow CH_3OH$	553.15	442	Cu / ZnO / Al_2O_3	RGibbs	1:2
	$2CH_3OH \leftrightarrow CH_3OCH_3 + H_2O$	523.15 - 673.15	25	Alumina Based	87.2 %	n/a
# 39	$CO_2 + H_2 \leftrightarrow CO + H_2O$	474	40	CZA – Pd modified	34.375 %	1:1
	$CO + 2H_2 \leftrightarrow CH_3OH$	533.15	330	Fe - Cu	RGibbs	1:2
	$2CH_3OH \leftrightarrow CH_3OCH_3 + H_2O$	523.15 - 673.15	25	Alumina Based	87.2 %	n/a
# 40	$CO_2 + H_2 \leftrightarrow CO + H_2O$	474	40	CZA – Pd modified	34.375 %	1:1
	$CO + 2H_2 \leftrightarrow CH_3OH$	523 - 543	20	Cu – Ga / ZnO	RGibbs	1:2
	$2CH_3OH \leftrightarrow CH_3OCH_3 + H_2O$	523.15 - 673.15	25	Alumina Based	87.2 %	n/a
# 41	$CO_2 + H_2 \leftrightarrow CO + H_2O$	533.15	330	Fe - Cu	RGibbs	1:1
# 42	$CO_2 + H_2 \leftrightarrow CO + H_2O$	533.15	330	Fe - Cu	RGibbs	1:1
	$CO + 2H_2 \leftrightarrow CH_3OH$	553.15	442	Cu / ZnO / Al_2O_3	RGibbs	1:2
# 43	$CO_2 + H_2 \leftrightarrow CO + H_2O$	533.15	330	Fe - Cu	RGibbs	1:1
	$CO + 2H_2 \leftrightarrow CH_3OH$	533.15	330	Fe - Cu	RGibbs	1:2
# 44	$CO_2 + H_2 \leftrightarrow CO + H_2O$	533.15	330	Fe - Cu	RGibbs	1:1
	$CO + 2H_2 \leftrightarrow CH_3OH$	523 - 543	20	Cu – Ga / ZnO	RGibbs	1:2
# 45	$CO_2 + H_2 \leftrightarrow CO + H_2O$	533.15	330	Fe - Cu	RGibbs	1:1
	$CO + 2H_2 \leftrightarrow CH_3OH$	553.15	442	Cu / ZnO / Al_2O_3	RGibbs	1:2
	$2CH_3OH \leftrightarrow CH_3OCH_3 + H_2O$	523.15 - 673.15	25	Alumina Based	87.2 %	n/a

Case Study	Reaction	Temp (Kelvin)	Pressure (bar)	Catalyst	X_{CO2}	CO_2 : H_2 Ratio
# 46	$CO_2 + H_2 \leftrightarrow CO + H_2O$	533.15	330	Fe - Cu	RGibbs	1:1
	$CO + 2H_2 \leftrightarrow CH_3OH$	533.15	330	Fe - Cu	RGibbs	1:2
	$2CH_3OH \leftrightarrow CH_3OCH_3 + H_2O$	523.15 - 673.15	25	Alumina Based	87.2 %	n/a
# 47	$CO_2 + H_2 \leftrightarrow CO + H_2O$	533.15	330	Fe - Cu	RGibbs	1:1
	$CO + 2H_2 \leftrightarrow CH_3OH$	523 - 543	20	Cu – Ga / ZnO	RGibbs	1:2
	$2CH_3OH \leftrightarrow CH_3OCH_3 + H_2O$	523.15 - 673.15	25	Alumina Based	87.2 %	n/a
# 48.1	$CO_2 + H_2 \leftrightarrow CO + H_2O$	623	15	Fe / ZrO_2	9.423 %	1:2
# 48.2	$CO_2 + H_2 \leftrightarrow CO + H_2O$	623	15	Fe / TiO_2	4.7941 %	1:2
# 49	$CO_2 + H_2 \leftrightarrow CO + H_2O$	623	15	Fe / ZrO_2	9.423 %	1:2
	$CO + 2H_2 \leftrightarrow CH_3OH$	553.15	442	Cu / ZnO / Al_2O_3	RGibbs	1:2
# 50	$CO_2 + H_2 \leftrightarrow CO + H_2O$	623	15	Fe / ZrO_2	9.423 %	1:2
	$CO + 2H_2 \leftrightarrow CH_3OH$	533.15	330	Fe - Cu	RGibbs	1:2
# 51	$CO_2 + H_2 \leftrightarrow CO + H_2O$	623	15	Fe / ZrO_2	9.423 %	1:2
	$CO + 2H_2 \leftrightarrow CH_3OH$	523 - 543	20	Cu – Ga / ZnO	RGibbs	1:2
# 52	$CO_2 + H_2 \leftrightarrow CO + H_2O$	623	15	Fe / ZrO_2	9.423 %	1:2
	$CO + 2H_2 \leftrightarrow CH_3OH$	553.15	442	Cu / ZnO / Al_2O_3	RGibbs	1:2
	$2CH_3OH \leftrightarrow CH_3OCH_3 + H_2O$	523.15 - 673.15	25	Alumina Based	87.2 %	n/a
# 53	$CO_2 + H_2 \leftrightarrow CO + H_2O$	623	15	Fe / ZrO_2	9.423 %	1:2
	$CO + 2H_2 \leftrightarrow CH_3OH$	533.15	330	Fe - Cu	RGibbs	1:2
	$2CH_3OH \leftrightarrow CH_3OCH_3 + H_2O$	523.15 - 673.15	25	Alumina Based	87.2 %	n/a

Case Study	Reaction	Temp (Kelvin)	Pressure (bar)	Catalyst	X_{CO2}	$CO_2 : H_2$ Ratio
# 54	$CO_2 + H_2 \leftrightarrow CO + H_2O$	623	15	Fe / ZrO_2	9.423 %	1:2
	$CO + 2H_2 \leftrightarrow CH_3OH$	523 - 543	20	Cu – Ga / ZnO	RGibbs	1:2
	$2CH_3OH \leftrightarrow CH_3OCH_3 + H_2O$	523.15 - 673.15	25	Alumina Based	87.2 %	n/a
# 55	$CO_2 + H_2 \leftrightarrow CO + H_2O$	498 - 548	50	Cu / ZnO / Al_2O_3	2.7025 %	1:1
# 56	$CO_2 + H_2 \leftrightarrow CO + H_2O$	498 - 548	50	Cu / ZnO / Al_2O_3	2.7025 %	1:1
	$CO + 2H_2 \leftrightarrow CH_3OH$	553.15	442	Cu / ZnO / Al_2O_3	RGibbs	1:2
# 57	$CO_2 + H_2 \leftrightarrow CO + H_2O$	498 - 548	50	Cu / ZnO / Al_2O_3	2.7025 %	1:1
	$CO + 2H_2 \leftrightarrow CH_3OH$	533.15	330	Fe - Cu	RGibbs	1:2
# 58	$CO_2 + H_2 \leftrightarrow CO + H_2O$	498 - 548	50	Cu / ZnO / Al_2O_3	2.7025 %	1:1
	$CO + 2H_2 \leftrightarrow CH_3OH$	523 - 543	20	Cu – Ga / ZnO	RGibbs	1:2
# 59	$CO_2 + H_2 \leftrightarrow CO + H_2O$	498 - 548	50	Cu / ZnO / Al_2O_3	2.7025 %	1:1
	$CO + 2H_2 \leftrightarrow CH_3OH$	553.15	442	Cu / ZnO / Al_2O_3	RGibbs	1:2
	$2CH_3OH \leftrightarrow CH_3OCH_3 + H_2O$	523.15 - 673.15	25	Alumina Based	87.2 %	n/a
# 60	$CO_2 + H_2 \leftrightarrow CO + H_2O$	498 - 548	50	Cu / ZnO / Al_2O_3	2.7025 %	1:1
	$CO + 2H_2 \leftrightarrow CH_3OH$	533.15	330	Fe - Cu	RGibbs	1:2
	$2CH_3OH \leftrightarrow CH_3OCH_3 + H_2O$	523.15 - 673.15	25	Alumina Based	87.2 %	n/a
# 61	$CO_2 + H_2 \leftrightarrow CO + H_2O$	498 - 548	50	Cu / ZnO / Al_2O_3	2.7025 %	1:1
	$CO + 2H_2 \leftrightarrow CH_3OH$	523 - 543	20	Cu – Ga / ZnO	RGibbs	1:2
	$2CH_3OH \leftrightarrow CH_3OCH_3 + H_2O$	523.15 - 673.15	25	Alumina Based	87.2 %	n/a
# 62	$CO_2 + H_2 \leftrightarrow CO + H_2O$	523 - 543	20	Cu – Ga / ZnO	0.75 %	1:1

Case Study	Reaction	Temp (Kelvin)	Pressure (bar)	Catalyst	X_{CO2}	$CO_2 : H_2$ Ratio
# 63	$CO_2 + H_2 \leftrightarrow CO + H_2O$	523 - 543	20	Cu – Ga / ZnO	0.75 %	1:1
	$CO + 2H_2 \leftrightarrow CH_3OH$	553.15	442	Cu / ZnO / Al_2O_3	RGibbs	1:2
# 64	$CO_2 + H_2 \leftrightarrow CO + H_2O$	523 - 543	20	Cu – Ga / ZnO	0.75 %	1:1
	$CO + 2H_2 \leftrightarrow CH_3OH$	533.15	330	Fe - Cu	RGibbs	1:2
# 65	$CO_2 + H_2 \leftrightarrow CO + H_2O$	523 - 543	20	Cu – Ga / ZnO	0.75 %	1:1
	$CO + 2H_2 \leftrightarrow CH_3OH$	523 - 543	20	Cu – Ga / ZnO	RGibbs	1:2
# 66	$CO_2 + H_2 \leftrightarrow CO + H_2O$	523 - 543	20	Cu – Ga / ZnO	0.75 %	1:1
	$CO + 2H_2 \leftrightarrow CH_3OH$	553.15	442	Cu / ZnO / Al_2O_3	RGibbs	1:2
	$2CH_3OH \leftrightarrow CH_3OCH_3 + H_2O$	523.15 - 673.15	25	Alumina Based	87.2 %	n/a
# 67	$CO_2 + H_2 \leftrightarrow CO + H_2O$	523 - 543	20	Cu – Ga / ZnO	0.75 %	1:1
	$CO + 2H_2 \leftrightarrow CH_3OH$	533.15	330	Fe - Cu	RGibbs	1:2
	$2CH_3OH \leftrightarrow CH_3OCH_3 + H_2O$	523.15 - 673.15	25	Alumina Based	87.2 %	n/a
# 68	$CO_2 + H_2 \leftrightarrow CO + H_2O$	523 - 543	20	Cu – Ga / ZnO	0.75 %	1:1
	$CO + 2H_2 \leftrightarrow CH_3OH$	523 - 543	20	Cu – Ga / ZnO	RGibbs	1:2
	$2CH_3OH \leftrightarrow CH_3OCH_3 + H_2O$	523.15 - 673.15	25	Alumina Based	87.2 %	n/a
# 69	$CO_2 + H_2 \leftrightarrow CO + H_2O$	298 - 363	70	Pt - Cu	RGibbs	1:1
# 70	$CO_2 + H_2 \leftrightarrow CO + H_2O$	298 - 363	70	Pt - Cu	RGibbs	1:1
	$CO + 2H_2 \leftrightarrow CH_3OH$	553.15	442	Cu / ZnO / Al_2O_3	RGibbs	1:2
# 71	$CO_2 + H_2 \leftrightarrow CO + H_2O$	298 - 363	70	Pt - Cu	RGibbs	1:1
	$CO + 2H_2 \leftrightarrow CH_3OH$	533.15	330	Fe - Cu	RGibbs	1:2

Case Study	Reaction	Temp (Kelvin)	Pressure (bar)	Catalyst	X_{CO2}	$CO_2 : H_2$ Ratio
# 72	$CO_2 + H_2 \leftrightarrow CO + H_2O$	298 - 363	70	Pt - Cu	RGibbs	1:1
	$CO + 2H_2 \leftrightarrow CH_3OH$	523 - 543	20	Cu – Ga / ZnO	RGibbs	1:2
# 73	$CO_2 + H_2 \leftrightarrow CO + H_2O$	298 - 363	70	Pt - Cu	RGibbs	1:1
	$CO + 2H_2 \leftrightarrow CH_3OH$	553.15	442	Cu / ZnO / Al_2O_3	RGibbs	1:2
	$2CH_3OH \leftrightarrow CH_3OCH_3 + H_2O$	523.15 - 673.15	25	Alumina Based	87.2 %	n/a
# 74	$CO_2 + H_2 \leftrightarrow CO + H_2O$	298 - 363	70	Pt - Cu	RGibbs	1:1
	$CO + 2H_2 \leftrightarrow CH_3OH$	533.15	330	Fe - Cu	RGibbs	1:2
	$2CH_3OH \leftrightarrow CH_3OCH_3 + H_2O$	523.15 - 673.15	25	Alumina Based	87.2 %	n/a
# 75	$CO_2 + H_2 \leftrightarrow CO + H_2O$	298 - 363	70	Pt - Cu	RGibbs	1:1
	$CO + 2H_2 \leftrightarrow CH_3OH$	523 - 543	20	Cu – Ga / ZnO	RGibbs	1:2
	$2CH_3OH \leftrightarrow CH_3OCH_3 + H_2O$	523.15 - 673.15	25	Alumina Based	87.2 %	n/a
# 76	$CO_2 + H_2 \leftrightarrow CO + H_2O$	433 - 513	80	Cu / Zn / Zr / Cr	5.76 %	1:1
# 77	$CO_2 + H_2 \leftrightarrow CO + H_2O$	433 - 513	80	Cu / Zn / Zr / Cr	5.76 %	1:1
	$CO + 2H_2 \leftrightarrow CH_3OH$	553.15	442	Cu / ZnO / Al_2O_3	RGibbs	1:2
# 78	$CO_2 + H_2 \leftrightarrow CO + H_2O$	433 - 513	80	Cu / Zn / Zr / Cr	5.76 %	1:1
	$CO + 2H_2 \leftrightarrow CH_3OH$	533.15	330	Fe - Cu	RGibbs	1:2
# 79	$CO_2 + H_2 \leftrightarrow CO + H_2O$	433 - 513	80	Cu / Zn / Zr / Cr	5.76 %	1:1
	$CO + 2H_2 \leftrightarrow CH_3OH$	523 - 543	20	Cu – Ga / ZnO	RGibbs	1:2
# 80	$CO_2 + H_2 \leftrightarrow CO + H_2O$	433 - 513	80	Cu / Zn / Zr / Cr	5.76 %	1:1
	$CO + 2H_2 \leftrightarrow CH_3OH$	553.15	442	Cu / ZnO / Al_2O_3	RGibbs	1:2
	$2CH_3OH \leftrightarrow CH_3OCH_3 + H_2O$	523.15 - 673.15	25	Alumina Based	87.2 %	n/a

Case Study	Reaction	Temp (Kelvin)	Pressure (bar)	Catalyst	X_{CO2}	$CO_2 : H_2$ Ratio
# 81	$CO_2 + H_2 \leftrightarrow CO + H_2O$	433 - 513	80	Cu / Zn / Zr / Cr	5.76 %	1:1
	$CO + 2H_2 \leftrightarrow CH_3OH$	533.15	330	Fe - Cu	RGibbs	1:2
	$2CH_3OH \leftrightarrow CH_3OCH_3 + H_2O$	523.15 - 673.15	25	Alumina Based	87.2 %	n/a
# 82	$CO_2 + H_2 \leftrightarrow CO + H_2O$	433 - 513	80	Cu / Zn / Zr / Cr	5.76 %	1:1
	$CO + 2H_2 \leftrightarrow CH_3OH$	523 - 543	20	Cu – Ga / ZnO	RGibbs	1:2
	$2CH_3OH \leftrightarrow CH_3OCH_3 + H_2O$	523.15 - 673.15	25	Alumina Based	87.2 %	n/a

10.2. Appendix B – Case study data (based on formulae)

This section shows the detailed case study data extracted from Aspen Plus ®. Table 37 contains the calculated values using the Aspen Plus ® data.

Table 37: Detailed case study data extracted from Aspen Plus ®

	4	5	6	7	8
Total Cost of Heat Exchangers (USD)	270,831.18	52,579.57	204,553.05	44,039.66	165,182.90
Total Cost of Pressure Changing Unit Operations (USD)	21,927,093.85	25,425,223.10	12,045,312.02	20,504,118.66	11,457,203.81
Total Cost of Separation Unit Operations (USD)	421,787.26	9,161,685.98	694,776.55	6,137,350.62	1,312,015.22
Total Cost of these Three Major Unit Operation Types	22,619,712.29	34,639,488.65	12,944,641.62	26,685,508.95	12,934,401.92
Main Product Being Produced	MeOH	MeOH	MeOH	MeOH	MeOH
Production Rate of Main Product (tonnes/year)	14,123.89	24,023.66	23,458.33	24,626.53	24,983.01
Secondary Product	Water	Water	Water	Water	Water
Production Rate of Secondary Product (tonnes/year)	8,021.38	13,508.19	13,196.38	13,846.54	14,046.99
Total Energy needed per Annum to Operate the Plant (GJ)	564,130.40	738,053.56	366,971.71	610,358.62	364,076.43
Mass of Natural Gas to Operate the Plant (tonnes/year)	10,256.92	13,419.16	6,672.21	11,097.43	6,619.57
Mass of CO_2 Produced Natural Gas combustion (tonnes/year)	28,139.07	36,814.43	18,304.71	30,444.95	18,160.29
Total Natural Gas Cost (USD)	1,614,771.21	2,112,610.20	1,050,422.67	1,747,095.23	1,042,135.18
Amount of CO_2 to be Purchased (tonns/annum)	6,716.85	-1,958.51	16,551.21	4,410.97	16,695.63
Cost of Raw Materials / Reactants for the Process (USD/year)	5,461,701.44	4,790,016.00	6,445,137.40	5,231,113.09	6,459,579.19
Sales Potential of Products from the Process (USD/year)	6,696,335.30	11,389,384.11	11,121,392.16	11,675,196.46	11,844,199.86
Annual Profit/Loss (USD/year)	-380,137.36	4,486,757.91	3,625,832.09	4,696,988.14	4,342,485.48
Payback Period of Three Main Unit Operations (years)	Infeasible	7.72	3.57	5.68	2.98

	9	10	11	12	13
Total Cost of Heat Exchangers (USD)	298,517.86	424,897.54	352,989.81	301,392.54	93,561.01
Total Cost of Pressure Changing Unit Operations (USD)	19,674,257.30	36,753,330.89	37,633,170.66	22,308,818.93	27,504,516.13
Total Cost of Separation Unit Operations (USD)	419,476.15	428,821.97	1,256,849.91	526,995.46	9,351,132.84
Total Cost of these Three Major Unit Operation Types	20,392,251.31	37,607,050.40	39,243,010.38	23,137,206.93	36,949,209.97
Main Product Being Produced	MeOH	MeOH	MeOH	DME	DME
Production Rate of Main Product (tonnes/year)	16,856.53	8,447.31	16,938.88	9,791.75	16,631.89
Secondary Product	Water	Water	Water	MeOH	MeOH
Production Rate of Secondary Product (tonnes/year)	9,541.14	4,869.98	9,546.15	175.04	293.59
Total Energy needed per Annum to Operate the Plant (GJ)	524,676.97	858,568.99	1,001,934.55	582,683.83	769,551.96
Mass of Natural Gas to Operate the Plant (tonnes/year)	9,539.58	15,610.35	18,216.99	10,594.25	13,991.85
Mass of CO_2 Produced Natural Gas combustion (tonnes/year)	26,171.11	42,825.79	49,976.92	29,064.52	38,385.58
Total Natural Gas Cost (USD)	1,501,839.39	2,457,574.48	2,867,945.18	1,667,878.67	2,202,771.46
Amount of CO_2 to be Purchased (tonns/annum)	8,684.81	-7,969.87	-15,121.00	5,791.40	-3,529.66
Cost of Raw Materials / Reactants for the Process (USD/year)	5,658,496.86	4,790,016.00	4,790,016.00	5,369,156.17	4,790,016.00
Sales Potential of Products from the Process (USD/year)	7,991,782.39	4,005,292.25	8,030,648.52	7,181,910.68	12,196,638.61
Annual Profit/Loss (USD/year)	831,446.13	-3,242,298.23	372,687.34	144,875.84	5,203,851.15
Payback Period of Three Main Unit Operations (years)	24,53	Infeasible	105,30	159,70	7,10

	14	15	16	17	18
Total Cost of Heat Exchangers (USD)	244,530.86	85,853.01	207,475.37	330,089.23	452,449.99
Total Cost of Pressure Changing Unit Operations (USD)	14,055,300.93	22,596,912.20	13,550,356.56	21,912,522.32	37,660,556.73
Total Cost of Separation Unit Operations (USD)	920,552.14	6,326,815.14	1,501,495.23	604,734.52	618,302.13
Total Cost of these Three Major Unit Operation Types	15,220,383.93	29,009,580.35	15,259,327.16	22,847,346.07	38,731,308.85
Main Product Being Produced	DME	DME	DME	DME	DME
Production Rate of Main Product (tonnes/year)	16,258.39	17,061.76	17,319.93	11,686.55	5,856.26
Secondary Product	MeOH	MeOH	MeOH	MeOH	MeOH
Production Rate of Secondary Product (tonnes/year)	289.88	303.19	309.58	208.96	104.69
Total Energy needed per Annum to Operate the Plant (GJ)	397,743.70	642,686.42	396,902.01	546,747.50	946,618.90
Mass of Natural Gas to Operate the Plant (tonnes/year)	7,231.70	11,685.21	7,216.40	9,940.86	17,211.25
Mass of CO_2 Produced Natural Gas combustion (tonnes/year)	19,839.63	32,057.47	19,797.64	27,272.00	47,217.76
Total Natural Gas Cost (USD)	1,138,504.62	1,839,630.55	1,136,095.38	1,565,014.25	2,709,609.24
Amount of CO_2 to be Purchased (tonns/annum)	15,016.29	2,798.45	15,058.28	7,583.92	-12,361.84
Cost of Raw Materials / Reactants for the Process (USD/year)	6,291,645.44	5,069,860.68	6,295,843.79	5,548,408.10	4,790,016.00
Sales Potential of Products from the Process (USD/year)	11,924,086.40	12,512,794.20	12,702,964.85	8,571,570.95	4,295,665.92
Annual Profit/Loss (USD/year)	4,493,936.33	5,603,302.97	5,271,025.68	1,458,148.59	-3,203,959.32
Payback Period of Three Main Unit Operations (years)	3,39	5,18	2,89	15,67	Infeasible

	19	20	21	22	23
Total Cost of Heat Exchangers (USD)	399,799.85	51,131.80	82,893.40	60,018.99	452,562.67
Total Cost of Pressure Changing Unit Operations (USD)	39,238,256.95	2,571,563.52	14,533,599.30	12,047,640.18	2,571,564.23
Total Cost of Separation Unit Operations (USD)	1,446,302.47	131,734.31	659,375.83	733,701.31	587,212.57
Total Cost of these Three Major Unit Operation Types	41,084,359.26	2,754,429.63	15,275,868.53	12,841,360.48	3,611,339.47
Main Product Being Produced	DME	CO	MeOH	MeOH	MeOH
Production Rate of Main Product (tonnes/year)	11,729.77	615.39	7,896.05	7,968.33	1,811.17
Secondary Product	MeOH	Water	Water	Water	Water
Production Rate of Secondary Product (tonnes/year)	207.51	364.27	4,816.49	4,752.49	4,169.26
Total Energy needed per Annum to Operate the Plant (GJ)	1,024,140.74	48,041.24	225,310.53	179,611.30	65,854.74
Mass of Natural Gas to Operate the Plant (tonnes/year)	18,620.74	873.48	4,096.56	3,265.66	1,197.36
Mass of CO_2 Produced Natural Gas combustion (tonnes/year)	51,084.58	2,396.32	11,238.59	8,959.09	3,284.86
Total Natural Gas Cost (USD)	2,931,508.34	137,513.62	644,930.60	514,120.76	188,503.11
Amount of CO_2 to be Purchased (tonns/annum)	-16,228.66	32,459.60	23,617.33	25,896.83	31,571.06
Cost of Raw Materials / Reactants for the Process (USD/year)	4,790,016.00	4,842,632.24	3,958,405.44	4,186,355.18	4,753,777.75
Sales Potential of Products from the Process (USD/year)	8,602,067.63	1,522.66	3,745,014.30	3,778,846.55	871,829.39
Annual Profit/Loss (USD/year)	880,543.28	-4,978,623.19	-858,321.74	-921,629.39	-4,070,451.47
Payback Period of Three Main Unit Operations (years)	46,66	Infeasible	Infeasible	Infeasible	Infeasible

	24	25	26	27	28
Total Cost of Heat Exchangers (USD)	109,868.57	362,242.78	454,752.10	18,169.84	44,522.10
Total Cost of Pressure Changing Unit Operations (USD)	14,087,583.52	12,734,802.30	2,640,749.00	6,730,034.46	9,966,879.27
Total Cost of Separation Unit Operations (USD)	832,984.03	907,309.56	750,320.75	2,821,919.07	3,304,867.83
Total Cost of these Three Major Unit Operation Types	15,030,436.12	14,004,354.63	3,845,821.85	9,570,123.37	13,316,269.20
Main Product Being Produced	DME	DME	DME	CO	MeOH
Production Rate of Main Product (tonnes/year)	5,471.66	5,515.30	694.77	998.29	7,686.73
Secondary Product	MeOH	MeOH	MeOH	Water	Water
Production Rate of Secondary Product (tonnes/year)	92.53	92.24	11.94	621.50	4,643.41
Total Energy needed per Annum to Operate the Plant (GJ)	233,054.67	240,466.80	63,686.36	186,385.00	233,594.92
Mass of Natural Gas to Operate the Plant (tonnes/year)	4,237.36	4,372.12	1,157.93	3,388.82	4,247.18
Mass of CO_2 Produced Natural Gas combustion (tonnes/year)	11,624.87	11,994.59	3,176.70	9,296.96	11,651.81
Total Natural Gas Cost (USD)	667,097.47	688,314.02	182,296.31	533,509.85	668,643.89
Amount of CO_2 to be Purchased (tonns/annum)	23,231.05	22,861.33	31,679.22	25,558.96	23,204.11
Cost of Raw Materials / Reactants for the Process (USD/year)	3,919,777.36	3,882,805.32	4,764,593.74	4,152,567.67	3,917,082.58
Sales Potential of Products from the Process (USD/year)	4,012,164.21	4,043,243.07	520,818.59	2,597.87	3.645.547.05
Annual Profit/Loss (USD/year)	-574,710.62	-527,876.27	-4,426,071.47	-4,683,479.65	-940,179.42
Payback Period of Three Main Unit Operations (years)	Infeasible	Infeasible	Infeasible	Infeasible	Infeasible

	29	30	31	32	33
Total Cost of Heat Exchangers (USD)	322,776.88	275,857.68	101,734.53	228,853.40	297,017.20
Total Cost of Pressure Changing Unit Operations (USD)	13,588,586.10	17,211,009.86	10,564,113.89	11,331,561.73	13,713,999.77
Total Cost of Separation Unit Operations (USD)	3,444,918.26	3,266,897.25	3,452,224.02	3,597,693.32	3,440,505.50
Total Cost of these Three Major Unit Operation Types	17,356,281.23	20,753,764.79	14,118,072.45	15,158,108.45	17,451,522.47
Main Product Being Produced	MeOH	MeOH	DME	DME	DME
Production Rate of Main Product (tonnes/year)	7,968.53	1,018.41	5,326.24	5,419.72	706.91
Secondary Product	Water	Water	MeOH	MeOH	MeOH
Production Rate of Secondary Product (tonnes/year)	4,761.60	3,406.10	90.01	90.50	12.15
Total Energy needed per Annum to Operate the Plant (GJ)	279,233.45	295,654.85	242,778.54	249,716.16	257,858.92
Mass of Natural Gas to Operate the Plant (tonnes/year)	5,076.97	5,375.54	4,414.16	4,540.29	4,688.34
Mass of CO_2 Produced Natural Gas combustion (tonnes/year)	13,928.28	14,747.39	12,109.90	12,455.95	12,862.11
Total Natural Gas Cost (USD)	799,279.98	846,284.72	694,931.15	714,789.47	738,097.36
Amount of CO_2 to be Purchased (tonns/annum)	20,927.64	20,108.53	22,746.02	22,399.97	21,993.81
Cost of Raw Materials / Reactants for the Process (USD/year)	3,689,435.61	3,607,524.97	3,871,274.29	3,836,669.10	3,796,052.69
Sales Potential of Products from the Process (USD/year)	3,778,979.07	494,663.02	3,905,315.75	3,973,015.75	530,089.19
Annual Profit/Loss (USD/year)	-709,736.53	-3,959,146.67	-660,889.69	-578,442.82	-4,004,060.86
Payback Period of Three Main Unit Operations (years)	Infeasible	Infeasible	Infeasible	Infeasible	Infeasible

	34	35	36	37	38
Total Cost of Heat Exchangers (USD)	62,410.03	96,107.53	191,331.06	330,855.76	123,004.84
Total Cost of Pressure Changing Unit Operations (USD)	3,185,652.47	7,739,004.90	9,363,062.36	5,260,180.58	8,366,302.27
Total Cost of Separation Unit Operations (USD)	216,432.33	701,640.22	855,285.84	673,782.69	857,136.16
Total Cost of these Three Major Unit Operation Types	3,464,494.83	8,536,752.64	10,409,679.26	6,264,819.03	9,346,443.27
Main Product Being Produced	CO	MeOH	MeOH	MeOH	DME
Production Rate of Main Product (tonnes/year)	7,625.83	7,439.65	7,710.70	1,192.47	5,133.63
Secondary Product	Water	Water	Water	Water	MeOH
Production Rate of Secondary Product (tonnes/year)	4,888.96	5,316.82	5,305.65	5,737.01	83.32
Total Energy needed per Annum to Operate the Plant (GJ)	78,365.78	168,337.81	191,673.60	97,684.17	178,006.22
Mass of Natural Gas to Operate the Plant (tonnes/year)	1,424.83	3,060.69	3,484.97	1,776.08	3,236.48
Mass of CO_2 Produced Natural Gas combustion (tonnes/year)	3,908.92	8,396.76	9,560.76	4,872.53	8,879.03
Total Natural Gas Cost (USD)	224,314.81	481,851.46	548,648.00	279,611.92	509,526.38
Amount of CO_2 to be Purchased (tonns/annum)	30,947.00	26,459.16	25,295.16	29,983.39	25,976.89
Cost of Raw Materials / Reactants for the Process (USD/year)	4,691,372.15	4,242,587.78	4,126,187.87	4,595,011.19	4,194,361.36
Sales Potential of Products from the Process (USD/year)	20,435.86	3,531,804.73	3,659,624.17	586,516.90	3,765,939.10
Annual Profit/Loss (USD/year)	-4,895,251.10	-1,192,634.52	-1,015,211.70	-4,288,106.21	-937,948.64
Payback Period of Three Main Unit Operations (years)	Infeasible	Infeasible	Infeasible	Infeasible	Infeasible

	39	40	41	42	43
Total Cost of Heat Exchangers (USD)	218,612.03	347,635.02	18,244.11	69,322.12	184,440.57
Total Cost of Pressure Changing Unit Operations (USD)	10,111,309.77	5,345,948.82	6,251,660.95	9,577,631.08	10,262,981.72
Total Cost of Separation Unit Operations (USD)	1,284,578.14	845,846.24	1,887,245.50	2,349,291.43	2,496,423.55
Total Cost of these Three Major Unit Operation Types	11,614,499.94	6,539,430.08	8,157,150.56	11,996,244.63	12,943,845.84
Main Product Being Produced	DME	DME	CO	MeOH	MeOH
Production Rate of Main Product (tonnes/year)	5,277.04	827.34	2,638.79	7,693.15	7,847.55
Secondary Product	MeOH	MeOH	Water	Water	Water
Production Rate of Secondary Product (tonnes/year)	78.62	14.15	1,680.86	4,702.03	4,700.63
Total Energy needed per Annum to Operate the Plant (GJ)	201,597.70	99,253.39	169,477.97	220,285.43	231,789.93
Mass of Natural Gas to Operate the Plant (tonnes/year)	3,665.41	1,804.61	3,081.42	4,005.19	4,214.36
Mass of CO_2 Produced Natural Gas combustion (tonnes/year)	10,055.78	4,950.80	8,453.63	10,987.93	11,561.78
Total Natural Gas Cost (USD)	577,054.81	284,103.66	485,115.05	630,546.70	663,477.29
Amount of CO_2 to be Purchased (tonns/annum)	24,800.14	29,905.12	26,402.29	23,867.99	23,294.14
Cost of Raw Materials / Reactants for the Process (USD/year)	4,076,686.05	4,587,183.86	4,236,900.64	3,983,470.88	3,926,085.91
Sales Potential of Products from the Process (USD/year)	3,867,083.91	627,672.25	7,025.98	3,648,820.09	3,721,650.88
Annual Profit/Loss (USD/year)	-786,656.95	-4,243,615.27	-4,714,989.71	-965,197.49	-867,912.32
Payback Period of Three Main Unit Operations (years)	Infeasible	Infeasible	Infeasible	Infeasible	Infeasible

	44	45	46	47	48.1
Total Cost of Heat Exchangers (USD)	330,710.85	96,344.13	211,612.01	347,077.08	46,719.74
Total Cost of Pressure Changing Unit Operations (USD)	8,127,061.76	10,181,945.70	10,901,492.91	8,203,172.22	2,322,347.95
Total Cost of Separation Unit Operations (USD)	2,326,230.71	2,522,900.03	2,670,031.79	2,499,838.99	103,803.45
Total Cost of these Three Major Unit Operation Types	10,784,003.32	12,801,189.86	13,783,136.71	11,050,088.30	2,472,871.14
Main Product Being Produced	MeOH	DME	DME	DME	CO
Production Rate of Main Product (tonnes/year)	1,089.30	5,327.51	5,424.13	756.07	2,090.42
Secondary Product	Water	MeOH	MeOH	MeOH	Water
Production Rate of Secondary Product (tonnes/year)	3,859.87	89.53	89.50	12.98	1,305.56
Total Energy needed per Annum to Operate the Plant (GJ)	184,709.85	230,309.72	254,345.51	181,228.41	50,071.34
Mass of Natural Gas to Operate the Plant (tonnes/year)	3,358.36	4,187.45	4,624.46	3,295.06	910.39
Mass of CO_2 Produced Natural Gas combustion (tonnes/year)	9,213.41	11,487.95	12,686.86	9,039.75	2,497.58
Total Natural Gas Cost (USD)	528,714.89	659,240.32	728,040.56	518,749.60	143,324.58
Amount of CO_2 to be Purchased (tonns/annum)	25,642.51	23,367.97	22,169.06	25,816.17	32,358.34
Cost of Raw Materials / Reactants for the Process (USD/year)	4,160,923.39	3,933,469.26	3,813,577.70	4,178,288.95	4,832,506.03
Sales Potential of Products from the Process (USD/year)	529,999.02	3,906,242.84	3,975,929.22	567,856.15	5,457.22
Annual Profit/Loss (USD/year)	-4,159,639.26	-686,466.75	-565,689.04	-4,129,182.39	-4,970,373.39
Payback Period of Three Main Unit Operations (years)	Infeasible	Infeasible	Infeasible	Infeasible	Infeasible

	48.2	49	50	51	52
Total Cost of Heat Exchangers (USD)	46,290.19	85,247.92	229,837.19	356,864.01	112,262.54
Total Cost of Pressure Changing Unit Operations (USD)	2,322,347.95	7,690,743.12	8,647,800.13	3,442,073.41	8,219,211.52
Total Cost of Separation Unit Operations (USD)	103,803.45	565,527.74	712,659.49	728,680.46	739,134.63
Total Cost of these Three Major Unit Operation Types	2,472,441.58	8,341,518.78	9,590,296.80	4,527,617.88	9,070,608.69
Main Product Being Produced	CO	MeOH	MeOH	MeOH	DME
Production Rate of Main Product (tonnes/year)	1,063.53	7,691.43	7,842.05	1,064.63	5,327.59
Secondary Product	Water	Water	Water	Water	MeOH
Production Rate of Secondary Product (tonnes/year)	644.16	4,678.95	4,680.96	3,690.55	89.73
Total Energy needed per Annum to Operate the Plant (GJ)	49,897.53	171,146.08	195,867.60	58,153.44	181,177.42
Mass of Natural Gas to Operate the Plant (tonnes/year)	907.23	3,111.75	3,561.23	1,057.34	3,294.13
Mass of CO_2 Produced Natural Gas combustion (tonnes/year)	2,488.91	8,536.84	9,769.96	2,900.72	9,037.21
Total Natural Gas Cost (USD)	142,827.07	489,889.85	560,652.93	166,458.85	518,603.64
Amount of CO_2 to be Purchased (tonns/annum)	32,367.01	26,319.08	25,085.96	31,955.20	25,818.71
Cost of Raw Materials / Reactants for the Process (USD/year)	4,833,372.99	4,228,580.05	4,105,268.04	4,792,192.16	4,178,543.30
Sales Potential of Products from the Process (USD/year)	2,692.57	3,647,912.45	3,718,974.91	517,653.51	3,906,298.23
Annual Profit/Loss (USD/year)	-4,973,507.49	-1,070,557.45	-946,946.06	-4,440,997.50	-790,848.70
Payback Period of Three Main Unit Operations (years)	Infeasible	Infeasible	Infeasible	Infeasible	Infeasible

	53	54	55	56	57
Total Cost of Heat Exchangers (USD)	255,654.33	382,953.87	56,651.41	94,308.05	219,698.67
Total Cost of Pressure Changing Unit Operations (USD)	8,973,371.23	4,390,799.73	3,388,098.91	8,253,387.34	8,084,756.23
Total Cost of Separation Unit Operations (USD)	886,267.74	902,288.71	259,713.29	716,238.83	861,708.32
Total Cost of these Three Major Unit Operation Types	10,115,293.30	5,676,042.31	3,704,463.62	9,063,934.21	9,166,163.22
Main Product Being Produced	DME	DME	CO	MeOH	MeOH
Production Rate of Main Product (tonnes/year)	5,423.12	738.98	599.48	7,684.74	7,827.65
Secondary Product	MeOH	MeOH	Water	Water	Water
Production Rate of Secondary Product (tonnes/year)	89.93	12.69	369.26	4,632.02	4,640.24
Total Energy needed per Annum to Operate the Plant (GJ)	201,419.95	44,421.02	84,530.73	176,456.69	170,465.14
Mass of Natural Gas to Operate the Plant (tonnes/year)	3,662.18	807.65	1,536.92	3,208.30	3,099.37
Mass of CO_2 Produced Natural Gas combustion (tonnes/year)	10,046.91	2,215.74	4,216.43	8,801.74	8,502.87
Total Natural Gas Cost (USD)	576,546.01	127,151.06	241,961.40	505,091.00	487,940.74
Amount of CO_2 to be Purchased (tonns/annum)	24,809.01	32,640.18	30,639.49	26,054.18	26,353.05
Cost of Raw Materials / Reactants for the Process (USD/year)	4,077,572.70	4,860,690.06	4,660,621.12	4,202,090.46	4,231,976.59
Sales Potential of Products from the Process (USD/year)	3,975,324.12	554,673.11	1,543.50	3,644,559.37	3,712,010.34
Annual Profit/Loss (USD/year)	-678,794.58	-4,433,168.02	-4,901,039.03	-1,062,622.09	-1,007,906.99
Payback Period of Three Main Unit Operations (years)	Infeasible	Infeasible	Infeasible	Infeasible	Infeasible

	58	59	60	61	62
Total Cost of Heat Exchangers (USD)	374,549.74	121,309.31	212,105.64	390,521.36	54,735.65
Total Cost of Pressure Changing Unit Operations (USD)	6,282,923.32	8,849,047.11	7,761,449.37	6,352,137.94	2,571,563.52
Total Cost of Separation Unit Operations (USD)	704,691.48	889,847.08	1,035,328.07	878,299.73	131,734.31
Total Cost of these Three Major Unit Operation Types	7,362,164.55	9,860,203.50	9,008,883.07	7,620,959.04	2,758,033.48
Main Product Being Produced	MeOH	DME	DME	DME	CO
Production Rate of Main Product (tonnes/year)	1,001.23	5,325.40	5,335.25	695.01	166.38
Secondary Product	Water	MeOH	MeOH	MeOH	Water
Production Rate of Secondary Product (tonnes/year)	3,308.90	90.09	89.31	11.95	90.50
Total Energy needed per Annum to Operate the Plant (GJ)	110,692.09	186,496.39	167,867.80	112,026.86	57,763.92
Mass of Natural Gas to Operate the Plant (tonnes/year)	2,012.58	3,390.84	3,052.14	2,036.85	1,050.25
Mass of CO_2 Produced Natural Gas combustion (tonnes/year)	5,521.37	9,302.52	8,373.32	5,587.95	2,881.29
Total Natural Gas Cost (USD)	316,845.89	533,828.71	480,506.08	320,666.54	165,343.90
Amount of CO_2 to be Purchased (tonns/annum)	29,334.55	25,553.40	26,482.60	29,267.97	31,974.63
Cost of Raw Materials / Reactants for the Process (USD/year)	4,530,127.12	4,152,012.03	4,244,932.24	4,523,469.24	4,794,135.07
Sales Potential of Products from the Process (USD/year)	486,151.64	3,904,700.92	3,911,132.23	521,000.48	378.27
Annual Profit/Loss (USD/year)	-4,360,821.38	-781,139.82	-814,306.09	-4,323,135.30	-4,959,100.70
Payback Period of Three Main Unit Operations (years)	Infeasible	Infeasible	Infeasible	Infeasible	Infeasible

	63	64	65	66	67
Total Cost of Heat Exchangers (USD)	93,376.60	222,040.94	227,635.82	120,374.31	249,170.05
Total Cost of Pressure Changing Unit Operations (USD)	7,581,400.13	7,793,668.77	2,571,563.55	8,175,667.65	8,410,790.67
Total Cost of Separation Unit Operations (USD)	588,080.72	733,550.45	549,209.59	761,688.93	907,158.65
Total Cost of these Three Major Unit Operation Types	8,262,857.45	8,749,260.16	3,348,408.95	9,057,730.89	9,567,119.37
Main Product Being Produced	MeOH	MeOH	MeOH	DME	DME
Production Rate of Main Product (tonnes/year)	7,682.30	7,823.25	982.26	5,324.28	5,416.28
Secondary Product	Water	Water	Water	MeOH	MeOH
Production Rate of Secondary Product (tonnes/year)	4,620.33	4,629.90	3,205.73	90.16	90.81
Total Energy needed per Annum to Operate the Plant (GJ)	168,161.12	167,081.40	62,236.75	178,203.44	177,289.64
Mass of Natural Gas to Operate the Plant (tonnes/year)	3,057.47	3,037.84	1,131.58	3,240.06	3,223.45
Mass of CO_2 Produced Natural Gas combustion (tonnes/year)	8,387.95	8,334.09	3,104.40	8,888.86	8,843.28
Total Natural Gas Cost (USD)	481,345.69	478,255.10	178,146.95	510,090.91	507,475.22
Amount of CO_2 to be Purchased (tonns/annum)	26,467.97	26,521.83	31,751.52	25,967.06	26,012.64
Cost of Raw Materials / Reactants for the Process (USD/year)	4,243,469.13	4,248,854.82	4,771,824.43	4,193,377.60	4,197,935.71
Sales Potential of Products from the Process (USD/year)	3,643,359.00	3,709,892.55	476,771.85	3,903,884.26	3,970,602.68
Annual Profit/Loss (USD/year)	-1,081,455.82	-1,017,217.37	-4,473,199.53	-799,584.26	-734,808.26
Payback Period of Three Main Unit Operations (years)	Infeasible	Infeasible	Infeasible	Infeasible	Infeasible

	68	69	70	71	72
Total Cost of Heat Exchangers (USD)	243,518.74	68,874.32	105,792.72	237,468.15	385,269.84
Total Cost of Pressure Changing Unit Operations (USD)	2,639,277.91	3,698,352.85	8,434,106.87	8,332,278.18	7,454,905.04
Total Cost of Separation Unit Operations (USD)	722,817.83	348,444.28	804,863.92	950,332.46	765,919.55
Total Cost of these Three Major Unit Operation Types	3,605,614.48	4,115,671.45	9,344,763.51	9,520,078.79	8,606,094.42
Main Product Being Produced	DME	CO	MeOH	MeOH	MeOH
Production Rate of Main Product (tonnes/year)	681.85	330.03	7,683.42	7,825.02	990.08
Secondary Product	MeOH	Water	Water	Water	Water
Production Rate of Secondary Product (tonnes/year)	11.72	204.71	4,625.00	4,634.05	3,247.33
Total Energy needed per Annum to Operate the Plant (GJ)	63,520.68	96,807.10	179,874.14	174,823.98	131,579.37
Mass of Natural Gas to Operate the Plant (tonnes/year)	1,154.92	1,760.13	3,270.44	3,178.62	2,392.35
Mass of CO_2 Produced Natural Gas combustion (tonnes/year)	3,168.44	4,828.78	8,972.20	8,720.29	6,563.24
Total Natural Gas Cost (USD)	181,822.09	277,101.39	514,873.13	500,417.51	376,633.79
Amount of CO_2 to be Purchased (tonns/annum)	31,687.48	30,027.14	25,883.72	26,135.63	28,292.68
Cost of Raw Materials / Reactants for the Process (USD/year)	4,765,420.12	4,599,386.04	4,185,044.09	4,210,234.51	4,425,940.50
Sales Potential of Products from the Process (USD/year)	510,969.60	855.68	3,643,907.69	3,710,747.52	480,632.80
Annual Profit/Loss (USD/year)	-4,436,272.61	-4,875,631.75	-1,056,009.53	-999,904.50	-4,321,941.49
Payback Period of Three Main Unit Operations (years)	Infeasible	Infeasible	Infeasible	Infeasible	Infeasible

	73	74	75	76	77
Total Cost of Heat Exchangers (USD)	132,791.77	264,597.26	401,198.64	62,354.90	98,547.79
Total Cost of Pressure Changing Unit Operations (USD)	9,028,824.47	8,950,431.52	7,523,027.27	3,823,260.67	8,470,411.00
Total Cost of Separation Unit Operations (USD)	978,471.15	1,123,941.31	939,527.80	395,971.25	852,806.63
Total Cost of these Three Major Unit Operation Types	10,140,087.39	10,338,970.09	8,863,753.71	4,281,586.81	9,421,765.42
Main Product Being Produced	DME	DME	DME	CO	MeOH
Production Rate of Main Product (tonnes/year)	5,324.84	5,417.06	687.27	1,277.81	7,688.19
Secondary Product	MeOH	MeOH	MeOH	Water	Water
Production Rate of Secondary Product (tonnes/year)	90.14	90.75	11.81	814.74	4,652.71
Total Energy needed per Annum to Operate the Plant (GJ)	189,914.08	185,030.42	132,896.35	101,817.87	181,704.39
Mass of Natural Gas to Operate the Plant (tonnes/year)	3,452.98	3,364.19	2,416.30	1,851.23	3,303.72
Mass of CO_2 Produced Natural Gas combustion (tonnes/year)	9,473.00	9,229.40	6,628.93	5,078.72	9,063.49
Total Natural Gas Cost (USD)	543,611.52	529,632.51	380,403.53	291,444.25	520,112.05
Amount of CO_2 to be Purchased (tonns/annum)	25,382.92	25,626.52	28,226.99	29,777.20	25,792.43
Cost of Raw Materials / Reactants for the Process (USD/year)	4,134,964.47	4,159,324.34	4,419,371.35	4,574,392.12	4,175,914.72
Sales Potential of Products from the Process (USD/year)	3,904,290.66	3,971,154.69	515,098.93	3,405.60	3,646,276.60
Annual Profit/Loss (USD/year)	-774,285.32	-717,802.16	-4,284,675.94	-4,862,430.77	-1,049,750.18
Payback Period of Three Main Unit Operations (years)	Infeasible	Infeasible	Infeasible	Infeasible	Infeasible

	78	79	80	81	82
Total Cost of Heat Exchangers (USD)	209,921.12	370,618.01	125,555.17	237,030.92	386,729.74
Total Cost of Pressure Changing Unit Operations (USD)	7,778,213.56	7,870,222.56	9,068,584.51	8,398,780.71	7,941,755.99
Total Cost of Separation Unit Operations (USD)	998,284.76	871,425.50	1,026,414.88	1,171,893.02	1,045,033.75
Total Cost of these Three Major Unit Operation Types	8,986,419.44	9,112,266.07	10,220,554.56	9,807,704.65	9,373,519.47
Main Product Being Produced	MeOH	MeOH	DME	DME	DME
Production Rate of Main Product (tonnes/year)	7,774.54	1,031.53	5,326.74	5,379.47	716.02
Secondary Product	Water	Water	MeOH	MeOH	MeOH
Production Rate of Secondary Product (tonnes/year)	4,616.32	3,483.47	89.94	89.69	12.30
Total Energy needed per Annum to Operate the Plant (GJ)	169,256.10	140,108.90	191,740.98	179,386.03	141,450.73
Mass of Natural Gas to Operate the Plant (tonnes/year)	3,077.38	2,547.43	3,486.20	3,261.56	2,571.83
Mass of CO_2 Produced Natural Gas combustion (tonnes/year)	8,442.57	6,988.69	9,564.12	8,947.85	7,055.62
Total Natural Gas Cost (USD)	484,479.98	401,048.80	548,840.87	513,475.95	404,889.66
Amount of CO_2 to be Purchased (tonns/annum)	26,413.35	27,867.23	25,291.80	25,908.07	27,800.30
Cost of Raw Materials / Reactants for the Process (USD/year)	4,238,007.32	4,383,394.81	4,125,851.77	4,187,478.82	4,376,701.71
Sales Potential of Products from the Process (USD/year)	3,686,858.25	501,175.13	3,905,681.09	3,943,452.87	537,062.14
Annual Profit/Loss (USD/year)	-1,035,629.05	-4,283,268.48	-769,011.55	-757,501.91	-4,244,529.23
Payback Period of Three Main Unit Operations (years)	Infeasible	Infeasible	Infeasible	Infeasible	Infeasible

10.3. Appendix C - Costing procedure (constants and graphs)

This appendix details the constants and graph required for the costing procedure detailed in Section 5.2.

10.3.1. Purchased equipment cost constants

The constants that are required for Equation (33) are shown in Table 38.

Table 38: Equipment cost data to be utilized with Equation (33)

Equipment	Description	K_1	K_2	K_3	Min	Max
Compressors (kW)	Centrifugal, Axial & Reciprocating	2.2897	1.3604	-0.1027	450	3,000
	Rotary	5.0355	-1.8002	0.8253	18	950
Heat Exchangers (m^2)	Scraped Wall	3.7803	0.8569	0.0349	2	20
	Teflon Tube	3.8062	0.8924	-0.1647	1	10
	Bayonet	4.2768	-0.0495	0.1431	10	1,000
	Floating Head	4.8306	-0.8509	0.3187	10	1,000
	Fixed Tube	4.3247	-0.3030	0.1634	10	1,000
	U-Tube	4.1884	-0.2503	0.1974	10	1,000
	Kettle Reboiler	4.4646	-0.5277	0.3955	10	100
	Double Pipe	3.3444	0.2745	-0.0472	1	10
	Multiple Pipe	2.7652	0.7282	0.0783	10	100
	Flat Plate	4.6656	-0.1557	0.1547	10	1,000
	Spiral Plate	4.6561	-0.2947	0.2207	1	100
	Air Cooler	4.0336	0.2341	0.0497	10	10,000
	Spiral Tube	3.9912	0.0668	0.2430	1	100
Packing (m^3)	Loose	2.4493	0.9744	0.0055	0.03	628
Process Vessels (m^3)	Horizontal	3.5565	0.3776	0.0905	0.1	628
	Vertical	3.4974	0.4483	0.1074	0.3	520
Pumps (kW)	Reciprocating	3.8696	0.3161	0.1220	0.1	200
	Positive Displacement	3.4771	0.1350	0.1438	1	100
	Centrifugal	3.3892	0.0536	0.1538	1	300

Equipment	Description	K_1	K_2	K_3	Min	Max
Reactor (m^3)	Autoclave	4.5587	-0.7014	0.0020	1	15
	Fermenter	4.1052	-0.4680	-0.0005	0.1	35
	Inoculum Tank	3.7957	-0.5407	0.0160	0.07	1
	Jacketed Agitated	4.1052	-0.4680	-0.0005	0.1	35
	Jacketed Non-agitated	3.3496	-0.2765	0.0025	5	45
	Mixer/Settler	4.7116	-0.5521	0.0004	0.04	60
Towers (m^3)	Tray and Packed	3.4974	0.44885	0.1074	0.3	520
Trays (m^2)	Sieve	2.9949	0.4465	0.3961	0.07	12.30
	Valve	3.3322	0.4838	0.3434	0.70	10.50
	Demisters	3.2353	0.4838	0.3434	0.70	10.50
Turbines (kW)	Axial Gas	2.7051	1.4398	-0.1776	100	4,000
	Radial Gas/ Liquid Expanders	2.2476	1.4965	-0.1618	100	1,500

10.3.2. Pressure factors for non-pressure driven unit operations

The constants required to utilize Equation (34) are shown in Table 39.

Table 39: Pressure factors for process equipment utilized in Equation (34)

Equipment	Description	C_1	C_2	C_3	Range (barg)
Compressors	Centrifugal, Axial, Rotary and Reciprocating	0	0	0	-
Heat Exchangers	Scraped Wall	0	0	0	P < 40
		0.6072	-0.9120	0.3327	40 < P < 100
		13.1467	-12.6574	3.0705	100 < P < 400
	Teflon Tube	0	0	0	P < 15
	Bayonet, Fixed Tube Sheet, Floating Head, Kettle Reboiler, U-Tube (Shall & Tube)	0	0	0	P < 5
		0.03881	-0.11272	0.08183	5 < P < 140
	Bayonet, Fixed Tube Sheet, Floating Head, Kettle Reboiler, U-Tube (Tube)	0	0	0	P < 5
		-0.00164	-0.00627	0.0123	5 < P < 40

	Double Pipe and Multiple Pipe	0	0	0	P < 40
		0.6072	-0.9120	0.3327	40 < P < 100
		13.1467	-12.6574	3.0705	100 < P < 300
	Flat Plate and Spiral Plate	0	0	0	P < 19
	Air Cooler	0	0	0	P < 10
		-0.1250	0.15361	-0.02861	10 < P < 100
	Spiral Tube (Shell & Tube)	0	0	0	P < 150
		-0.4045	0.1859	0	150 < P < 400
	Spiral Tube (Tube)	0	0	0	P < 150
		-0.2115	0.09717	0	150 < P < 400
Packing	Loose	0	0	0	-
Pumps	Reciprocating	0	0	0	P < 10
		-0.245382	0.259016	-0.01363	10 < P < 100
	Positive Displacement	0	0	0	P < 10
		-0.245382	0.259016	-0.01363	10 < P < 100
	Centrifugal	0	0	0	P < 10
		-0.3935	0.3957	-0.00226	10 < P < 100
Trays	Sieve, Valve and Demisters	0	0	0	-
Turbines	Axial Gas, Radial Gas, Liquid Expanders	0	0	0	-

10.3.3. Bare module and material factors for heat exchangers, process vessels and pumps

Table 40 details the identification numbers that are associated with each unit operation, and is utilized in association with Figure 22.

Table 40: Identification numbers for material factors for heat exchangers, process vessels and pumps

Identification Number	Equipment	Description	Material of Construction
1	Heat Exchanger	Double pipe, multiple pipe, fixed tube sheet, floating head, U-Tube, bayonet, kettle	CS-Shell/CS-Tube
2			CS-Shell/Cu-Tube
3			Cu-Shell/Cu-Tube
4			CS-Shell/SS-Tube
5			SS-Shell/SS-Tube

6		reboiler, scraped wall and spiral tube	CS-Shell/Ni Alloy Tube
7			Ni Alloy Shell/Ni Alloy Tube
8			CS-Shell/Ti-Tube
9			Ti-Shell/Ti-Tube
10		Air Cooler	CS Tube
11			Al Tube
12			SS Tube
13		Flat Plate and Spiral Plate	CS (in contact with fluid)
14			Cu (in contact with fluid)
15			SS (in contact with fluid)
16			Ni Alloy (in contact with fluid)
17			Ti (in contact with fluid)
18	Process Vessels	Horizontal and Vertical (Including Towers)	CS
19			SS Clad
20			SS
21			Ni Alloy Clad
22			Ni Alloy
23			Ti Clad
24			Ti
25	Pumps	Reciprocating	Cast Iron
26			Carbon Steel
27			Cu Alloy
28			SS
29			Ni Alloy
30			Ti
31		Positive Displacement	Cast Iron
32			Carbon Steel
33			Cu Alloy
34			SS
35			Ni Alloy
36			Ti
37		Centrifugal	Cast Iron
38			Carbon Steel
39			SS
40			Ni Alloy

Figure 22 utilizes the aforementioned identification numbers, with each number being associated with its own material factor, based on the type of equipment in question, as well as the material from which it is constructed.

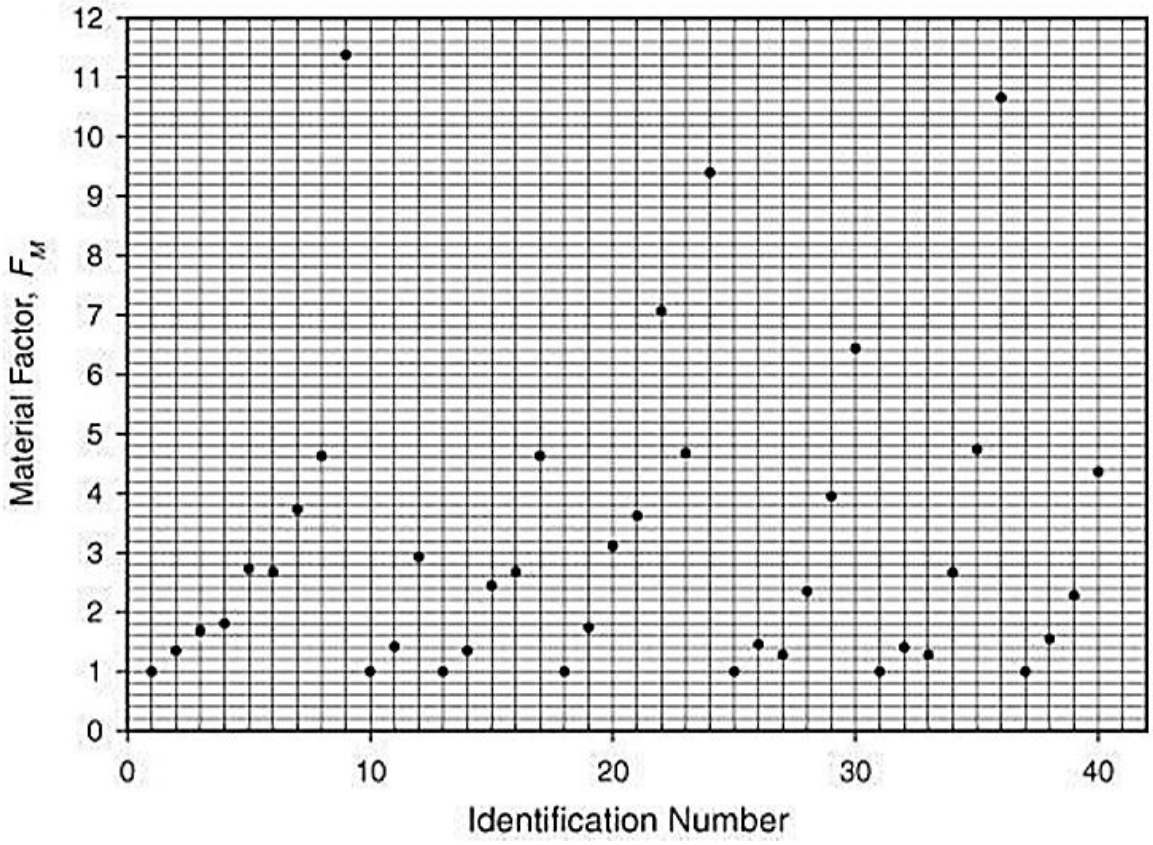

Figure 22: Material factors for the equipment in Table 40

The bare module cost factors required in Equation (36) are shown in Table 41.

Table 41: Constants for bare module factors utilized in Equation (36)

Equipment	Description	B_1	B_2
Heat Exchanger	Double pipe, multiple pipe, scraped wall and spiral tube	1.74	1.55
	Fixed tube sheet, floating head, U-Tube, bayonet, kettle reboiler and Teflon tube	1.63	1.66
	Air cooler, spiral plate and flat plate	0.96	1.21
Process Vessels	Horizontal	1.49	1.52
	Vertical (including towers)	2.25	1.82
Pumps	Reciprocating, Positive Displacement and Centrifugal	1.89	1.35

The bare module factors for the remaining process equipment utilized in these processes/case studies, are shown in Table 42.

Table 42: Identification numbers for material factors for the rest of the unit operations

Identification Number	Equipment	Description	Material of Construction
1	Compressors	Centrifugal	CS
2			SS
3			Ni Alloy
4		Axial	CS
5			SS
6			Ni Alloy
7		Rotary	CS
8			SS
9			Ni Alloy
10		Reciprocating	CS
11			SS
12			Ni Alloy
57	Power Recovery Equipment	Turbines	CS
58			SS
59			Ni Alloy
60	Trays and Demister Pads	Sieve and Valve Trays	CS
61			SS
62			Ni Alloy
63		Demister Pads	SS
64			Fluorocarbon
65			Ni Alloy
66	Tower Packing	Packing	Metal (304SS)
67			Polyethylene
68			Ceramic

Figure 23 shows the material factors that are associated with each of the identification numbers given in Table 42.

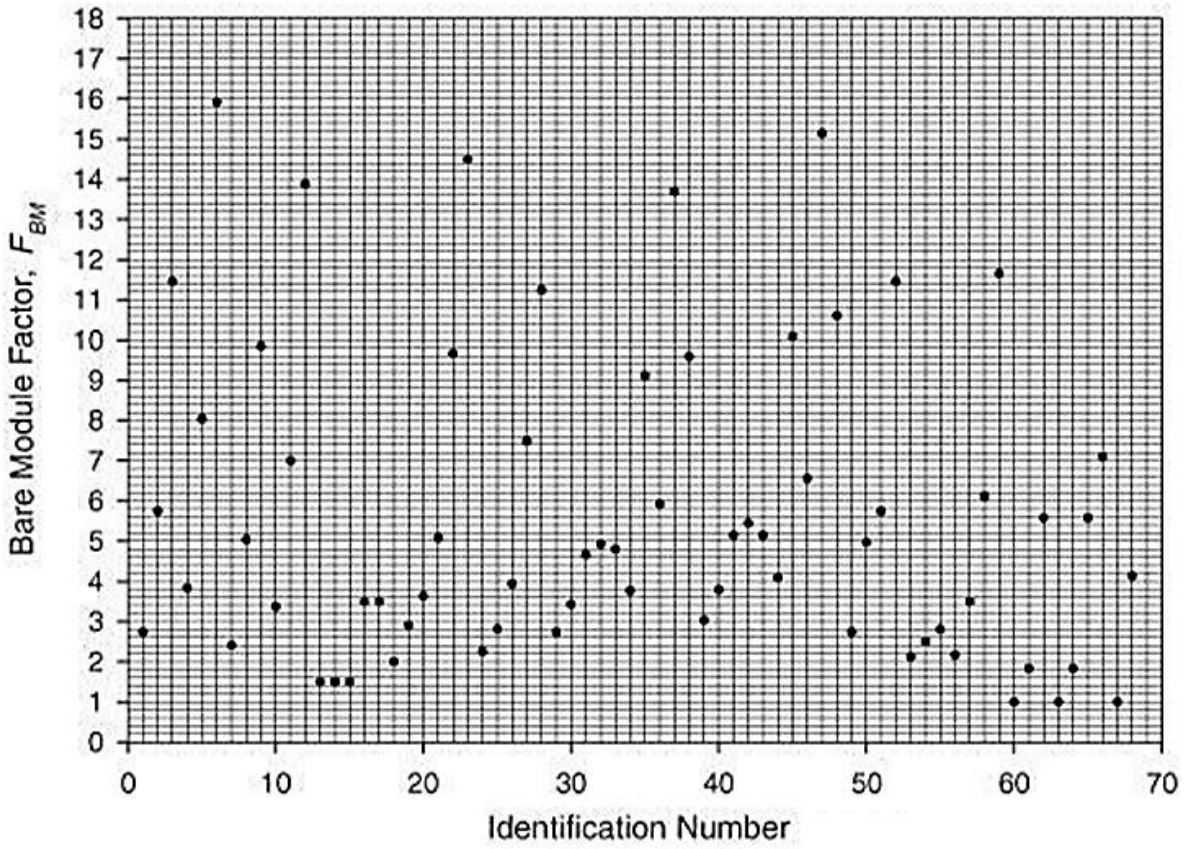

Figure 23: Material factors for the equipment in Table 42

10.4. Appendix D – MATLAB ® codes for costing equipment

This appendix details the MATLAB codes utilized in the costing of each unit operation, using the procedure detailed in Section 5.2, and the constants given in Appendix C.

10.4.1. Code for the costing of compressors

```
disp('Types of Compressors for Costing')

disp('Type 1 - Centrifugal (For capacities ranging between 450 and 3000 kW)')
disp('Type 2 - Axial (For capacities ranging between 450 and 3000 kW)')
disp('Type 3 - Reciprocating (For capacities ranging between 450 and 3000 kW)')
disp('Type 4 - Rotary (For capacities ranging between 18 and 950 kW)')

disp('Materials of Construction for Compressors:')

disp('')

disp('Material 1 - Carbon Steel (CS)')
disp('Material 2 - Stainless Steel (SS)')
disp('Material 3 - Ni Alloy')

Material_Factors_Centrifugal = [ 1 2.7 ; 2 5.7 ; 3 11.5];
Material_Factors_Axial = [ 1 3.8 ; 2 8 ; 3 15.9];
Material_Factors_Rotary = [ 1 2.4 ; 2 5 ; 3 9.8];
Material_Factors_Reciprocating = [ 1 3.3 ; 2 7 ; 3 13.9];

disp('')

Exchange_Rate = 11.98;

disp('')

CEPCI_2001 = 397;

disp('')

CEPCI_2018 = 576.40;

disp('')

Type = input('Select the type of Compressor that will be used from option 1, 2, 3 and 4');

disp('')

Capacity = input('Input the capacity of the Compressor in kilowatts (kW)');

if Type == 1

  Material = input('Input the type of material for contruction from option 1, 2, 3 and 4');
```

```
  K1 = 2.2897;
  K2 = 1.3604;
  K3 = -0.1027;

  Cpo = 10^(K1 + (K2 * log10(Capacity)) + (K3 *((log10(Capacity))^2)));

  F_BM = Material_Factors_Centrifugal(Material,2);

  Bare_Module_Cost = Cpo * F_BM;

elseif Type == 2

  Material = input('Input the type of material for contruction from option 1, 2, 3 and 4');

  K1 = 2.2897;
  K2 = 1.3604;
  K3 = -0.1027;

  Cpo = 10^(K1 + (K2 * log10(Capacity)) + (K3 *((log10(Capacity))^2)));

  F_BM = Material_Factors_Axial(Material,2);

  Bare_Module_Cost = Cpo * F_BM;

elseif Type == 3

  Material = input('Input the type of material for contruction from option 1, 2, 3 and 4');

  K1 = 5.0355;
  K2 = -1.8002;
  K3 = 0.8253;

  Cpo = 10^(K1 + (K2 * log10(Capacity)) + (K3 *((log10(Capacity))^2)));

  F_BM = Material_Factors_Rotary(Material,2);

  Bare_Module_Cost = Cpo * F_BM;

elseif Type == 4

  Material = input('Input the type of material for contruction from option 1, 2, 3 and 4');

  K1 = 2.2897;
  K2 = 1.3604;
  K3 = -0.1027;

  Cpo = 10^(K1 + (K2 * log10(Capacity)) + (K3 *((log10(Capacity))^2)));

  F_BM = Material_Factors_Reciprocating(Material,2);

  Bare_Module_Cost = Cpo * F_BM;

end

New_Price_2018 = Bare_Module_Cost * ((CEPCI_2018)/(CEPCI_2001));
```

10.4.2. Code for the costing of heat exchangers

```
disp('Types of Heat Exchangers for Costing')

disp('')

disp('Type 1 - Scraped Wall (For capacities ranging between 2 and 20 m2)')
disp('Type 2 - Teflon Tube (For capacities ranging between 1 and 10 m2)')
disp('Type 3 - Bayonet (For capacities ranging between 10 and 1000 kW)')
disp('Type 4 - Floating Head (For capacities ranging between 10 and 1000 kW)')
disp('Type 5 - Fixed Tube (For capacities ranging between 10 and 1000 kW)')
disp('Type 6 - U-Tube (For capacities ranging between 10 and 1000 kW)')
disp('Type 7 - Kettle Reboiler (For capacities ranging between 10 and 100 kW)')
disp('Type 8 - Double Pipe (For capacities ranging between 1 and 10 kW)')
disp('Type 9 - Multiple Pipe (For capacities ranging between 10 and 100 kW)')
disp('Type 10 - Flat Pipe (For capacities ranging between 10 and 1000 kW)')
disp('Type 11 - Spiral Plate (For capacities ranging between 1 and 100 kW)')
disp('Type 12 - Air Cooler (For capacities ranging between 10 and 10000 kW)')
disp('Type 13 - Spiral Tube (For capacities ranging between 1 and 100 kW)')

disp('')

disp('Materials of Construction for Heat Exchangers depending on Type:')

disp('')

disp('Materials for Type 1, 2, 3, 4, 5, 6, 7, 8, 9, 13 (Category 1)')

disp('')

disp('Material 1 - CS-Shell / CS-Tube')
disp('Material 2 - CS-Shell / Cu-Tube')
disp('Material 3 - Cu-Shell / Cu-Tube')
disp('Material 4 - CS-Shell / SS-Tube')
disp('Material 5 - SS-Shell / SS-Tube')
disp('Material 6 - CS-Shell / Ni Alloy Tube')
disp('Material 7 - Ni Alloy Shell / Ni Alloy Tube')
disp('Material 8 - CS-Shell / Ti-Tube')
disp('Material 9 - Ti-Shell / Ti-Tube')

disp('')

disp('Material for Type 12 (Category 2)')

disp('')

disp('Material 1 - CS Tube')
disp('Material 2 - Al Tube')
disp('Material 3 - SS Tube')

disp('')

disp('Material for 10 and 12 (Category 3)')

disp('')
```

```
disp('Material 1 - CS in contact with fluid')
disp('Material 2 - Cu in contact with fluid')
disp('Material 3 - SS in contact with fluid')
disp('Material 4 - Ni Alloy in contact with fluid')
disp('Material 5 - Ti in contact with fluid')

disp('')

Material_Factors_Category_1 = [ 1 1 ; 2 1.4 ; 3 1.7 ; 4 1.8 ; 5 2.7 ; 6 2.7 ; 7 3.7 ; 8 4.6 ;
9 11.4];
Material_Factors_Category_2 = [ 1 1 ; 2 1.4 ; 3 2.9];
Material_Factors_Category_3 = [ 1 1 ; 2 1.3 ; 3 2.5 ; 4 2.7 ; 5 4.6];

disp('')

Exchange_Rate = 11.98;

disp('')

CEPCI_2001 = 397;

disp('')

CEPCI_2018 = 576.40;

disp('')

Type = input('Select the type of Heat Exchanger that will be used from option 1 through to
13');

disp('')

Capacity = input('Input the capacity of the Heat Exchanger in square meters (m2)');

if Type == 1

   K1 = 3.7803;
   K2 = 0.8569;
   K3 = 0.0349;

elseif Type == 2

   K1 = 3.8062;
   K2 = 0.8924;
   K3 = -0.1671;

elseif Type == 3

   K1 = 4.2768;
   K2 = -0.0495;
   K3 = 0.1431;

elseif Type == 4

   K1 = 4.8306;
   K2 = -0.8509;
   K3 = 0.3187;
```

```
elseif Type == 5

   K1 = 4.3247;
   K2 = -0.303;
   K3 = 0.1634;

elseif Type == 6

   K1 = 4.1884;
   K2 = -0.2503;
   K3 = 0.1974;

elseif Type == 7

   K1 = 4.4646;
   K2 = -0.5277;
   K3 = 0.3955;

elseif Type == 8

   K1 = 3.3444;
   K2 = 0.2745;
   K3 = -0.0472;

elseif Type == 9

   K1 = 2.7652;
   K2 = 0.7282;
   K3 = 0.0783;

elseif Type == 10

   K1 = 4.6656;
   K2 = -0.1557;
   K3 = 0.1547;

elseif Type == 11

   K1 = 4.6561;
   K2 = -0.2947;
   K3 = 0.2207;

elseif Type == 12

   K1 = 4.0336;
   K2 = 0.2341;
   K3 = 0.0497;

elseif Type == 13

   K1 = 3.9912;
   K2 = 0.0668;
   K3 = 0.243;

end

Cpo = 10^(K1 + (K2 * log10(Capacity)) + (K3 *((log10(Capacity))^2)));
```

```
Category = input('Please choose the category from the above list (Choose from 1, 2 and 3)');

disp('')

Material = input('Choose a material from the category');

if Category == 1

   Fm = Material_Factors_Category_1(Material,2);

elseif Category == 2

   Fm = Material_Factors_Category_2(Material,2);

elseif Category == 3

   Fm = Material_Factors_Category_3(Material,2);

end

if Type == 1 || 8 || 9 || 13

   B1 = 1.74;
   B2 = 1.55;

elseif Type == 2 || 3 || 4 || 5 || 6 || 7

   B1 = 1.63;
   B2 = 1.66;

elseif Type == 10 || 11 || 12

   B1 = 0.96;
   B2 = 1.21;

end

P = input('Input the pressure that the heat exchanger is operating at in barg');

if Type == 1 || 8 || 9

   if P < 40

   C1 = 0;
   C2 = 0;
   C3 = 0;

   elseif P > 40 && P < 100

   C1 = 0.6072;
   C2 = -0.912;
   C3 = 0.3327;

   elseif P > 100 && P < 300

   C1 = 13.1467;
   C2 = -12.6574;
```

```
    C3 = 3.0705;

    end

elseif Type == 2 || 10 || 11

    C1 = 0;
    C2 = 0;
    C3 = 0;

elseif Type == 12

    if P < 10

    C1 = 0;
    C2 = 0;
    C3 = 0;

    elseif P > 10 && P < 100

    C1 = -0.125;
    C2 = 0.15361;
    C3 = -0.02861;

    end

elseif Type == 13

    if P < 150

    C1 = 0;
    C2 = 0;
    C3 = 0;

    elseif P > 150 && P < 400

    C1 = -0.4045;
    C2 = 0.1895;
    C3 = 0;

    end

elseif Type == 3 || 4 || 5 || 6 || 7

    if P < 5

    C1 = 0;
    C2 = 0;
    C3 = 0;

    elseif P > 5 && P < 140

    C1 = 0.03881;
    C2 = -0.11272;
    C3 = 0.08183;

    end
```

```
end

Fp = 10^(C1 + (C2 * log10(P)) + (C3 *((log10(P))^2)));

Bare_Module_Cost = Cpo * (B1 + (B2 * Fm * Fp));

New_Price_2018 = Bare_Module_Cost * ((CEPCI_2018)/(CEPCI_2001));
```

10.4.3. Code for the costing of pumps

```
disp('Types of Pumps for Costing')

disp('')

disp('Type 1 - Reciprocating (For capacities ranging between 0.1 and 200 kW)')
disp('Type 2 - Positive Displacement (For capacities ranging between 1 and 100 kW)')
disp('Type 3 - Centrifugal (For capacities ranging between 1 and 300 kW)')

disp('')

disp('Materials of Construction for Pumps:')

disp('')

disp('Material 1 - Cast Iron')
disp('Material 2 - Carbon Steel')
disp('Material 3 - Cu Alloy')
disp('Material 4 - Stainless Steel')
disp('Material 5 - Ni Alloy')
disp('Material 6 - Ti')

Material_Factors_Reciprocating = [ 1 1 ; 2 1.5 ; 3 1.3 ; 4 2.4 ; 5 3.9 ; 6 6.4];
Material_Factors_Positive_Displacement = [ 1 1 ; 2 1.4 ; 3 1.3 ; 4 2.7 ; 5 4.7 ; 6 10.6];
Material_Factors_Centrifugal = [ 1 1 ; 2 1.6 ; 3 2.2 ; 4 4.3];

disp('')

Exchange_Rate = input('Input the exchange rate in ZAR per USD');

disp('')

CEPCI_2001 = 397;

disp('')

CEPCI_2018 = input('Input the CEPCI at the date at which this unit operation is being
evaluated');

disp('')

Type = input('Select the type of Pump that will be used from option 1, 2 and 3');

disp('')

Capacity = input('Input the capacity of the Pump in kilowatts (kW)');

if Type == 1

  Material = input('Input the type of material for contruction from option 1, 2, 3 , 4, 5 and
6');

  disp('')
```

```
  P = input('Input the pressure that the pump is operating at from 0 to 100 barg');

  disp('')

  K1 = 3.8696;
  K2 = 0.3161;
  K3 = 0.122;

  Cpo = 10^(K1 + (K2 * log10(Capacity)) + (K3 *((log10(Capacity))^2)));

    if P  < 10

      C1 = 0;
      C2 = 0;
      C3 = 0;

      Fp = 10^(C1 + (C2 * log10(P)) + (C3 *((log10(P))^2)));

    elseif P > 10

      C1 = -0.245382;
      C2 = 0.259016;
      C3 = -0.01363;

      Fp = 10^(C1 + (C2 * log10(P)) + (C3 *((log10(P))^2)));

    end

  Fm = Material_Factors_Reciprocating(Material,2);

  Bare_Module_Cost = Cpo * (1.89 + (1.35 * Fm * Fp));

elseif Type == 2

  Material = input('Input the type of material for contruction from option 1, 2, 3 , 4, 5 and
6');

  disp('')

  P = input('Input the pressure that the pump is operating at from 0 to 100 barg');

  disp('')

  K1 = 3.4771;
  K2 = 0.135;
  K3 = 0.1438;

  Cpo = 10^(K1 + (K2 * log10(Capacity)) + (K3 *((log10(Capacity))^2)));

    if P  < 10

      C1 = 0;
      C2 = 0;
      C3 = 0;

      Fp = 10^(C1 + (C2 * log10(P)) + (C3 *((log10(P))^2)));

    elseif P > 10
```

```
      C1 = -0.245382;
      C2 = 0.259016;
      C3 = -0.01363;

      Fp = 10^(C1 + (C2 * log10(P)) + (C3 *((log10(P))^2)));

    end

  Fm = Material_Factors_Reciprocating(Material,2);

  Bare_Module_Cost = Cpo * (1.89 + (1.35 * Fm * Fp));

elseif Type == 3

  Material = input('Input the type of material for contruction from option 1, 2, 3(SS), and
4(Cu Alloy)');

  disp('')

  P = input('Input the pressure that the pump is operating at from 0 to 100 barg');

  disp('')

  K1 = 3.3892;
  K2 = 0.0536;
  K3 = 0.1538;

  Cpo = 10^(K1 + (K2 * log10(Capacity)) + (K3 *((log10(Capacity))^2)));

    if P  < 10

      C1 = 0;
      C2 = 0;
      C3 = 0;

      Fp = 10^(C1 + (C2 * log10(P)) + (C3 *((log10(P))^2)));

    elseif P > 10

      C1 = -0.3935;
      C2 = 0.3957;
      C3 = -0.00226;

      Fp = 10^(C1 + (C2 * log10(P)) + (C3 *((log10(P))^2)));

    end

  Fm = Material_Factors_Reciprocating(Material,2);

  Bare_Module_Cost = Cpo * (1.89 + (1.35 * Fm * Fp));

end

New_Price_2018 = Bare_Module_Cost * ((CEPCI_2018)/(CEPCI_2001));
```

10.4.4. Code for the costing of turbines

```
disp('The following programme is used in order to cost the Turbines that are needed in the
Process')

disp('')

disp('In this programme the following options are available:')

disp('')

disp('Types of Turbines for Costing')

disp('')

disp('Type 1 - Axial Gas Turbines (For capacities ranging between 100 and 4000 kW)')
disp('Type 2 - Radial Gas / Liquid Expanders (For capacities ranging between 100 and 1500
kW)')

disp('')

disp('Materials of Construction for Turbines:')

disp('')

disp('Material 1 - Carbon Steel (CS)')
disp('Material 2 - Stainless Steel (SS)')
disp('Material 3 - Ni Alloy')

Material_Factors = [ 1 3.6 ; 2 6.1 ; 3 11.6];

disp('')

Exchange_Rate = 11.98;

disp('')

CEPCI_2001 = 397;

disp('')

CEPCI_2018 = 576.40;

disp('')

Type = input('Select the type of Turbine that will be used from option 1 and 2');

disp('')

Capacity = input('Input the capacity of the Turbine in kilowatts (kW)');

if Type == 1

  Material = 2;
```

```
  K1 = 2.7051;
  K2 = 1.4398;
  K3 = -0.1776;

  Cpo = 10^(K1 + (K2 * log10(Capacity)) + (K3 *((log10(Capacity))^2)));

  F_BM = Material_Factors(Material,2);

  Bare_Module_Cost = Cpo * F_BM;

elseif Type == 2

  Material = input('Input the type of material for contruction from option 1, 2 and 3');

  K1 = 2.2476;
  K2 = 1.4965;
  K3 = -0.1618;

  Cpo = 10^(K1 + (K2 * log10(Capacity)) + (K3 *((log10(Capacity))^2)));

  F_BM = Material_Factors(Material,2);

  Bare_Module_Cost = Cpo * F_BM;

end

New_Price_2018 = Bare_Module_Cost * ((CEPCI_2018)/(CEPCI_2001));
```

10.4.5. Code for the costing of process vessels

```
disp('Types of process vessels')

disp('')

disp('Type 1 - Horizontal Process Vessel (Range of 0.1 and 628 m3)')
disp('Type 2 - Vertical Process Vessel (Range of 0.3 and 520 m3)')

disp('')

disp('Materials of Construction for Towers:')

disp('')

disp('Material 1 - CS')
disp('Material 2 - SS Clad')
disp('Material 3 - SS')
disp('Material 4 - Ni Alloy Clad')
disp('Material 5 - Ni Alloy')
disp('Material 6 - Ti Clad')
disp('Material 7 - Ti')

Material_Factors = [ 1 1 ; 2 1.7 ; 3 3.1 ; 4 3.6 ; 5 7.1 ; 6 4.7 ; 7 9.4];

disp('')

Exchange_Rate = input('Input the exchange rate in ZAR per USD');

disp('')

CEPCI_2001 = 397;

disp('')

CEPCI_2018 = input('Input the CEPCI at the date at which this unit operation is being
evaluated');

disp('')

Type = input('Choose the type of process vessel to cost');

disp('')

Capacity = input('Input the capacity of the Tower in cubic meters (m3)');

if Type == 1

   K1 = 3.5565;
   K2 = 0.3776;
   K3 = 0.0905;

elseif Type == 2

   K1 = 3.4974;
```

```
    K2 = 0.4485;
    K3 = 0.1074;

end

Cpo = 10^(K1 + (K2 * log10(Capacity)) + (K3 *((log10(Capacity))^2)));

P = input('Please insert the pressure of the vessel in barg');

disp('')

D = input('Please input the diameter of the tower vessel');

if P < 0.5

    Fp = 1.25;

else

    Fp = ((((P+1)/D)/(2*(850-0.6*(P+1))))+0.00315)/0.0063;

end

Material = input('Choose a material from the seven options that are provided above');

Fm = Material_Factors(Material,2);

Orientation = input('Choose the orientation of the vessel in question - be it vertical(Option
1) or horizontal (Options 2)');

if Orientation == 1

    B1 = 2.25;
    B2 = 1.82;

elseif Orientation == 2

    B1 = 1.49;
    B2 = 1.52;

end

Bare_Module_Cost = Cpo * (B1 + (B2 * Fm * Fp));

New_Price_2018 = Bare_Module_Cost * ((CEPCI_2018)/(CEPCI_2001));
```

10.4.6. Code for the costing of towers

```
disp('In this programme there is only one option available for costing, This is the packing
and the trayed tower, which will be costed in the same way.')
disp('The size of the tower must be between 0.3m3 and 520m3 for this programme to work
accurately')

disp('')

disp('Materials of Construction for Towers:')

disp('')

disp('Material 1 - CS')
disp('Material 2 - SS Clad')
disp('Material 3 - SS')
disp('Material 4 - Ni Alloy Clad')
disp('Material 5 - Ni Alloy')
disp('Material 6 - Ti Clad')
disp('Material 7 - Ti')

Material_Factors = [ 1 1 ; 2 1.7 ; 3 3.1 ; 4 3.6 ; 5 7.1 ; 6 4.7 ; 7 9.4];

disp('')

Exchange_Rate = input('Input the exchange rate in ZAR per USD');

disp('')

CEPCI_2001 = 397;

disp('')

CEPCI_2018 = input('Input the CEPCI at the date at which this unit operation is being
evaluated');

disp('')

Capacity = input('Input the capacity of the Tower in cubic meters (m3)');

K1 = 3.4974;
K2 = 0.4485;
K3 = 0.1074;

Cpo = 10^(K1 + (K2 * log10(Capacity)) + (K3 *((log10(Capacity))^2)));

P = input('Please insert the pressure of the vessel in barg');

disp('')

D = input('Please input the diameter of the tower vessel');

if P < 0.5

   Fp = 1.25;
```

```
else

   Fp = ((((P+1)/D)/(2*(850-0.6*(P+1))))+0.00315)/0.0063;

end

Material = input('Choose a material from the seven options that are provided above');

Fm = Material_Factors(Material,2);

Orientation = input('Choose the orientation of the vessel in question - be it vertical(Option
1) or horizontal (Options 2)');

if Orientation == 1

    B1 = 2.25;
    B2 = 1.82;

elseif Orientation == 2

    B1 = 1.49;
    B2 = 1.52;

end

Bare_Module_Cost = Cpo * (B1 + (B2 * Fm * Fp));

New_Price_2018 = Bare_Module_Cost * ((CEPCI_2018)/(CEPCI_2001));
```

10.4.7. Code for the costing of trays

```
disp('Types of Trays for Costing')

disp('')

disp('Type 1 - Sieve (For capacities ranging between 0.07 and 12.3 m2)')
disp('Type 2 - Valve (For capacities ranging between 0.7 and 10.5 m2)')

disp('')

disp('Materials of Construction for Trays:')

disp('')

disp('Material 1 - Carbon Steel (CS)')
disp('Material 2 - Stainless Steel (SS)')
disp('Material 3 - Ni Alloy')

Material_Factors = [ 1 1 ; 2 1.8 ; 3 5.6];

disp('')

Exchange_Rate = input('Input the exchange rate in ZAR per USD');

disp('')

CEPCI_2001 = 397;

disp('')

CEPCI_2018 = input('Input the CEPCI at the date at which this unit operation is being
evaluated');

disp('')

Type = input('Select the type of Tray that will be used from option 1 and 2');

disp('')

Capacity = input('Input the capacity of the Tray in square meters');

disp('')

N = input('Input the number of trays in the tower');

if N < 20

    Fq = 10^(0.4771 + (0.08516 * log10(N)) - 0.3473 * ((log10(N))^2));

  elseif N > 20

    Fq = 1;

end
```

```
if Type == 1

  Material = input('Input the type of material for construction from option 1, 2 and 3');

  K1 = 2.9949;
  K2 = 0.4465;
  K3 = 0.3961;

  Cpo = 10^(K1 + (K2 * log10(Capacity)) + (K3 *((log10(Capacity))^2)));

  F_BM = Material_Factors(Material,2);

  Bare_Module_Cost = Cpo * N * F_BM * Fq;


elseif Type == 2

  Material = input('Input the type of material for construction from option 1, 2 and 3');

  K1 = 3.3322;
  K2 = 0.4838;
  K3 = 0.3434;

  Cpo = 10^(K1 + (K2 * log10(Capacity)) + (K3 *((log10(Capacity))^2)));

  F_BM = Material_Factors(Material,2);

  Bare_Module_Cost = Cpo * N * F_BM * Fq;

end

New_Price_2018 = Bare_Module_Cost * ((CEPCI_2018)/(CEPCI_2001));
```